



U.S. Department
of Transportation
**Federal Railroad
Administration**

RAILROAD WHEEL RESIDUAL STRESS DETECTION PROGRAM

Office of Research and
Development
Washington, D.C. 20590

AN EVALUATION OF RESIDUAL STRESS IN CAST STEEL RAILROAD WHEELS USING ELECTROMAGNETIC ACOUSTIC TRANSDUCERS (EMATs)

DOT/FRA/ORD-99/06

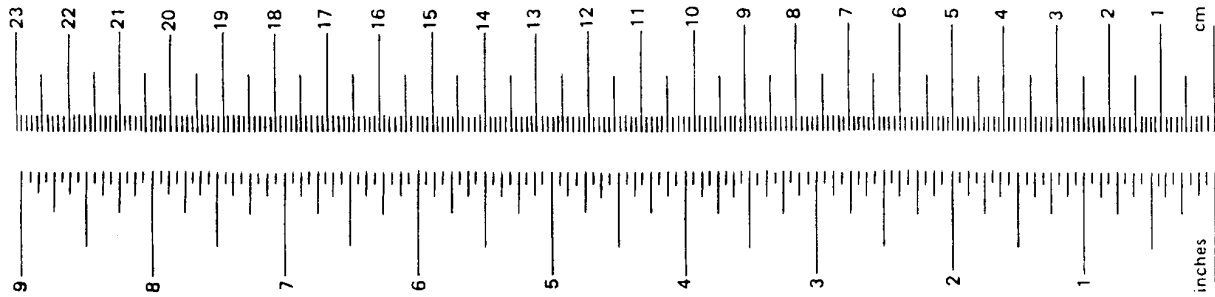
December 1998
Final Report

This document is available to the
U.S. public through the National
Technical Information Service
Springfield, Virginia 22161

Disclaimer: This document is disseminated under the sponsorship of the Department of Transportation in the interest of information exchange. The United States Government assumes no liability for the contents or use thereof. The United States Government does not endorse products or manufacturers. Trade or manufacturers' names appear herein solely because they are considered essential to the object of this report.

1. Report No. FRA/ORD-99/06	2. Government Accession No.	3. Recipient's Catalog No.	
4. Title and Subtitle Wheel Residual Stress Detection Program An Evaluation of Residual Stress in Cast Steel Railroad Wheels using Electromagnetic Acoustic Transducers (EMATS)		5. Report Date December 1998	
		6. Performing Organization Code	
7. Authors Dan Stone, Greg Garcia and Scott Burnett		8. Performing Organization Report No.	
9. Performing Organization Name and Address Association of American Railroads Transportation Technology Center, Inc. P.O. Box 11130 Pueblo, CO 81001		10. Work Unit N o. (TRAIS)	
		11. Contract or Grant No. DTFR53-93-C-00001	
12. Sponsoring Agency Name and Address U.S. Department of Transportation Federal Railroad Administration Office of Research and Development 1120 Vermont Avenue, NW Washington, DC 20590		13. Type of Report or Period Covered	
		14. Sponsoring Agency Code	
15. Supplemental Notes			
16. Abstract A nondestructive testing (NDT) method to determine the residual stress in the rims of cast steel railroad wheels has been evaluated by the Association of American Railroads (AAR), at the Transportation Technology Center (TTC), Pueblo, Colorado. The National Institute of Standards and Technology (NIST), Boulder, Colorado, has developed an ultrasonic system which uses electromagnetic acoustic transducers (EMATs) to determine the residual stress in cast steel railroad wheels. The system is designed to induce polarized shear waves into the rim of the wheel and measures the thickness averaged stress from the return sound signal. A similar ultrasonic system, known as the DEBRO-30, is commercially available in Europe and uses conventional piezoelectric transducers (PET) to measure the thickness averaged stress in rail and forged railroad wheels. These two ultrasonic systems were used during this project and the ultrasonic data obtained by the systems have been evaluated in this report. The measurement results show good correlation between EMAT and PET readings. NIST has identified a systematic offset between the two systems of approximately 40 Mega Pascals (Mpa) (6ksi) or less. Results from destructive tests with saw cutting starting at the flange tip and progressing into the wheel hub, correlated with ultrasonic measurements taken on as-manufactured, induction-heated and drag-braked railroad wheels. Saw cut displacements indicating compression agreed with ultrasonic measurements showing that the wheel rim was in compression. This was also true of wheels showing a state of rim residual tension. Comparisons between ultrasonic data and finite element analysis (FEA), performed at the TTC, also show a correlation between theoretical hoop residual stress estimates and ultrasonic residual stress measurements.			
17. Key Words electromagnetic acoustic transducer (EMAT), piezoelectric transducer (PET), nondestructive testing (NDT), birefringence, residual stress, finite element analysis (FEA), ultrasonic		18. Distribution Statement This document is available through National Technical Information Service Springfield, VA 22161	
19. Security Classification <i>(of the report)</i>	20. Security Classification <i>(of this page)</i>	21. No of Pages 84	22. Price

METRIC CONVERSION FACTORS



Approximate Conversions to Metric Measures

Symbol	When You Know	Multiply by	To Find	Symbol
in	inches	*2.50	centimeters	cm
ft	feet	30.00	centimeters	cm
yd	yards	0.90	meters	m
mi	miles	1.60	kilometers	km

AREA

in ²	square inches	6.50	square centimeters	cm ²
ft ²	square feet	0.09	square meters	m ²
yd ²	square yards	0.80	square meters	m ²
mi ²	square miles	2.60	square kilometers	km ²
	acres	0.40	hectares	ha

MASS (weight)

oz	ounces	28.00	grams	g
lb	pounds	0.45	kilograms	kg
	short tons (2000 lb)	0.90	tonnes	t

VOLUME

tsp	teaspoons	5.00	milliliters	ml
Tbsp	tablespoons	15.00	milliliters	ml
fl oz	fluid ounces	30.00	milliliters	ml
c	cups	0.24	liters	l
pt	pints	0.47	liters	l
qt	quarts	0.95	liters	l
gal	gallons	3.80	liters	l
ft ³	cubic feet	0.03	cubic meters	m ³
yd ³	cubic yards	0.76	cubic meters	m ³

TEMPERATURE (exact)

°F	Fahrenheit temperature	5/9 (after subtracting 32)	Celsius temperature	°C
----	------------------------	----------------------------	---------------------	----

Approximate Conversions from Metric Measures

Symbol	When You Know	Multiply by	To Find	Symbol
mm	millimeters	0.04	inches	in
cm	centimeters	0.40	inches	in
m	meters	3.30	feet	ft
m	meters	1.10	yards	yd
km	kilometers	0.60	miles	mi

LENGTH

AREA

cm ²	square centim.	0.16	square inches	in ²
m ²	square meters	1.20	square yards	yd ²
km ²	square kilom.	0.40	square miles	mi ²
ha	hectares (10,000 m ²)	2.50	acres	

MASS (weight)

g	grams	0.035	ounces	oz
kg	kilograms	2.2	pounds	lb
t	tonnes (1000 kg)	1.1	short tons	

VOLUME

ml	milliliters	0.03	fluid ounces	fl oz
l	liters	2.10	pints	pt
l	liters	1.06	quarts	qt
l	liters	0.26	gallons	gal
m ³	cubic meters	36.00	cubic feet	ft ³
m ³	cubic meters	1.30	cubic yards	yd ³

TEMPERATURE (exact)

°C	Celsius temperature	9/5 (then add 32)	Fahrenheit temperature	°F
----	---------------------	-------------------	------------------------	----



* 1 in. = 2.54 cm (exactly)

ACKNOWLEDGEMENTS

The Wheel Residual Stress Detection Program has been a cooperative project between the Federal Railroad Administration (FRA), the National Institute of Standards and Technology (NIST), the Institute of Fundamental Technological Research, Polish Academy of Sciences, Warsaw, Volpe National Transportation Systems Center (VNTSC), Griffin Wheel Company, Concurrent Technologies Corporation (CTC) and the Association of American Railroads (AAR). Special thanks to Don Gray and Monique Stewart of the FRA, Ray Schramm, Dr. Van Clark and George Aylers of NIST, Dr. Jacek Szelazek guest researcher from the Polish Academy of Sciences, Dr. Oscar Orringer and Dr. Jeff Gordon of VNTSC, John Oliver, Richard Pilon and the staff from Griffin Wheel Company, Dr. Robert Czarnek and Dr. Shih-Yung Lin of CTC and the staff of the AAR/TTC.

EXECUTIVE SUMMARY

A nondestructive testing (NDT) method to determine the residual stress in the rims of cast steel railroad wheels has been evaluated by the Association of American Railroads (AAR), at the Federal Railroad Administration's Transportation Technology Center (TTC), Pueblo, Colorado. The National Institute of Standards and Technology (NIST), Boulder, Colorado, has developed an ultrasonic system which uses an electromagnetic acoustic transducer (EMAT) technique to determine the residual stress in cast steel railroad wheels. The system is designed to induce polarized shear waves into the rim of the wheel and measures the thickness averaged stress from the return sound signal. A similar ultrasonic system, known as the DEBRO-30, is commercially available in Europe and uses a conventional piezoelectric transducer (PET) to measure the thickness averaged stress in rail and forged railroad wheels. These two ultrasonic systems were used during this project and the ultrasonic data obtained by the systems have been evaluated in this report.

The measurement results show good correlation between EMAT and PET readings. NIST has identified a systematic offset between the two systems of approximately 40 Mega Pascals (Mpa) (6 ksi) or less. Results from destructive tests with saw cutting starting at the flange tip and progressing into the wheel hub, correlated with ultrasonic measurements taken on as-manufactured, induction-heated and drag-braked railroad wheels. Saw cut displacements indicating compression agreed with ultrasonic measurements showing that the wheel rim was in compression. This was also true of wheels showing a state of rim residual tension. Comparisons between ultrasonic data and finite element analysis (FEA), performed at the TTC, also show a correlation between theoretical hoop residual stress estimates and ultrasonic residual stress measurements.

The EMAT system has produced positive results, under controlled environments, to determine the residual stress state of cast railroad wheels. NIST has further developed the system for portability since the conclusion of this work. AAR recommends that the portable EMAT ultrasonic system be further evaluated on both new railroad wheels and in-service wheels which can be ultrasonically measured for residual stress and compared with destructive forms of stress determination such as saw cutting. Once a level of confidence is demonstrated by in-service evaluation results, the system should then be made available to wheel manufacturers and wheel shops as both a quality control and safety tool for the railroad industry.

Table of Contents

1.0	Background	1
1.1	Previous Work.....	3
2.0	Objective	7
3.0	Procedures	7
3.1	Test Parameters	7
3.2	Test Wheels	8
3.3	Induction Heating	9
3.4	Drag Braking	11
3.5	Wheel Residual Stress Measurements	19
3.6	Standard Saw Cutting	25
3.7	Precision Saw Cutting	26
3.8	Finite Element Analysis	28
3.8.1	Induction Heat Finite Element Analysis	29
3.8.2	Saw Cut FEA Model	32
4.0	Results.....	34
4.1	Birefringence Measurements	34
4.2	Residual Stress Measurements	48
4.3	Standard Saw Cut Measurements	64
4.4	Finite Element Analysis (FEA)	75
4.4.1	Induction Heat FEA	75
4.4.2	Saw Cut FEA	78
4.4.3	Saw Cut FEA Relevant Error Sources	79
5.0	Conclusions	79
6.0	Recommendations	82
	References	83

List of Figures

Figure 1. Effect of Drag Testing on Residual Stress Distribution in Rim of Rim-Quenched Wheels	3
Figure 2. Typical Saw Cut Displacement Behavior of a New or Undamaged Rim-Quenched Wheel	4
Figure 3. Typical Saw Cut Displacement Behavior of a Thermally Damaged Wheel..	4
Figure 4. Calculated Distribution of Circumferential Residual Stresses (ksi) in a Thermally Damaged Wheel	5
Figure 5. Photograph of Coil Configuration for the Induction Heating Setup.....	10
Figure 6. Wheel Markings Identifying the Wheel at 3-inch Increments Around the Radius	10
Figure 7. Wheel to Rail Dynamometer at Griffin Wheel Company	12
Figure 8. Wheel to Rail Contact with the Griffin Wheel Dynamometer.....	12
Figure 9. Wheel to Rail Dynamometer Load Cell Arrangement Designed for Simulating Centered and Flange Crowded Brake Shoe Conditions	12
Figure 10. Brake Shoe to Wheel Tread Orientation.....	13
Figure 11. Brake Shoe Deterioration during Drag Braking at 90 hp with Brake Shoe Centered	14
Figure 12. Front View Comparison of Non-conditioned and Conditioned Brake Shoes used during 90 and 100 hp Drag Braking Runs	15
Figure 13. Side View Comparison of Non-conditioned and Conditioned Brake Shoes used during 90 and 100 hp Drag Braking Runs	15
Figure 14. Heat Band Origination during Drag Braking	17
Figure 15. Full Heat Band Across the Wheel Tread during Drag Braking.....	18
Figure 16. Water Spray of Drag Braked Wheels	18
Figure 17. Ultrasonic Measurement Locations from the Front Rim Face of the Railroad Wheels.....	20
Figure 18. Transducer Location on the Front Rim Face and Direction of Wave Propagation during Ultrasonic Inspection of Railroad Wheels	20
Figure 19. DEBRO-30 Ultrasonic Measurement System using PET.....	23
Figure 20. NIST Ultrasonic Measurement System using EMAT	23
Figure 21. Transducer Locations for the PET and EMAT Ultrasonic Measurement Systems.....	24
Figure 22. 85 hp Flange Crowded Wheels Showing Saw Cut Locations and Risers..	25
Figure 23. Standard Saw Cutting at Griffin Wheel	26
Figure 24. Precision Saw Cut Instrumentation Setup at CTC	27
Figure 25. Strain Gage Setup Across the Tread of the Wheel at CTC	27
Figure 26. Interferometer Setups at CTC	28

Figure 27. Finite Element Analysis of a Test Wheel Induction Heated at 38 kW (51 hp) for 30 Minutes and Air Cooled for 5 Hours	30
Figure 28. Finite Element Analysis of a Test Wheel Induction Heated at 42 kW (56 hp) for 30 Minutes and Air Cooled for 5 Hours	31
Figure 29. Finite Element Analysis of a Test Wheel Induction Heated at 45 kW (60 hp) for 30 Minutes and Air Cooled for 5 Hours	32
Figure 30. Three Dimensional 90 Degree Wheel Slice used in Developing the Finite Element Analysis Model.....	33
Figure 31. Residual Stress UT Birefringence Measurement Comparison between the PET and EMAT Systems for the Railroad Wheels Drag Braked at 75 hp and the Brake Shoe Positioned at the Flange Corner	37
Figure 32. Residual Stress UT Birefringence Measurement Comparison between the PET and EMAT Systems for the Railroad Wheels Drag Braked at 80 hp and the Brake Shoe Positioned at Tread Center.....	38
Figure 33. Residual Stress UT Birefringence Measurements using the EMAT System for the Railroad Wheels Drag Braked at 80 hp and the Brake Shoe Positioned at the Flange Corner	39
Figure 34. `Residual Stress UT Birefringence Measurement Comparison between the PET and EMAT Systems for the Railroad Wheels Drag Braked at 85 hp and 60 mph with the Brake Shoe Positioned at the Tread Center.....	40
Figure 35. Residual Stress UT Birefringence Measurement Comparison between the PET and EMAT systems for the Railroad Wheels Drag Braked at 85 hp and 60 mph with the Brake Shoe Positioned at the Flange Corner.....	41
Figure 36. Residual Stress UT Birefringence Measurement from the EMAT System for the Railroad Wheels Drag Braked at 85 hp and 70 mph with the Brake Shoe Positioned at the Tread Center	42
Figure 37. Residual Stress UT Birefringence Measurement from the EMAT System for the Railroad Wheels Drag Braked at 85 hp and 70 mph with the Brake Shoe Positioned at the Flange Corner	43
Figure 38. Residual Stress UT Birefringence Measurement from the EMAT System for the Railroad Wheels Drag Braked at 90 hp and the Brake Shoe Positioned at the Tread Center	44
Figure 39. Residual Stress UT Birefringence Measurement Comparison between the PET and EMAT Systems for the Railroad Wheels Drag Braked at 90 hp and the Brake Shoe Positioned at the Flange Corner	45
Figure 40. Residual Stress UT Birefringence Measurement Comparison between the PET and EMAT Systems for the Railroad Wheels Drag Braked at 100 hp and 70 mph with the Brake Shoe Positioned at the Tread Center.	46

Figure 41. Average UT Birefringence Measurement Comparison between the PET and EMAT Systems for Drag Braked Railroad Wheels	48
Figure 42. Residual Stress UT Measurement Comparison between the PET and EMAT Systems for the Railroad Wheels Drag Braked at 75 hp and the Brake Shoe Positioned at the Flange Corner.....	51
Figure 43. Residual Stress UT Measurement Comparison between the PET and EMAT Systems for the Railroad Wheels Drag Braked at 80 hp and the Brake Shoe Positioned at Tread Center	52
Figure 44. Residual Stress UT Measurement Comparison between the PET and EMAT Systems for the Railroad Wheels Drag Braked at 80 hp and the Brake Shoe Positioned at the Flange Corner	53
Figure 45. Residual Stress UT Measurement Comparison between the PET and EMAT Systems for the Railroad Wheels Drag Braked at 85 hp and 60 mph with the Brake Shoe Positioned at the Tread Center	54
Figure 46. Residual Stress UT Measurement Comparison between the PET and EMAT Systems for the Railroad Wheels Drag Braked at 85 hp and 60 mph with the Brake Shoe Positioned at the Flange Corner	55
Figure 47. Residual Stress UT Measurements using the EMAT System for Railroad Wheels Drag Braked at 85 hp and 70 mph with the Brake Shoe Positioned at the Tread Center	56
Figure 48. Residual Stress UT Measurements using the EMAT Systems for Railroad Wheels Drag Braked at 85 hp and 70 mph with the Brake Shoe Positioned at the Flange Corner	57
Figure 49. Residual Stress UT Measurement Comparison between the PET and EMAT Systems for the Railroad Wheels Drag Braked at 90 hp and the Brake Shoe Positioned at the Tread Center	58
Figure 50. Residual Stress UT Measurement Comparison between the PET and EMAT Systems for the Railroad Wheels Drag Braked at 90 hp and the Brake Shoe Positioned at the Flange Corner	59
Figure 51. Residual Stress UT Measurement Comparison between the PET and EMAT Systems for the Railroad Wheels Drag Braked at 100 hp and 70 mph with the Brake Shoe Positioned at the Tread Center	60
Figure 52. Average UT Residual Stress Measurement Comparison between the PET and EMAT Systems for As-Manufactured Railroad Wheels	62
Figure 53. Average UT Residual Stress Measurement Comparison between the PET and EMAT Systems for Induction Heated Railroad Wheels	62
Figure 54. Average UT Residual Stress Measurements Comparison between the PET and EMAT Systems for the Drag Braked Railroad Wheels	63
Figure 55. Direct Comparison of Average Stress Measured between EMAT and PET Ultrasonic Systems	63
Figure 56. Radial Displacements, after Standard Saw Cutting, of the 56 kW (75hp) Wheels Drag Braked at 60 mph for Three 30-Minute Cycles	65
Figure 57. Radial Displacements, after Standard Saw Cutting, of the 60 kW (80 hp) Wheels Drag Braked at 60 mph for Three 30-Minute Cycles	66
Figure 58. Radial Displacements, after Standard Saw Cutting, of the 63 kW (85 hp) Wheels Drag Braked at 60 mph for Three 30-Minute Cycles	67

Figure 59. Radial Displacements, after Standard Saw Cutting, of the 63 kW (85 hp) Wheels Drag Braked at 70 mph for Three 30-Minute Cycles	68
Figure 60. Radial Displacements, after Standard Saw Curring, of the 67 kW (90 hp) Wheels Drag Braked at 60 mph for Three 30-Minute Cycles	69
Figure 61. Radial Displacements, after Standard Saw Cutting, of the 75 kW (100 hp) Wheel Drag Braked at 70 mph for Three 30-Minute Cycles.....	70
Figure 62. Radial Displacements, after Standard Saw Cutting, of Railroad Wheels in the As-Manufactured Condition.....	71
Figure 63. Radial Displacements, after Standard Saw Cutting, of Railroad Wheels Induction Heated at 45 kW (60 hp) for 30 Minutes and Air Cooled for 5 Hours	72
Figure 64. Radial Displacement Comparison at a Cut Depth of 2 Inches for As-Manufactured, Induction Heated and Drag Braked Railroad Wheels	74
Figure 65. Fractured Railroad Wheel—Drag Braked at 70 mph, 3 Runs at a Minimum of 50 Minutes Each Run.....	74
Figure 66. Fractured Railroad Wheel—Drag Braked at 70 mph, 3 Runs at a Minimum of 50 Minutes Each Run.....	75
Figure 67. Residual Stress Comparison between Finite Element Analysis and Ultrasonic Measurements using PET and EMATs for Evaluating Induction Heated Railroad Wheels.....	77
Figure 68. Residual Stress Comparison between the Finite Element Analysis Heat Model and Ultrasonic Measurements using PET and EMATs with a -80 MPa Offset to Compensate for Stresses Generated during Manufacturing	77
Figure 69. Residual Stress Comparison between the Finite Element Analysis Saw Cut Displacement Model and Ultrasonic Measurements using PET and EMATs	78
Figure 70. Ultrasonic Measurement to Finite Element Analysis Comparison of Induction Heated Railroad Wheels.....	81
Figure 71. Comparison of Test Results obtained from Destructive and Non-Destructive Evaluation of Drag Braked Railroad Wheels	81

List of Tables

Table 1.	CH36, Class C Wheels Evaluated during Testing.....	8
Table 2.	Induction Heating Parameters for the Eight Test Wheels	11
Table 3.	CH36, Class C, Drag Braked Wheels	16
Table 4.	Acoustic Birefringence System Comparisons	21
Table 5.	PET and EMAT Ultrasonic Front Rim Phase Averaged Birefringence ($\times 10^{-4}$) (MPa) at Each Riser Location.....	34
Table 6.	PET and EMAT Ultrasonic Birefringence ($\times 10^{-4}$) Front Rim Face Measurements.....	47
Table 7.	PET and EMAT Ultrasonic Front Rim Phase Averaged Stress Values in MPA at Each Riser Location.....	49
Table 8.	PET and EMAT Ultrasonic Front Rim Phase Averaged Stress Values.....	61
Table 9.	Saw Cut Depth to Displacement Measurements for Railroad Wheels Drag Braked at 75 hp and 60 mph	64
Table 10.	Saw Cut Depth to Displacement Measurements for Railroad Wheels Drag Braked at 80 hp and 60 mph	66
Table 11.	Saw Cut Depth to Displacement Measurements for Railroad Wheels Drag Braked at 85 hp and 60 mph	67
Table 12.	Saw Cut Depth to Displacement Measurements for Railroad Wheels Drag Braked at 85 hp and 60 mph	68
Table 13.	Saw Cut Depth to Displacement Measurements for Railroad Wheels Drag Braked at 90 hp and 60 mph	69
Table 14.	Saw Cut Depth to Displacement Measurements for a Railroad Wheel Drag Braked at 100 hp and 70 mph.....	70
Table 15.	Saw Cut Depth to Displacement Measurements for Railroad Wheels in the As-Manufactured and Induction Heated (45 kW (60 hp)) Conditions ...	71
Table 16.	Saw Cut Depth to Displacement Measurements at a Cut Depth of 2 inches on As-Manufactured, Induction Heated and Drag Braked Railroad Wheels	73
Table 17.	Average Hoop Stress as Generated by the FEA Heat Model.....	76
Table 18.	Average Hoop Stress as Generated by the Saw Cut Displacement Model.....	78

1.0 BACKGROUND

In order for thermal failure to occur in a railway wheel, three conditions must be present. First, a thermal crack must be present on the rim of the wheel. Second, a residual tensile stress must be present to permit crack opening. And third, the wheel must be subjected to a set of alternating loads to advance the thermal crack until it reaches a critical size and fracture occurs. If any of the preceding three conditions are missing, failure will not occur.

Currently, thermal cracks are visually inspected as a normal part of terminal inspection. However, there exists no reliable non-destructive method for determining the state or magnitude of residual stress.

Residual stresses develop in a railroad wheel when the wheel is subject to inelastic deformation. When a wheel is heat treated, the heat treating process creates a circumferential compressive stress in the rim of the wheel. To create the residual compressive rim stress, the wheel is first heated uniformly. Heating the wheel uniformly causes all parts of the wheel to expand uniformly. If the wheel were cooled uniformly, there would be no change in the residual stresses in the cooled wheel.

The heat treatment process, however, cools the rim of the wheel much faster than the plate of the wheel. The rim is sprayed with water (rim quenched). The water cools the rim and as the rim cools, it contracts. The plate of the wheel, however, has not been cooled as rapidly and does not contract at the same rate as the rim. The radial stresses caused by the rim contracting and the plate, to which it is securely attached, not contracting, eventually exceed the yield point of the steel and the wheel suffers inelastic deformation. In this case, the hot plate is deformed in the radial direction to reduce its radius and thus relieve the radial stresses caused by the contracting cooled rim. When the plate itself cools it also contracts. The contracting plate is securely attached to the now cooled rim. The contraction of the deformed (smaller radius) plate causes radial tensile stresses to develop between the cool plate and the cool rim. In

addition to causing a radial tensile stress in the plate and the rim, the mismatch between the two causes the rim to go into compression. In summary, a residual compressive rim stress is created when an inelastic deformation makes the cool rim too large for the cool plate if both were in an unstressed condition. Radial tensile stresses between the plate and the rim and circumferential compressive stresses in the rim result from the fact that the two mismatched geometries of the wheel are securely attached. Most important is that the compressive stress imparted by rim quenching prevents crack opening and thus crack growth.

The mechanism also works the other way so that when the rim is heated it expands. The rim's expansion is resisted by the cool plate causing radial tensile stresses between the rim and the plate. If the rim is heated sufficiently between the rim and the plate, the radial tensile stresses will exceed the yield point of the steel and the rim will be inelastically (permanently) deformed. The hot rim, when cooled, will become smaller in radius, thereby reducing the tensile stresses between the hot rim and the cool plate.

However, when the rim cools it contracts. Because of the inelastic deformation that occurred when the rim was hot, as the deformed rim cools and contracts it becomes too small to fit on the plate when both are cool and in an unstressed state. Since the rim and plate are securely attached, a radial compressive stress develops between them making the plate smaller in radius thus creating a circumferential tensile stress in the rim of the wheel. This phenomenon forces the rim to become larger in radius to accommodate the fit with the plate. In summary, a residual tensile rim stress is caused when the wheel is deformed in such a way as to make the cool unstressed rim too small for the cool unstressed plate. By implementing a cost effective nondestructive test method to measure the state of stress in railroad wheels, thermal failures can be

A qualitative method for determining the state of rim residual stresses was accomplished by making a radial saw cut starting at the flange tip. If the saw cut opened, the rim had a net residual circumferential tensile stress. Jones³ improved this method by attaching a clip gage across the cut and a string potentiometer to the saw carriage. The outputs of the clip gage and the potentiometer are input into an X-Y recorder to yield a plot of opening versus distance. A new rim-quenched wheel will produce a plot typical of that shown in Figure 2 while a thermally damaged wheel, that has produced a net tensile stress will have a plot as shown in Figure 3.⁴

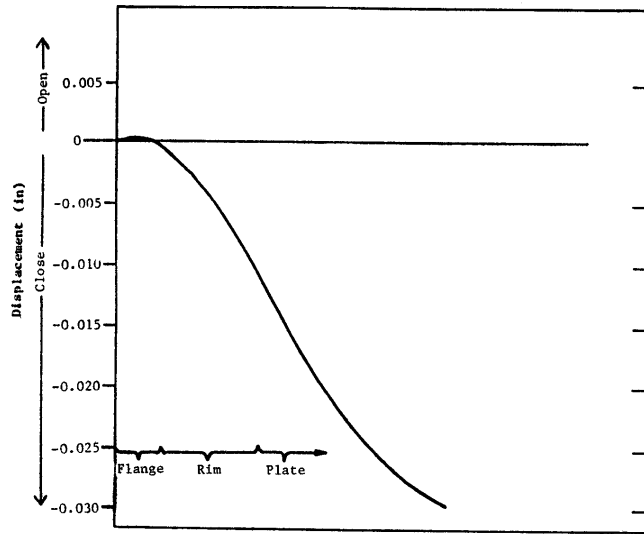


Figure 2. Typical Saw Cut Displacement Behavior of a New or Undamaged Rim-Quenched Wheel

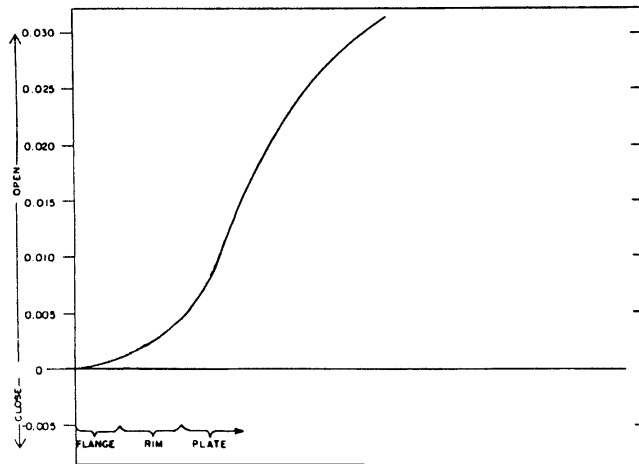


Figure 3. Typical Saw Cut Displacement Behavior of a Thermally Damaged Wheel

A good estimate of the distribution and magnitude of the residual stresses in a wheel can be obtained from a three dimensional finite element calculation using the displacement data along the length of the cut.⁵ The wheel with the saw cut is represented by a finite element mesh with displacements imposed on the free surface of the cut which are sufficient to restore it to the original state. The resulting stresses calculated on the free surface represent the original residual stress state within the

wheel. Figure 4 shows an example of such a calculation. Notice that the residual stress is not uniform across the rim and that both tensile and compressive stresses are present.

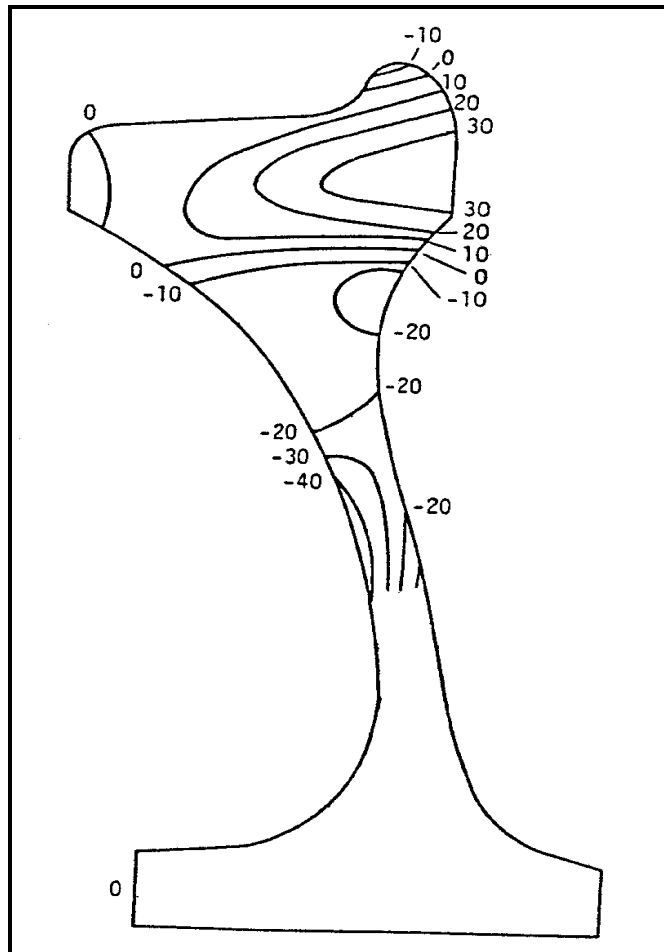


Figure 4. Calculated Distribution of Circumferential Residual Stresses (ksi) in a Thermally Damaged Wheel

Many attempts have been made to develop nondestructive methods to determine the residual stress state in wheels. Two approaches have been the principal methods of investigation. The first methods attempted used ultrasonic birefringence, and magnetics to include Barkhausen methods. Bray and his coworkers attempted to employ ultrasonic birefringence to residual stresses in rails in the early 1970's, but encountered difficulties when measuring wheel stresses due to the non uniformity of

the wheel microstructure and the difficulty of measuring a second order effect with the equipment available at the time.⁶

Concurrently, researchers at Southwest Research Institute began the evaluation of Barkhausen techniques to determine the residual stress state in wheels. The Barkhausen method measures the noise of magnetic domain wall shift as a magnetic field is applied. The method relies on the dependence of domain alignment on the existing stress state. The research was continued through 1987 in cooperation with the Burlington Northern Railroad, but it was found that the technique had to be calibrated for each manufacturer, wheel size, and heat-treatment.⁷ In 1992 Australian researchers reported the adaptation of a magnetomechanical system for determining wheel residual stresses.⁸ However, application of this method on various Australian rail systems concluded that while the magnetomechanical system showed promise, it was not ready to be used as a stand-alone system.⁹

However, ultrasonic birefringence has been established as the principal technique for application to nondestructive residual stress determination in the railroad industry (where birefringence is the relative change in sound velocity when the polarization direction rotates). Researchers in Japan have applied the technique to railroad wheels and found good correlation between stress and ultrasonic velocity when texture is taken into account in wrought wheels.¹⁰ German researchers have employed the technique to separate wheels with minor thermal damage to those with dangerous levels of residual stress.¹¹ French engineers are applying the technique as a production tool to ensure the proper stress state in wheels after heat-treatment.¹² And the Polish Academy of Sciences has developed a commercial system, the DEBRO unit, which has successfully evaluated the residual stresses in roller-straightened rails.¹³ Concurrent with the above developments, workers at NIST have been applying ultrasonic birefringence to obtain a more qualitative evaluation of the state of stress in wheels which is the subject of this report.

2.0 OBJECTIVE

The objective of this project was to evaluate the accuracy and reliability of the prototype residual stress measurement system developed by the National Institute of Standards and Technology (NIST), Boulder, Colorado. The electromagnetic acoustic transducer (EMAT) system, developed by NIST, was used to access the residual stress state of as-manufactured, induction heated, and drag braked railroad wheels.

3.0 PROCEDURES

The current phase of the Wheel Residual Stress Detection Program began in December 1994. The accuracy of the EMAT system was assessed by comparing EMAT ultrasonic measurements with ultrasonic measurements taken with the DEBRO-30. Developed by the Polish Academy of Sciences, the DEBRO-30 is an ultrasonic system, that uses piezoelectric transducer (PET) techniques. It is available for use commercially in Europe to determine residual stress in wrought railroad wheels. The residual stress measurements recorded by the two systems were compared to Finite Element Analysis (FEA) models developed at the TTC. The FEA models were developed by employing temperature dependant material properties for Class C wheel steel, provided by the wheel manufacturer (Griffin Wheel Company), to estimate residual stress distributions for induction heated wheels. The FEA was also used to perform an “unsawcutting”;i.e., reconstructing the wheel, using saw cut data compiled by Concurrent Technologies Corporation (CTC) in Johnstown, Pennsylvania, Griffin Wheel Company and the Transportation Technology Center, Pueblo, Colorado.

3.1 TEST PARAMETERS

There were 30 wheels tested, 2 of which remained in the as-manufactured condition, 8 were induction heated and 20 were drag braked. The induction heating and drag braking, performed to induce thermal damage into the railroad wheels, were accomplished at Griffin Wheel Company’s Technical Center in Bensenville, Illinois.

Ultrasonic measurements were made prior to and after inducing thermal damage into the wheels. The measurements were performed at Griffin Wheel Company and at NIST. The ultrasonic measurements were taken by researchers from NIST (EMAT), a guest researcher on leave from the Institute of Fundamental Technological Research, Polish Academy of Sciences, Warsaw, Poland (PET), and a representative from the AAR/TTC (EMAT).

3.2 TEST WHEELS

Table 1 identifies the serial numbers and conditions of the test wheels. There were three rim block specimens stress relieved and used as calibration samples for the test wheels. The rim block samples were stress relieved in accordance with parameters outlined by Griffin Wheel Company.

The calibration blocks were loaded into a pit furnace and the temperature of the furnace was raised to 800 degrees Fahrenheit (F) within 3 hours. The blocks were then soaked at 800 degrees F for 24 hours. At the completion of the soaking period, the furnace was turned off and the furnace covers opened. The rim blocks were then pit cooled for approximately 24 hours.

Table 1. CH36, Class C Wheels Evaluated during Testing

WHEEL IDENTIFICATION	WHEEL CONDITION
26508, 26512	As Manufactured
26515, 26529, 26506, 26520, 26522, 26513, 26524, 26526	Induction Heated
91768, 91817, 91807, 91813, 91778, 84967, 91784, 91777, 91847, 91843, 84972, 84758, 80887, 86398, 76896, 76933, 83991, 63764, 80582, 80742	Drag Braked

3.3 INDUCTION HEATING

The induction heating was performed at Griffin Wheel Company's Technical Center with each wheel supported by the hub with the back rim face oriented towards the floor. The induction heating coil was installed on the rim of the wheel with the wheel centered within the coil. Figure 5 shows the coil configuration for the induction heating setup. The wheel was then marked at 3-inch increments along the radius, starting at the hub and moving towards the flange, using a heat resistant marker as shown in Figure 6. Temperature data was collected using an infrared thermometer. Temperatures were collected at 10-minute intervals during the induction heating process. The axial wheel plate deflection was measured at the rim of the wheel. The maximum axial wheel plate deflection was recorded with any permanent axial deflection noted. During induction heating the induction coil voltage and current amplitude were monitored to ensure uniform heating. The duration of the heating procedure was controlled to the nearest 0.5 minute to ensure uniform heating conditions. The induction heated wheels were heated in accordance with the parameters identified in Table 2.



Figure 5. Photograph of Coil Configuration for the Induction Heating Setup

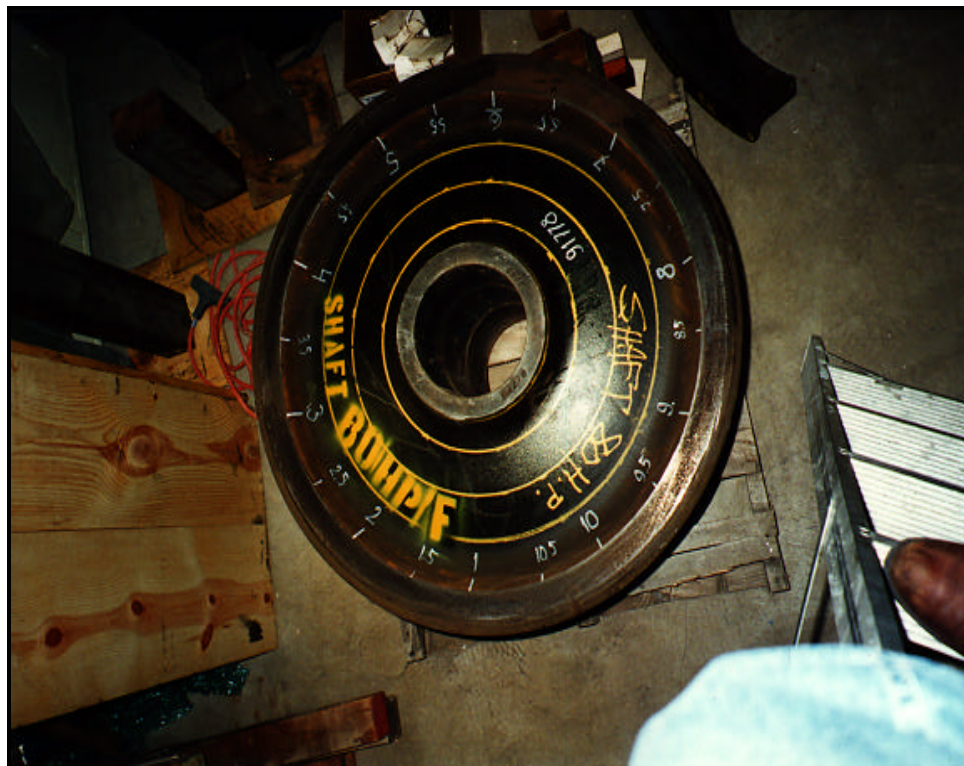


Figure 6. Wheel Markings Identifying the Wheel at 3-inch Increments Around the Radius

Table 2. Induction Heating Parameters For The Eight Test Wheels

Wheel Identification	Induction Heater Power Level (Kilowatts (hp))	Heating Duration (Minutes)
26515	38 (51)	30
26529	38 (51)	30
26506	42 (56)	30
26520	42 (56)	30
26522	42 (56)	30
26513	45 (60)	30
26524	45 (60)	30
26526	45 (60)	30

3.4 DRAG BRAKING

Drag braking was performed at Griffin Wheel Company's Technical Center on a wheel/rail dynamometer designed and constructed by Griffin Wheel Company (Figure 7). The dynamometer design consists of an inverted standard truck with a wheel set machined to a rail configuration. A second truck and wheel set is placed on the inverted truck which simulates the interaction between the wheel and the rail as shown in Figure 8. The normal load between the two trucks was approximately 25,000 pounds. The axle of the inverted truck is permanently mounted to a drive motor which can be set at various speeds. A combination of load cells are attached to the dynamometer to provide the proper simulation of center or flange crowded drag braking scenarios as shown in Figure 9. The brake shoe to wheel tread orientation can be seen in Figure 10.

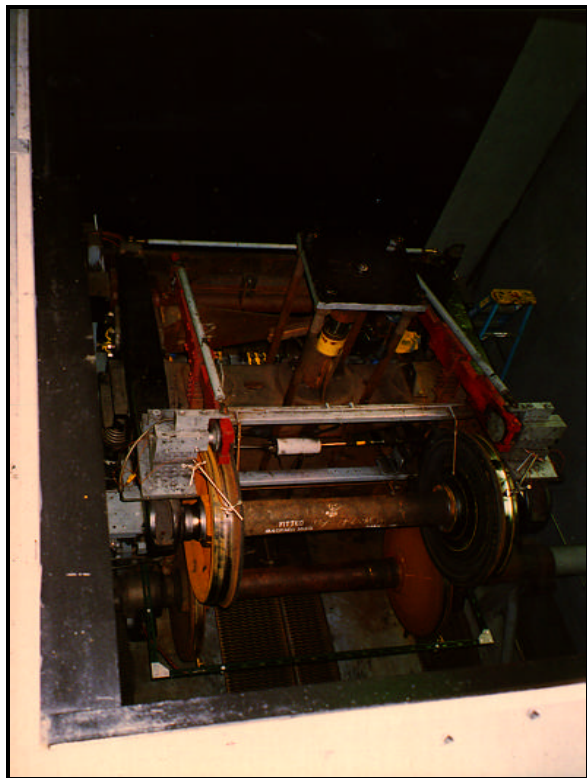


Figure 7. Wheel to Rail Dynamometer at Griffin Wheel Company

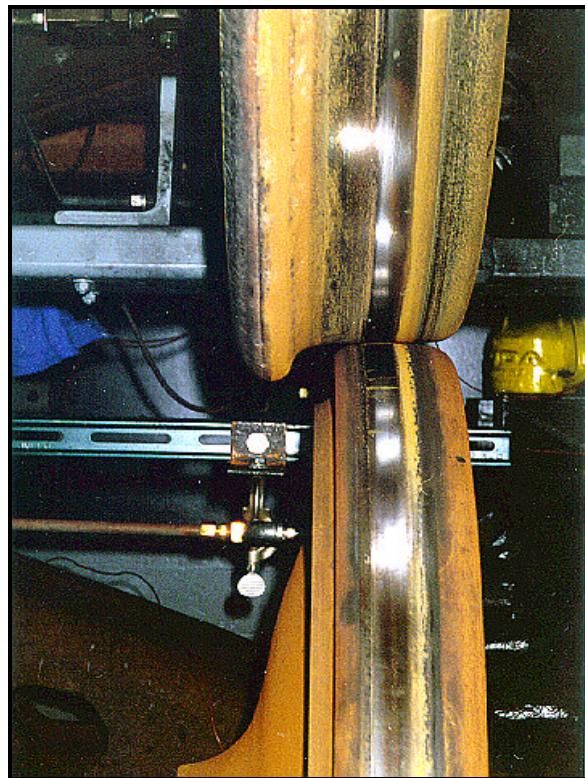


Figure 8. Wheel to Rail Contact With the Griffin Wheel Dynamometer

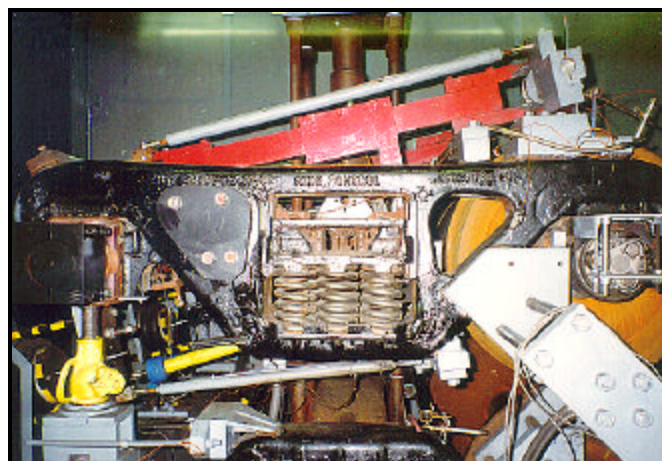


Figure 9. Wheel to Rail Dynamometer Load Cell Arrangement Designed for Simulating Centered and Flange Crowded Brake Shoe Conditions

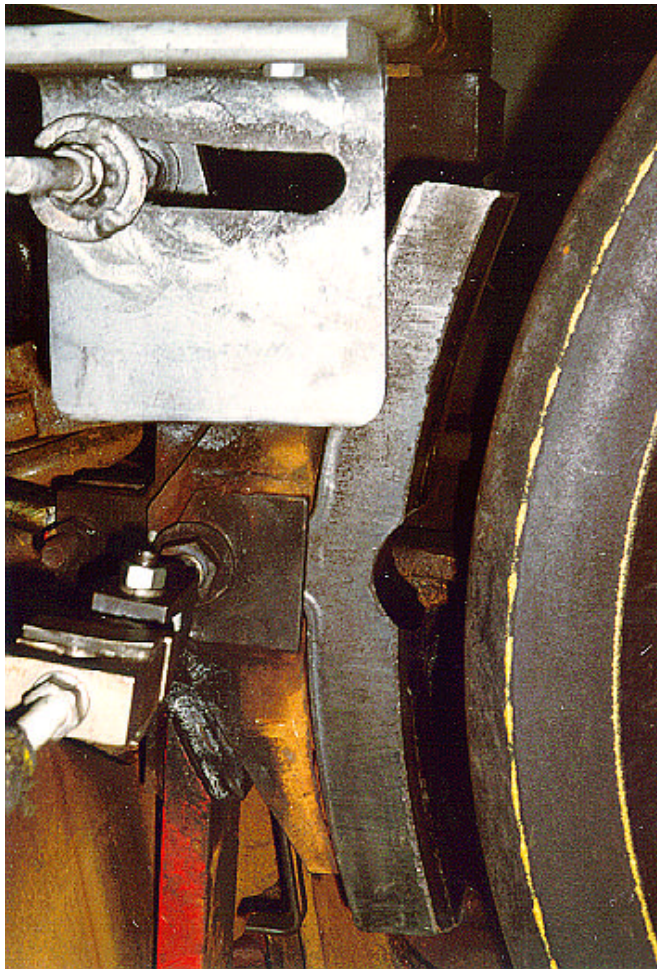


Figure 10. Brake Shoe to Wheel Tread Orientation

The dynamometer and test wheel sets were instrumented to provide the following information for both the shaft and end wheels with measurement intervals set at 5 seconds.

Wheel sets were scheduled to undergo drag braking in three 30-minute cycles to provide uniform thermal damage. The 30-minute cycle was not reached on some of the drag braking runs due to brake shoe deterioration. Figure 11 shows an example of brake shoe deterioration during the 90 horsepower (hp) runs with the brake shoe centered. Two of the 90 hp runs made it to a full 30 minutes but as seen in the

photograph one of the runs was stopped at 22 minutes due to deterioration and metal to metal contact.

After the 90 hp runs, an effort was made to minimize the effect from brake shoe deterioration by performing a pre-test brake shoe conditioning. Prior to actual test runs, the shoes were drag braked for 30 minutes at 45 hp. Figures 12 and 13 show front and side view comparisons of brake shoes which were not conditioned and shoes that were conditioned prior to drag braking. As seen in the photographs, the conditioned brake shoes held up better during drag braking. Brake shoes used during flange crowded runs were ground at the side in contact with the wheel flange corner to provide a matching profile for better contact in that area. Table 3 lists the horsepower, operating speed, drag braking duration, and brake shoe position for each railroad wheel drag braked.

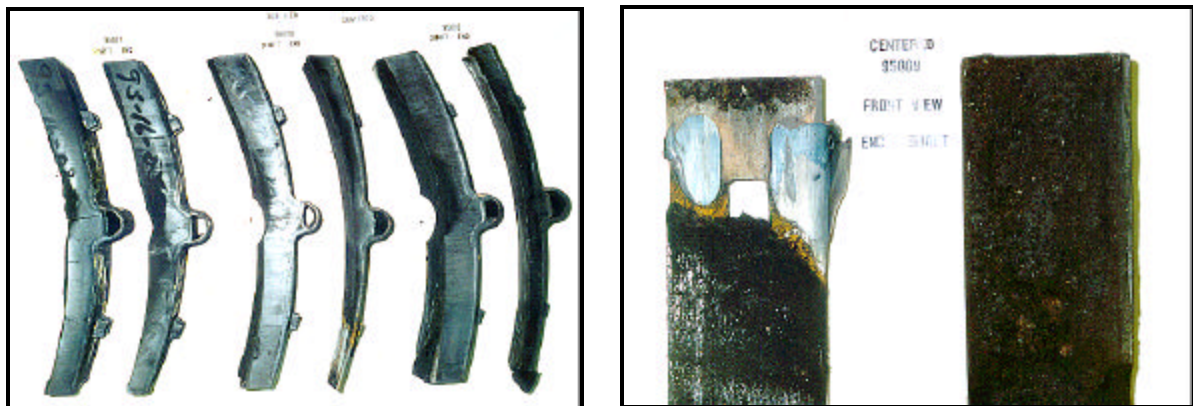


Figure 11. Brake Shoe Deterioration during Drag Braking at 90 Hp with the Brake Shoe Centered. (Left) Side View of the Brake Shoes after Drag Braking. (Right) Front View of the Brake Shoes Used during the 22-Minute Run Showing Shoe Deterioration to the Metal Backing Plate

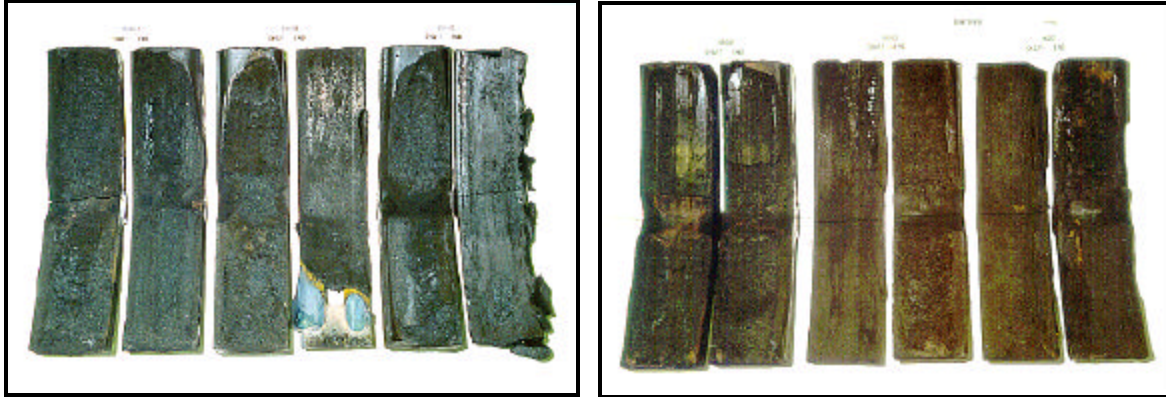


Figure 12. Front View Comparison of Non-conditioned and Conditioned Brake Shoes used during 90 and 100 hp Drag Braking Runs. (Left) 90 hp Non-Conditioned Brake Shoes (right) 100 hp Conditioned Brake Shoes

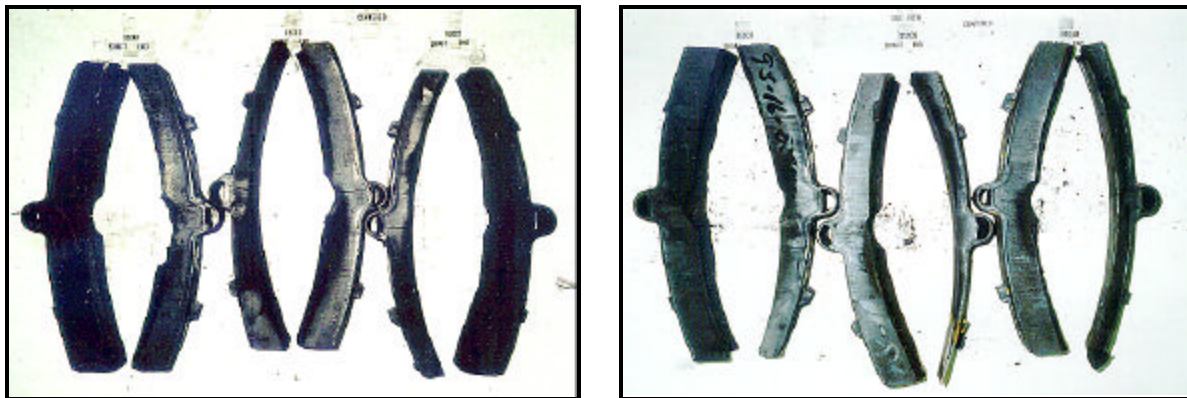


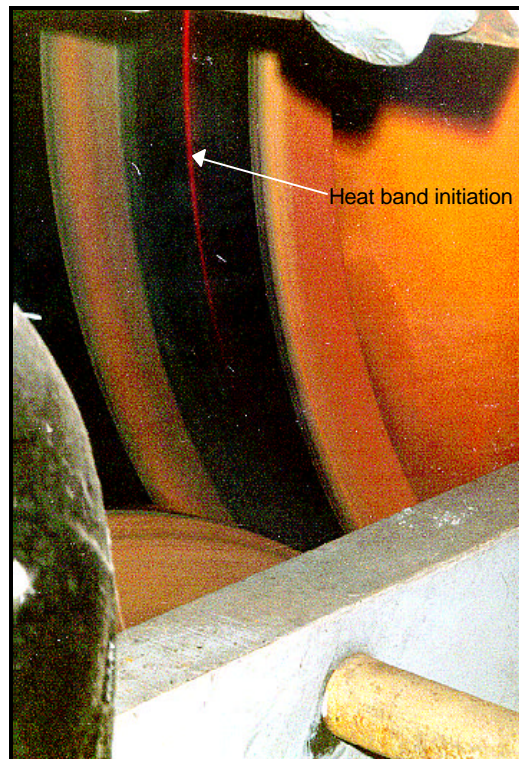
Figure 13. Side View Comparison of Non-Conditioned and Conditioned Brake Shoes Used during 90 and 100 Hp Drag Braking Runs. (Left) 90 Hp Non-Conditioned Brake Shoes. (Right) 100 Hp Conditioned Brake Shoes

Table 3. CH36, Class C, Drag Braked Wheels

Wheel Identification	Power Input Kilowatts (hp)	Operating Speed (mph)	Drag Braking Duration (Minutes)	Brake Shoe Position
91768	56 (75)	60	3 x 30	flange
91817	56 (75)	60	3 x 30	flange
91807	60 (80)	60	3 x 30	center
91813	60 (80)	60	3 x 30	center
91778	60 (80)	60	3 x 30	flange
84967	60 (80)	60	3 x 30	flange
91784	63 (85)	60	3 x 30	center
91777	63 (85)	60	3 x 30	center
91847	63 (85)	60	3 x 30	flange
91843	63 (85)	60	3 x 30	flange
84972	63 (85)	70	1 x 47.5 + 1 x 44	center
84758	63 (85)	70	1 x 47.5 + 1 x 44	center
80667	63 (85)	70	1 x 50, 1 x 56 + 1 x 60	flange
86398	63 (85)	70	1 x 50, 1 x 56 + 1 x 60	flange
76896	67 (90)	60	2 x 30 + 1 x 22	center
76933	67 (90)	60	2 x 30 + 1 x 22	center
83991	67 (90)	60	3 x 30	flange
63764	67 (90)	60	3 x 30	flange
80582	75 (100)	70	1 x 27, 1 x 45 + 1 x 29	center
80742	75 (100)	70	1 x 27, 1 x 45 + 1 x 29	center

Tread temperatures of approximately 1100-degrees Fahrenheit were reached during drag braking cycles. Heat bands at the wheel tread were especially apparent during the higher horsepower runs. Figures 14 and 15 show the beginning of the heat band and the full heat band across the wheel tread during the 85 hp center positioned drag braking run at 70 mph. The full heat band was developed at about 24 minutes into a 44 minute run.

At the completion of each drag braking cycle the railroad wheels were air cooled until the tread temperature had dropped to 500-degrees F or below. Once the wheels had cooled to 500-degrees Fahrenheit, they were further cooled to room temperature using a water spray as shown in Figure 16.



**Figure 14. Heat Band Origination
During Drag Braking**



Figure 15. Full Heat Band Across the Wheel Tread During Drag Braking

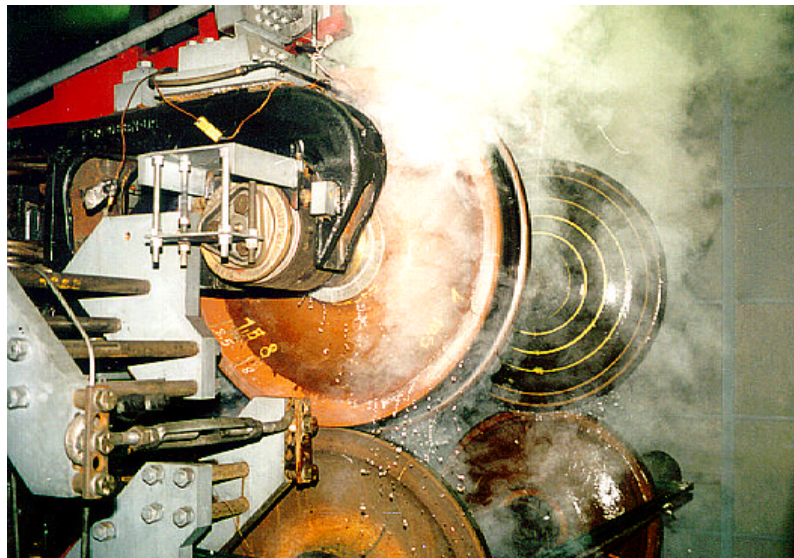


Figure 16. Water Spray of Drag Braked Wheels

3.5 WHEEL RESIDUAL STRESS MEASUREMENTS

A residual stress measurement was made at approximately 20 locations for each test wheel. The measurement locations correlated to 10 casting risers on the wheels and the midpoint between the risers. Figure 17 shows the approximate ultrasonic measurement locations for the railroad wheels. Measurements were taken using two ultrasonic systems; one system uses PET while the other uses EMAT. Figure 18 shows the transducer location at the front rim face and the wave direction during inspection. The amount of hoop residual stress was determined using through thickness birefringence measurements taken with the PET and EMAT systems. The birefringence data generated with the two ultrasonic systems was converted through thickness average stress using the measured birefringence's due to texture from the stress relieved rim block samples and the following relationship as derived by NIST.¹⁵

$$\Phi_2 = (B - B_{\equiv}) / C_A$$

where:

Φ_2	=	Through thickness average stress
B	=	Total birefringence
B_{\equiv}	=	Birefringence due to texture
C_A	=	Stress acoustic constant for shear waves traveling normal to the stress field



Figure 17. Ultrasonic Measurement Locations from the Front Rim Face of the Railroad Wheels

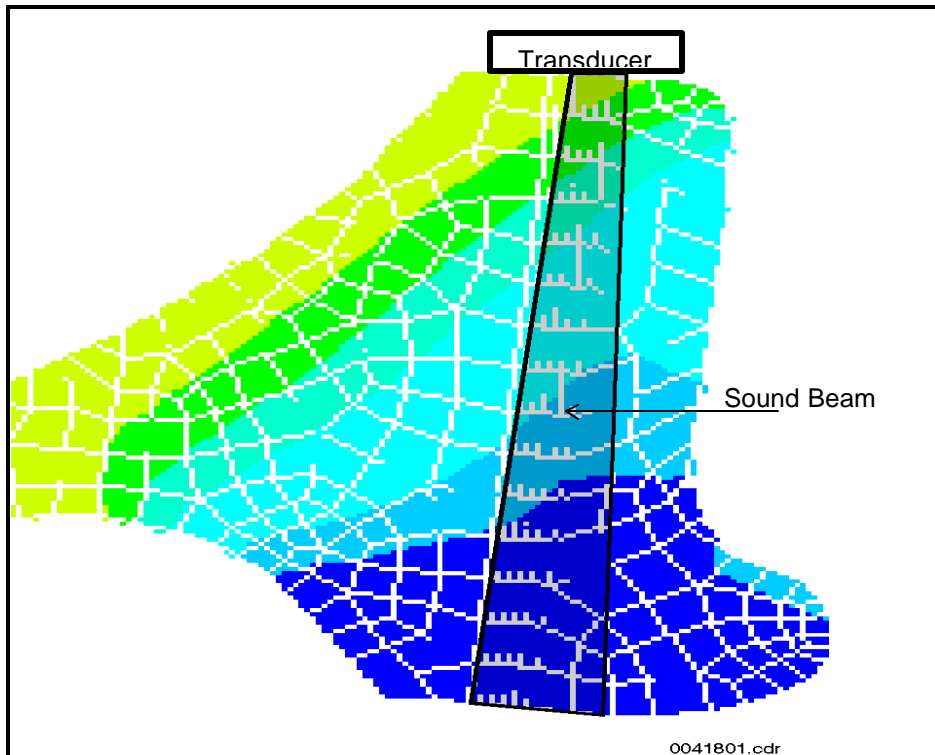


Figure 18. Transducer Location on the Front Rim Face and Direction of Wave Propagation During Ultrasonic Inspection of Railroad Wheels

When using standard piezoelectric transducers, a couplant (usually a liquid) is required to permit transmission of the ultrasonic signal into the material being evaluated. The EMAT system is electromagnetically coupled eliminating the need for a liquid couplant. The geometry of the beam spread differed slightly due to the difference in transducer window sizes and design with the EMAT system, providing less beam spread. This phenomenon may contribute to differences in stress readings. The difference in arrival time monitoring is primarily due to the PET system minimizing influences from variations in couplant thickness and surface roughness, which is accomplished by monitoring the arrival times between the first and second echoes. System comparisons performed by NIST are listed in Table 4.¹⁴

Table 4. Acoustic Birefringence System Comparisons

Parameter	PET	EMAT
Couplant Required	yes	no
Window Size	12mm x 12mm	10mm x 10mm
Measured Parameter	difference in 1 st and 2 nd arrival times	1 st echo arrival time
Timing Marker	manual, on peak	digital gate, on zero crossing
Measurement Location	1 st cycle	mid-pulse (usually)
Bandwidth	wide	narrow
Pulse Length	short	long
Transducer	Manually rotated for 2 polarizations	Automatic coil switching for 2 polarizations

Although the two systems are based on the same underlying laws of physics NIST has again stated that the measurements for this evaluation were made with two distinct systems designed to generate and detect ultrasonic waves.¹⁴

1. A piezoelectric transducer (PET). This transducer design represents the more conventional approach to ultrasonic evaluation. A small section of piezoelectric material is electrically shocked into mechanical resonance. The vibrations pass through a face plate and fluid couplant into the specimen. The return signal reverses this process.
2. An electromagnetic acoustic transducer (EMAT). This transducer is becoming more common with increasing availability of compatible electronics. It contains a wire coil and a magnet. A radio-frequency electrical pulse through the coil generates eddy currents into the specimen surface; the eddy currents interact with the magnetic field to produce mechanical vibrations of sound.

As mentioned previously, the PET system is commercially available and is currently used in some European applications.¹⁷ Both the PET and EMAT systems, built by NIST, use shear horizontal waves traveling through the rim thickness (giving the thickness averaged stress). Figures 19 and 20 show the PET and EMAT systems used during this project.



Figure 19. DEBRO-30 Ultrasonic Measurement System Using PET

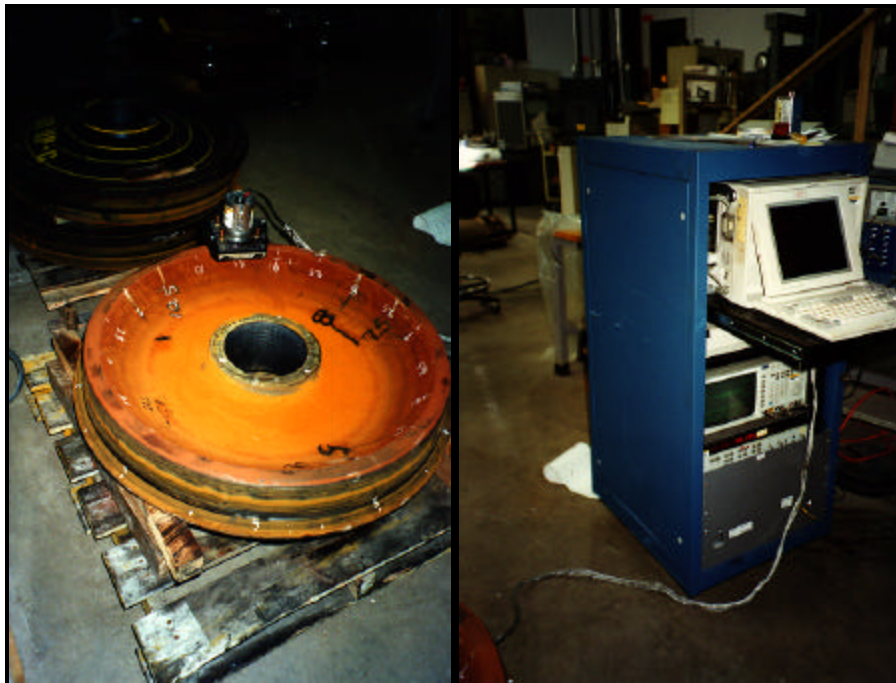


Figure 20. NIST Ultrasonic Measurement System Using EMAT. The EMAT is on the Left and the Control Console is on the Right

The front rim face (frf) birefringence measurements taken with both systems use the pulse-echo method of evaluation where one transducer is used for both transmitting and receiving ultrasonic signals. The transducer location for measurements from the frf was approximately midpoint of the frf. The PET system requires that the operator determine this location whereas the EMAT system finds this position automatically with the apparatus used to hold the transducer. Figure 21 shows the transducer location for both the PET and EMAT systems at the frf. The operation of these ultrasonic systems currently require some technical expertise to both produce the required settings and perform accurate evaluation of the data. Both system designs are being modified to reduce the amount of operator involvement to perform reliable evaluation.

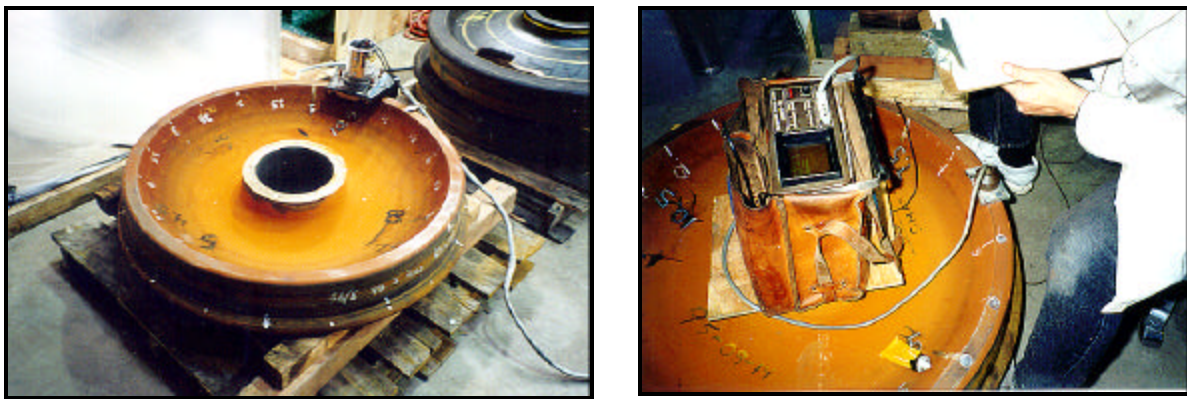


Figure 21. Transducer Locations for the PET and EMAT Ultrasonic Measurement Systems

3.6 STANDARD SAW CUTTING

Standard saw cutting was performed on two as-manufactured, two induction heated and eighteen drag braked railroad wheels. The saw cutting was accomplished at Griffin Wheel Company with cut locations determined from ultrasonic measurement data showing either areas of high compressive or tensile stress obtained after inducing thermal damage into the wheels. There were two areas cut on each of the wheels as shown in Figure 22.

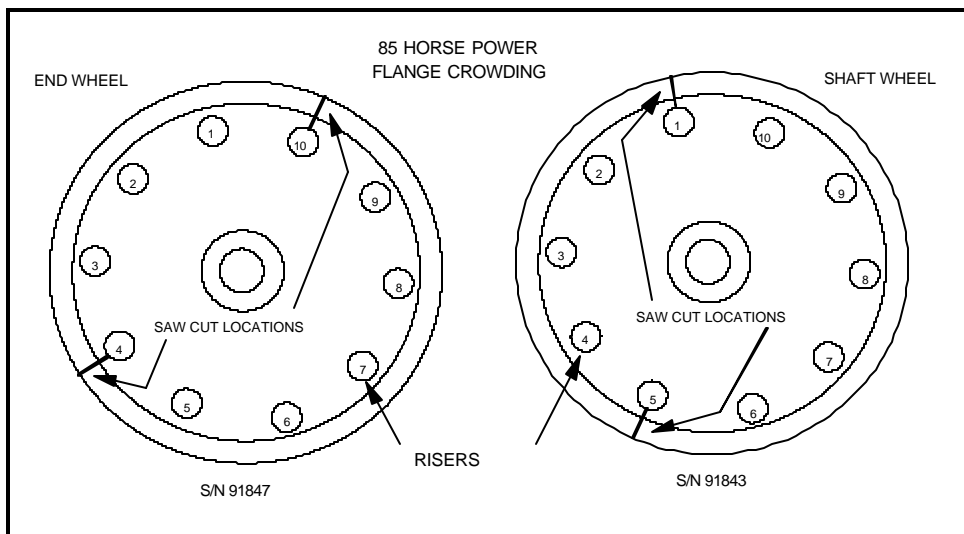


Figure 22. 85 hp Flange Crowded Wheels Showing Saw Cut Locations and Risers

The saw cutting was performed by placing the wheel on the bandsaw transfer table with the front rim face of the wheel oriented opposite the table surface. The surface of the flange tip was ground flat and two mounting blocks were attached to the wheel using an epoxy adhesive. A clip gage extensometer was installed on the mounting blocks to monitor saw cut circumferential displacement at the flange tip of the wheel. The wheels were cut approximately 5 inches deep using a band saw with a feed force of 60 pounds. The saw cut circumferential displacement and radial depth data was collected. Figure 23 shows the saw cut set up at Griffin Wheel.



Figure 23. Standard Saw Cutting at Griffin Wheel.
Extensometer Position on Left and Saw Cut Position on Right

3.7 PRECISION SAW CUTTING

Precision saw cutting was performed on two of the drag braked wheels. The saw cutting was performed at and by Concurrent Technologies Corporation (CTC) in Johnstown, Pennsylvania, who developed an approach utilizing various methods of interferometry to evaluate the radial and hoop displacement distribution along a saw cut. By combining high sensitivity Moiré interferometry with Michelson interferometry, full field information about the distribution of displacements around a saw cut notch on both flat surfaces of the rim of the wheel is provided.¹⁶ Figures 24 and 25 show the precision saw cutting set up at CTC. CTC estimates the precision of the displacement measurement to be better than 100 nanometers. Additional instrumentation and gauging is used to provide information about the absolute displacements of the points on the rim with respect to the center of the wheel and strains in selected locations.

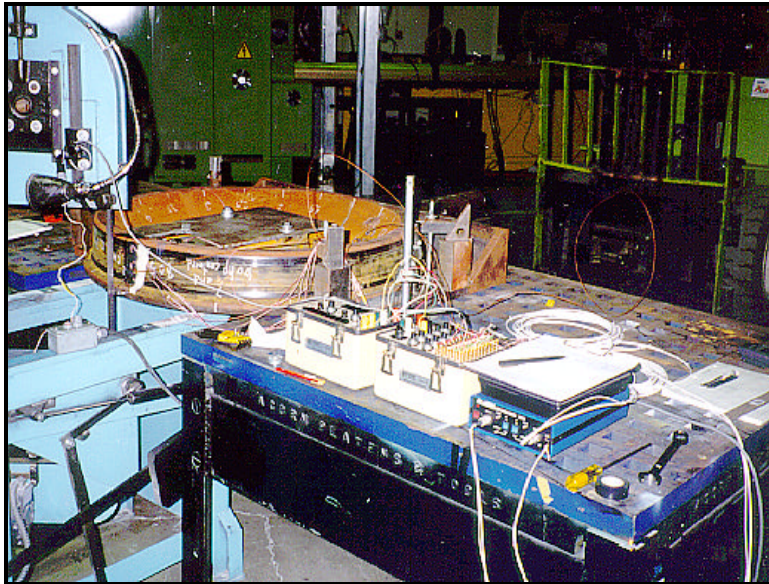


Figure 24. Precision Saw Cut Instrumentation Setup at CTC

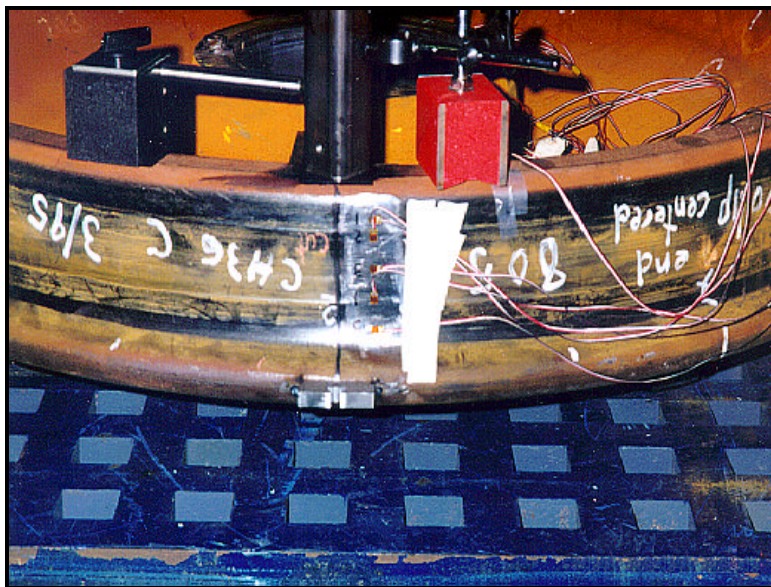


Figure 25. Strain Gage Setup Across the Tread of the Wheel at CTC

The resulting fringe patterns from the interferometry are generated as contour maps of the measured displacements. The in-plane displacement fields are recorded with Moiré interferometry while the out-of-plane fields are captured with the Michelson technique. Photographs of the interferometry setup for these techniques are shown in Figure 26. The fringe patterns are converted to contour maps of strains and if the material properties are known stresses can also be shown. The form of interferometry used by CTC is a cross between holography and the traditional Moiré method. The method contains all the sensitivity of holography while providing interpretation of interferograms typical for Moiré methods.

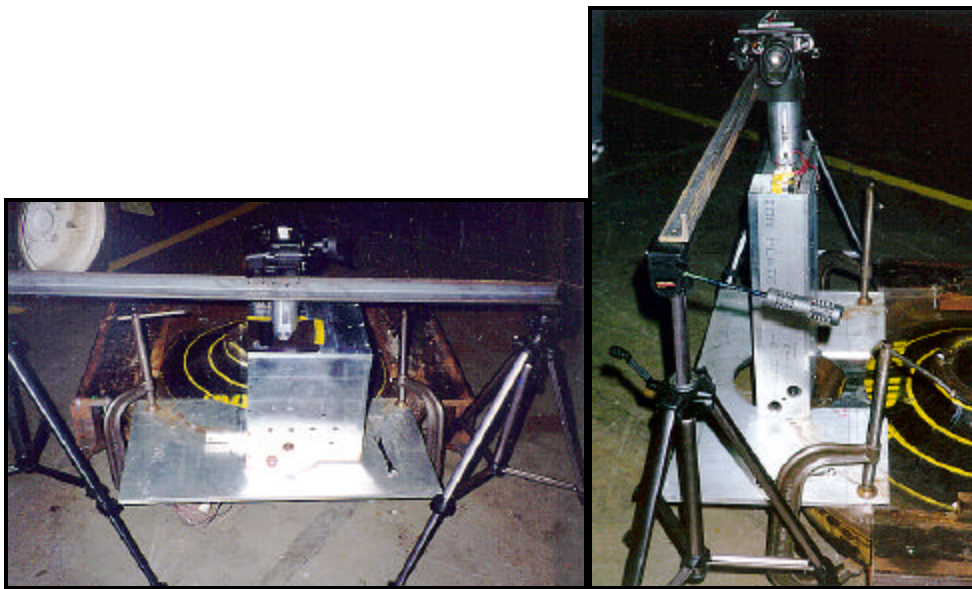


Figure 26. Interferometer Setups at CTC. Moire Interferometer on the Left and Michelson Interferometer on the Right

3.8 FINITE ELEMENT ANALYSIS

A finite element analysis (FEA) was used to obtain analytical results of wheel residual hoop stress for comparison to the nondestructive test (NDT) measurements. The FEA consists of two analyses. The first is the induction heat analysis, which simulates the induction heating of the wheels during the tests and calculates the resulting residual hoop stress directly. The second is the saw cut analysis, which calculates residual hoop

stress using saw cut opening displacement data measured at TTC on wheels saw cut at both Griffin Wheel Company and Concurrent Technologies Corporation.

3.8.1 Induction Heat Finite Element Analysis

The objective of the induction heat FEA is to calculate the wheel residual hoop stress caused by induction heating the wheel tread. The steps in constructing the induction heat FEA are specifying wheel geometry, wheel mesh and element types, material properties, and boundary conditions. The wheel geometry, provided by Griffin Wheel Company, is a CC38 2W wheel with AAR-1B tread profile. The wheel is a 2-D axis-symmetric model with the axle as the axis of symmetry. The mesh consists of 4- node rectangular plane elements in the NDT zone and 3-node triangle elements in the remaining area. The wheel material properties, which were provided by Griffin Wheel Company, are assumed to be homogeneous, isotropic, and temperature dependent.

The boundary conditions consist of applying heat to the tread nodes for 30 minutes and allowing the wheel to cool for 5 hours. This is accomplished for three different values of heat input (51, 56, and 60 hp) to simulate the actual tests that were conducted (see Figures 27, 28 and 29). Air convection boundary conditions are specified for wheel surface nodes not having heat applied. It should be noted that the FEA wheels start in the annealed condition (i.e. zero residual stress), whereas manufactured wheels initially have compressive residual stresses. However, the FEA results can still be compared to the test results if the FEA results are viewed as a change in residual hoop stress and not necessarily the absolute residual hoop stress in the wheel.

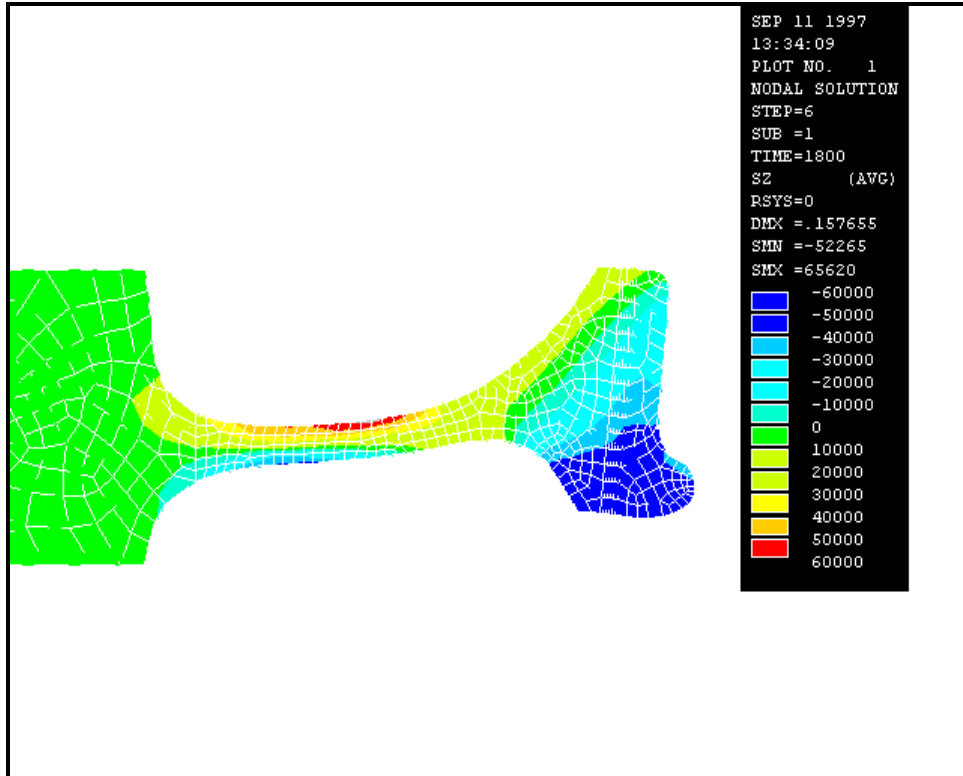


Figure 27. Finite Element Analysis of a Test Wheel Induction Heated at 38 kW (51 Hp) for 30 Minutes and Air Cooled for 5 Hours

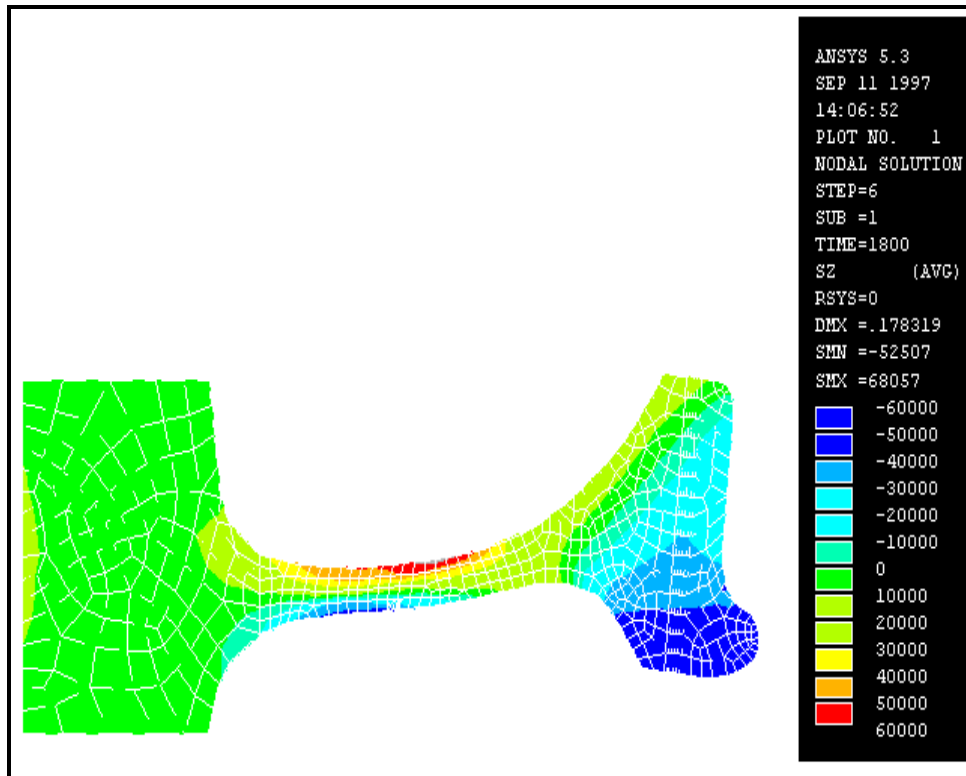


Figure 28. Finite Element Analysis of a Test Wheel Induction Heated at 42 kW (56 Hp) for 30 Minutes and Air Cooled for 5 Hours

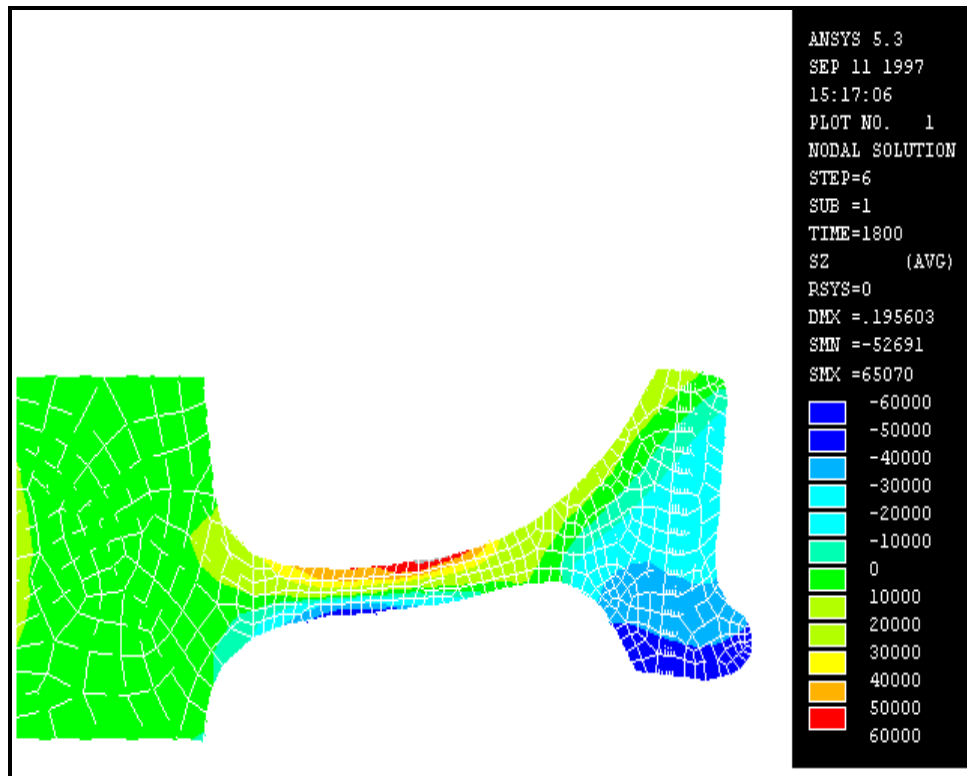


Figure 29. Finite Element Analysis of a Test Wheel Induction Heated at 45 kW (60 Hp) for 30 Minutes and Air Cooled for 5 Hours

3.8.2 Saw Cut FEA Model

The objective of the saw cut analysis is to calculate the residual hoop stress in the wheels using saw cut displacement data. The idea is the hoop displacements measured after saw cutting up to a depth of approximately 5 inches can be used to calculate the residual hoop stress in the wheel by effectively “unsawcutting” the wheel (i.e. returning it back to its original position). This is based on the assumption that after saw cutting the hoop residual stress in the wheel has been relieved.

The steps in constructing the saw cut FEA are specifying wheel geometry, wheel mesh and element types, material properties, and boundary conditions. The geometry, which was obtained from Griffin Wheel Company, is a 3-dimensional 90-degree slice of wheel as shown in Figure 30. The mesh consists of 8 node structural bricks in the NDT zone and 6 node structural tetrahedrons in the rest of the wheel. The material properties, which were provided by Griffin Wheel Company, are assumed to be homogeneous, linear, isotropic, and elastic. A modulus of elasticity of **30,000,000 psi** is used. The boundary conditions are hoop direction displacements applied to the two faces of the model. The cut face hoop displacements are obtained by interpolating the saw cut opening data, which consist of measured hoop displacements around the perimeter of the wheel, for the deepest depth of cut. Zero hoop displacement is applied to the other face of the model.

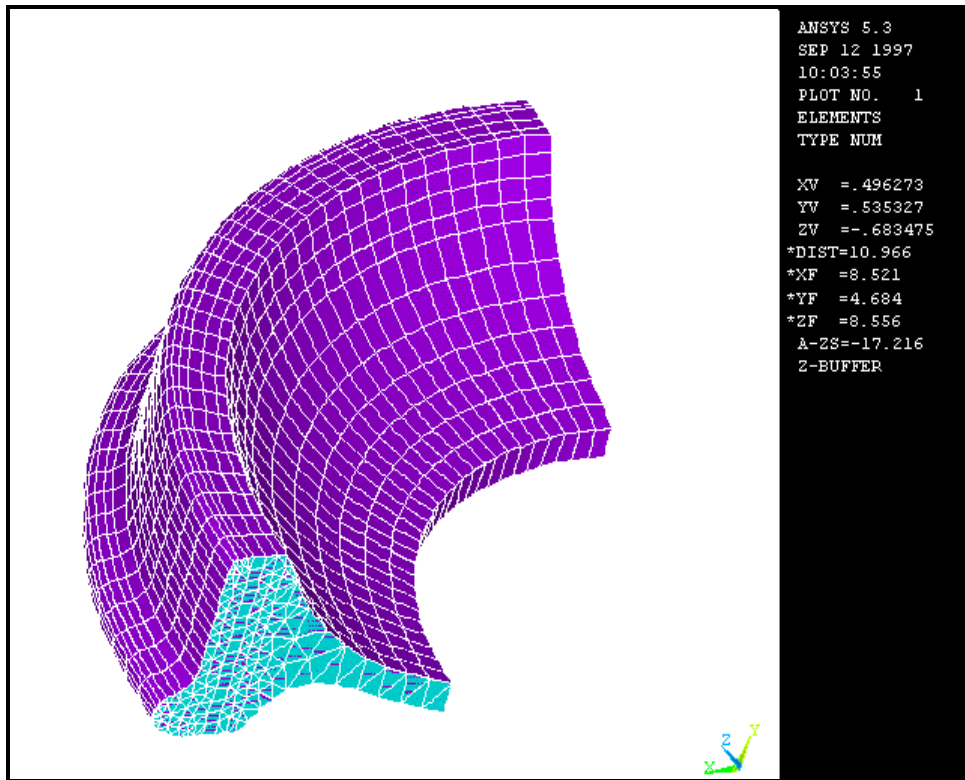


Figure 30. Three Dimensional 90 Degree Wheel Slice Used in Developing the Finite Element Analysis Model

4.0 RESULTS

4.1 BIREFRINGENCE MEASUREMENTS

Ultrasonic birefringence measurement results between the EMAT and PET systems for drag braked railroad wheels show similarities in data. These similarities provide confidence in the accuracy of the systems. There is some offset between systems, but in most instances the measurements replicate each other with some minor offset. The replication of results is especially apparent in railroad wheels which were subjected to greater thermal damage (i.e. 90 and 100 hp drag braking conditions). Table 5 lists the birefringence data measured at each of the 10 riser locations for each wheel tested. Figures 31 through 40 provide a graphic representation of the ultrasonic birefringence measurements.

Table 5. PET and EMAT Ultrasonic Front Rim Phase Averaged Birefringence ($\times 10^{-4}$) (MPA) at Each Riser Location

Wheel Description	1	2	3	4	5	6	7	8	9	10
75 hp flange (PET) SN 91817	0.2	2.4	3.0	3.3	1.3	1.6	1.5	1.9	3.7	2.0
75 hp flange (EMAT) SN 91817	7.8	9.0	8.0	7.2	8.9	8.2	6.8	6.1	5.0	7.6
75 hp flange (PET) SN 91768	-2.3	1.2	2.1	-0.1	-1.7	-0.5	1.1	0.3	0.3	-0.2
75 hp flange (EMAT) SN 91768	10.3	8.4	6.4	10.0	11.4	8.7	5.9	8.2	8.0	6.7
80 hp center (PET) SN 91807	1.1	0.8	3.0	1.2	3.0	-0.3	3.5	4.1	1.8	1.2
80 hp center (EMAT) SN 91807	9.2	7.7	6.4	7.6	8.3	9.8	5.9	6.4	6.2	9.0
80 hp center (PET) 91813	7.0	4.2	2.3	3.4	0.2	2.9	4.1	1.6	3.7	0.8
80 hp center (EMAT) 91813	7.6	8.3	10.9	10.9	11.6	10.1	8.4	10.1	11.1	11.0
80 hp flange (PET) SN 91778	NPM	NPM	NPM	NPM	NPM	NPM	NPM	NPM	NPM	NPM

**Table 5. PET and EMAT Ultrasonic Front Rim Phase Averaged
Birefringence ($\times 10^{-4}$) at Each Riser Location (continued)**

80 hp flange (EMAT) SN 91778	8.6	6.7	7.0	7.5	9.7	9.5	5.9	6.9	7.8	8.3
80 hp flange (PET) SN 84967	NPM									
80 hp flange (EMAT) SN 84967	7.5	6.7	8.7	7.7	4.4	9.6	8.4	8.7	4.2	5.1
85 hp center (60) (PET) SN 91777	1.3	1.2	3.9	4.2	1.0	3.5	-0.9	0.9	1.7	2.2
85 hp center (60) (EMAT) SN 91777	7.4	9.3	7.2	4.0	4.8	12.1	8.8	9.0	6.0	6.7
85 hp center (60) (PET) SN 91784	-7.1	-0.7	-8.1	-9.0	-5.7	-5.2	-2.7	-5.9	-9.4	-9.3
85 hp center (60) (EMAT) SN 91784	7.2	5.9	12.4	10.9	11.9	6.8	7.0	9.9	11.1	11.9
85 hp flange (60) (PET) SN 91847	1.6	2.3	2.3	1.8	0.6	0.7	3.5	2.1	1.6	2.4
85 hp flange (60) (EMAT) SN 91847	7.6	6.7	5.3	4.7	7.5	9.8	6.4	7.2	8.3	8.9
85 hp flange (60) (PET) SN 91843	-2.4	-1.2	-7.0	-7.3	-6.2	-4.1	-5.1	-7.4	-7.4	-6.6
85 hp flange (60) (EMAT) SN 91843	4.9	6.1	10.3	9.0	10	6.4	6.1	9.5	9.9	9.3
85 hp center (70) (PET) SN 84758	NPM									
85 hp center (70) (EMAT) SN 84758	1.8	1.3	6.7	4.6	6.4	2.2	4.1	4.9	3.7	3.4
85 hp center (70) (PET) SN 84972	NPM									
85 hp center (70) (EMAT) SN 84972	2.4	0.7	-0.4	-1.3	1.7	0.8	2.0	-3.0	-2.1	-0.6
85 hp flange (70) (PET) SN 86398	NPM									
85 hp flange (70) (EMAT) SN 86398	-3.3	0.9	2.4	0.4	1.2	-1.1	-1.0	-3.7	-2.4	0.1

Table 5. PET and EMAT Ultrasonic Front Rim Phase Averaged Birefringence ($\times 10^{-4}$) at Each Riser Location (continued)

85 hp flange (70) (PET) SN 80887	NPM									
85 hp flange (70) (EMAT) SN 80887	-8.4	-4.4	-7.6	-7.6	-6.5	-6.4	-7.1	-6.8	-7.2	-7.0
90 hp center (PET) SN 76933	5.5	5.9	2.1	3.5	3.2	7.0	5.1	4.4	5.1	6.0
90 hp center (EMAT) SN 76933	3.4	3.7	6.2	4.7	7.8	3.1	2.4	3.9	5.0	5.4
90 hp center (PET) SN 76896	9.6	10.4	8.8	8.7	6.2	5.6	7.8	6.6	7.6	9.2
90 hp center (EMAT) SN 76896	2.6	2.4	4.7	0.9	3.1	-0.2	3.9	6.7	3.7	2.8
90 hp flange (PET) SN 83991	1.3	1.5	1.2	2.3	2.6	3.4	0.8	2.0	0	2.0
90 hp flange (EMAT) SN 83991	5.4	6.3	9.0	6.9	5.2	6.3	6.8	7.5	6.5	3.2
90 hp flange (PET) SN 63764	1.1	3.0	4.9	3.3	3.9	0.2	3.5	5.5	4.8	2.0
90 hp flange (EMAT) SN 63764	7.8	6.2	5.1	4.3	5.4	7.2	5.2	1.8	5.2	7.3
100 hp center (PET) SN 80582	11.3	5.3	5.7	7.7	10.7	12.2	7.4	3.5	9.1	7.4
100 hp center (EMAT) SN 80582	3.0	5.6	7.2	3.6	1.9	1.3	3.5	4.7	3.1	5.9
100 hp flange (EMAT) SN 80742	-0.9	3.5	7.6	4.6	4.8	1.7	4.6	6.7	7.2	3.2
100 hp flange (EMAT) SN 80742	9.7	4.1	3.3	4.0	6.2	8.5	6.8	6.1	2.3	6.3

NPM-No PET measurements taken.

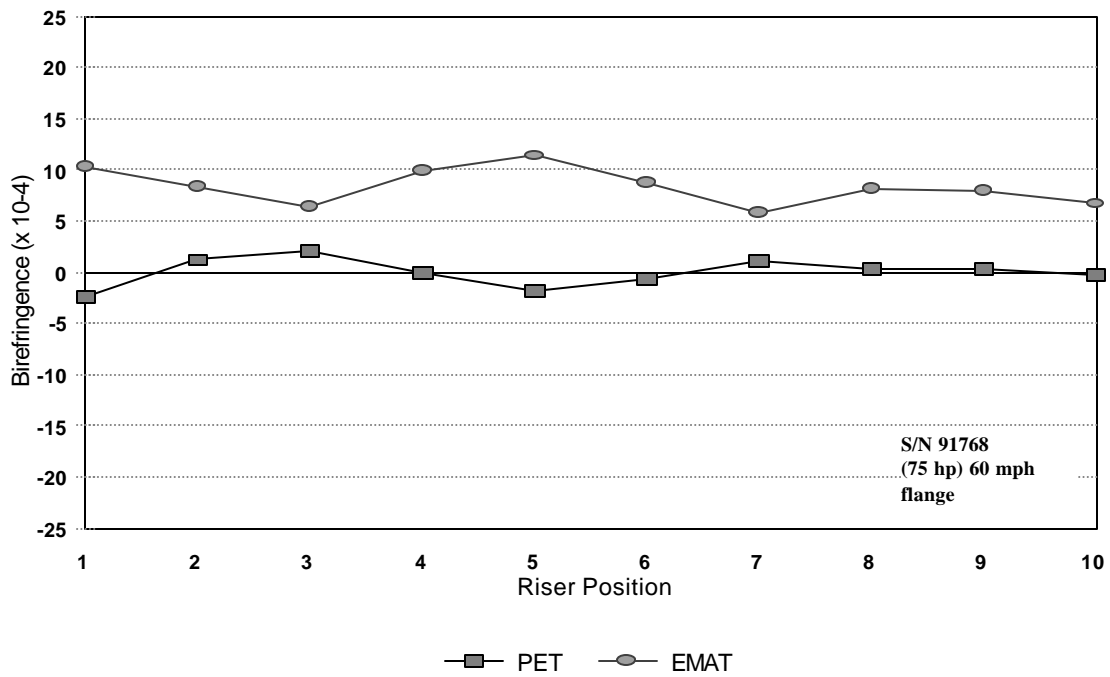
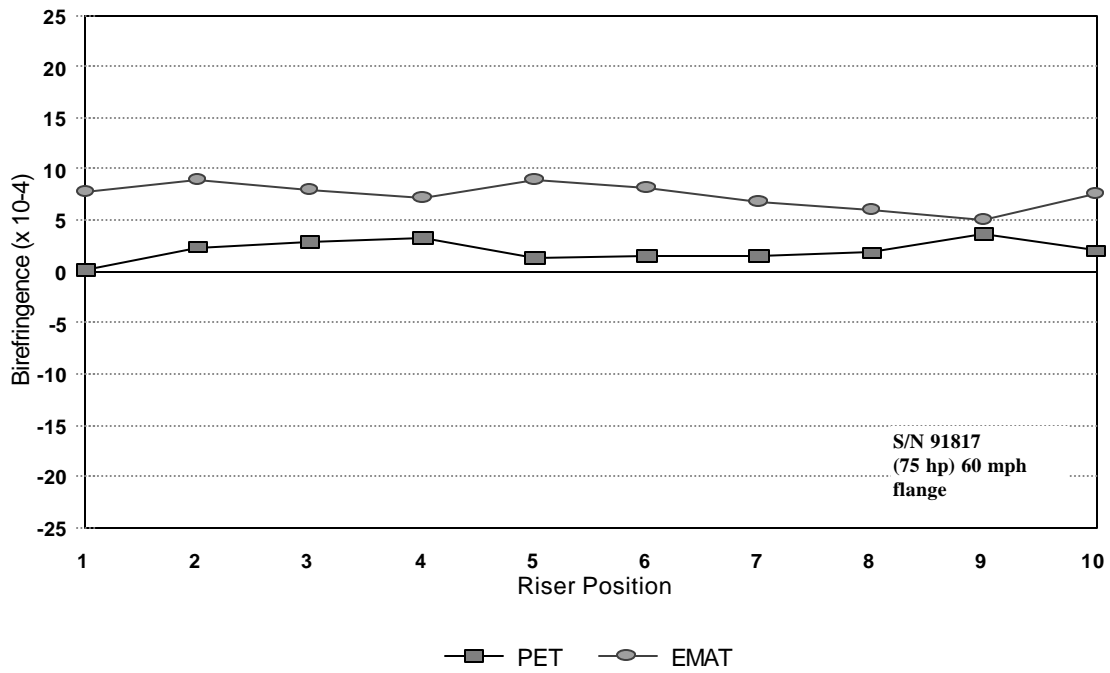


Figure 31. Residual Stress UT Birefringence Measurement Comparison Between the PET and EMAT Systems for the Railroad Wheels Drag Braked at 75 hp and the Brake Shoe Positioned at the Flange Corner

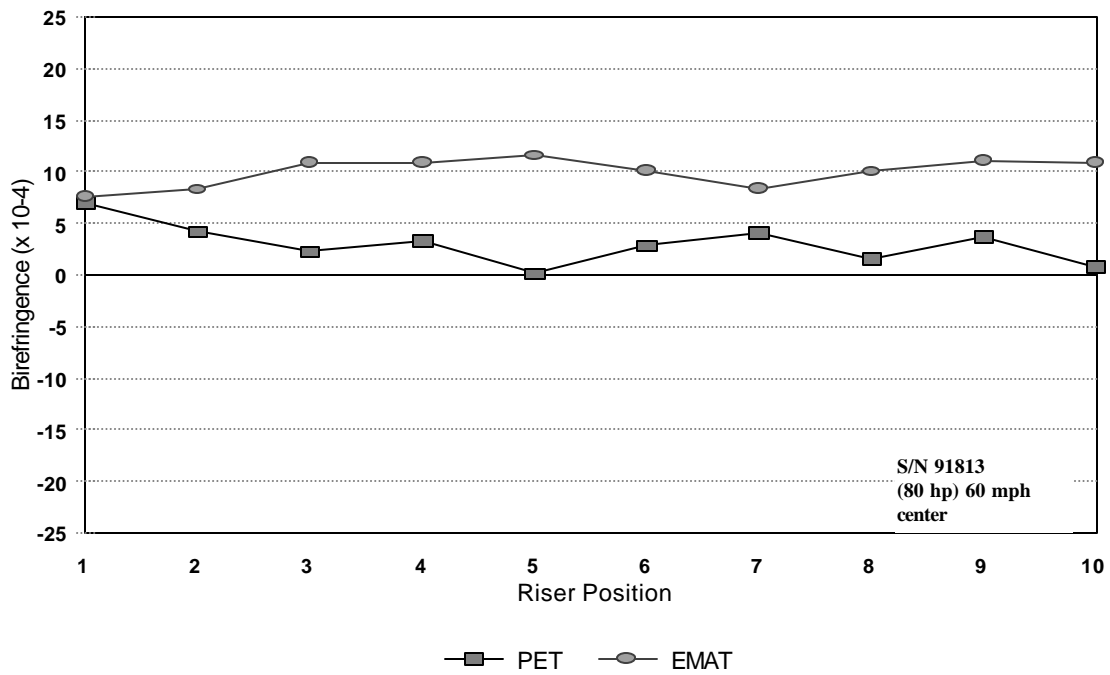
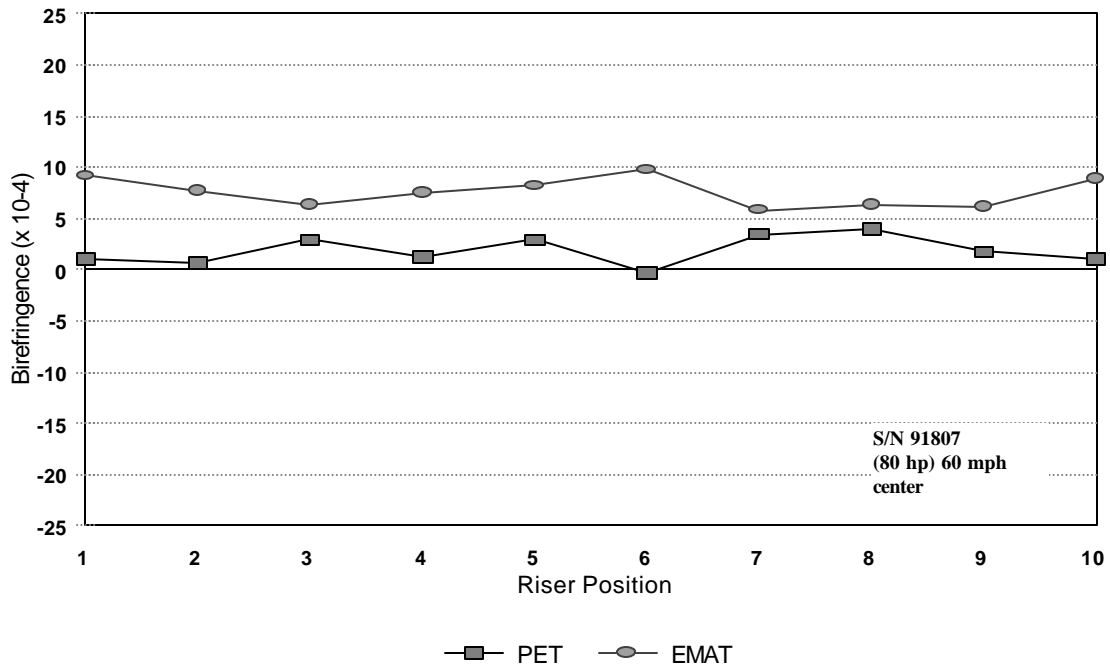


Figure 32. Residual Stress UT Birefringence Measurement Comparison Between the PET and EMAT Systems for the Railroad Wheels Drag Braked at 80 hp and the Brake Shoe Positioned at Tread Center

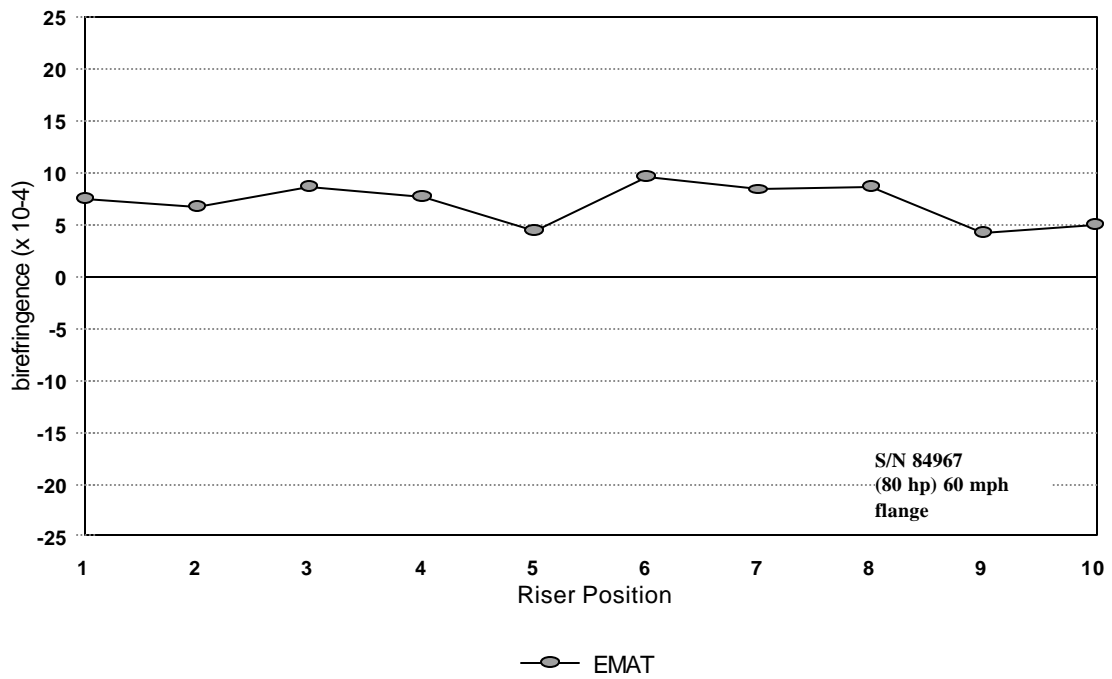
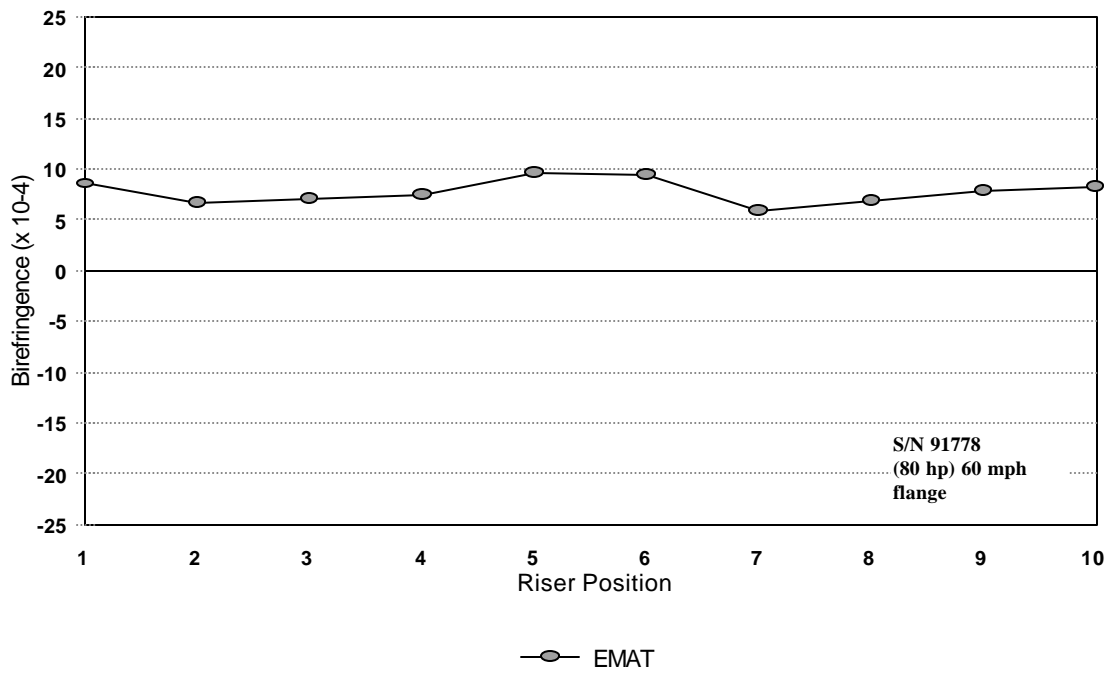


Figure 33. Residual Stress UT Birefringence Measurements using the EMAT System for the Railroad Wheels Drag Braked at 80 hp and the Brake Shoe Positioned at the Flange Corner

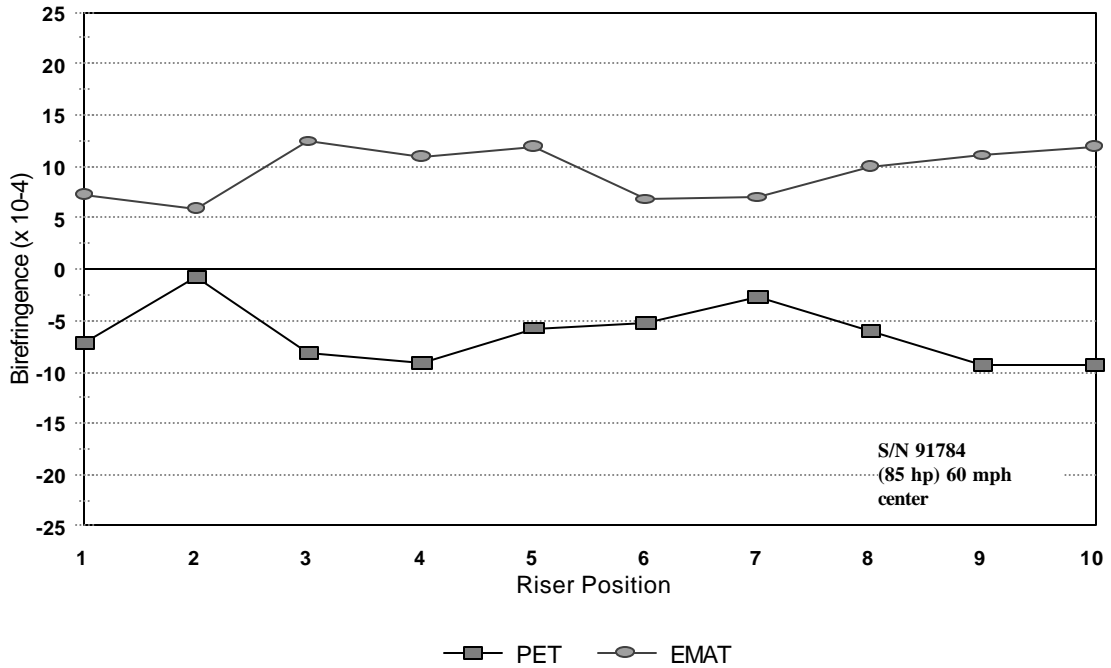
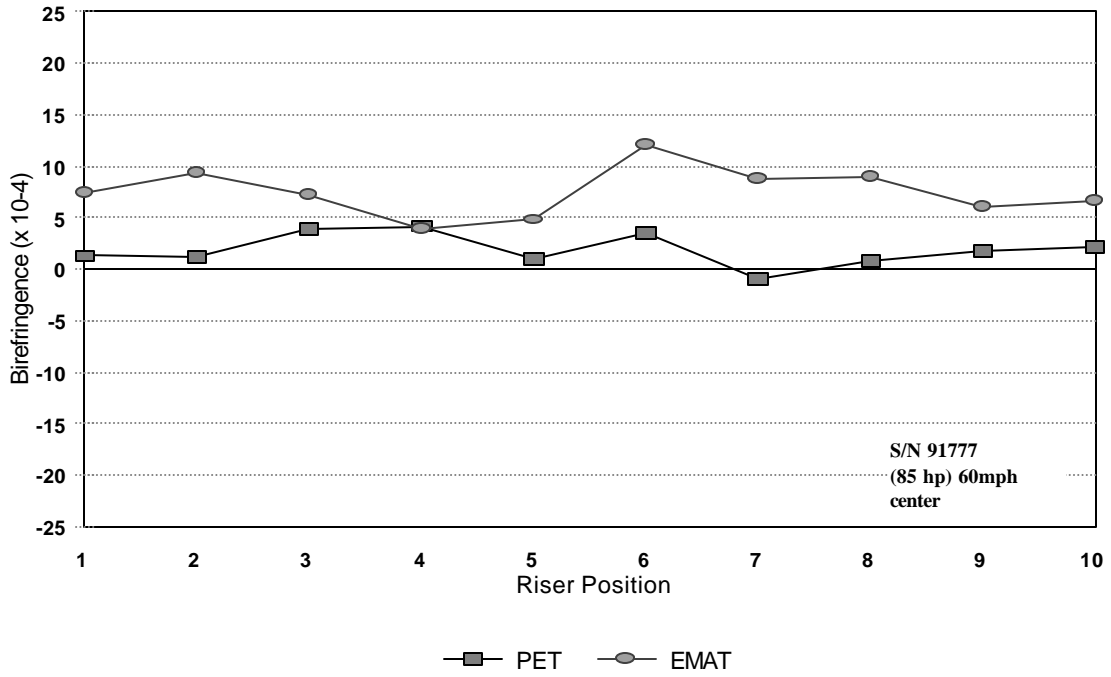


Figure 34. Residual Stress UT Birefringence Measurement Comparison Between the PET and EMAT Systems for the Railroad Wheels Drag Braked at 85 hp and 60 mph With the Brake Shoe Positioned at the Tread Center

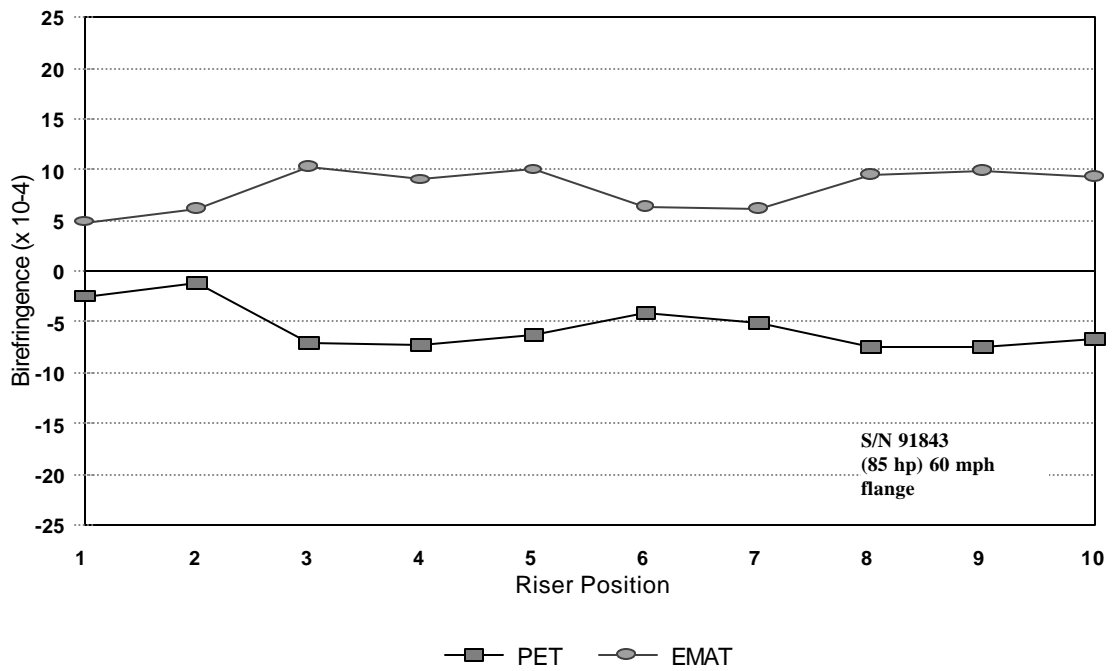
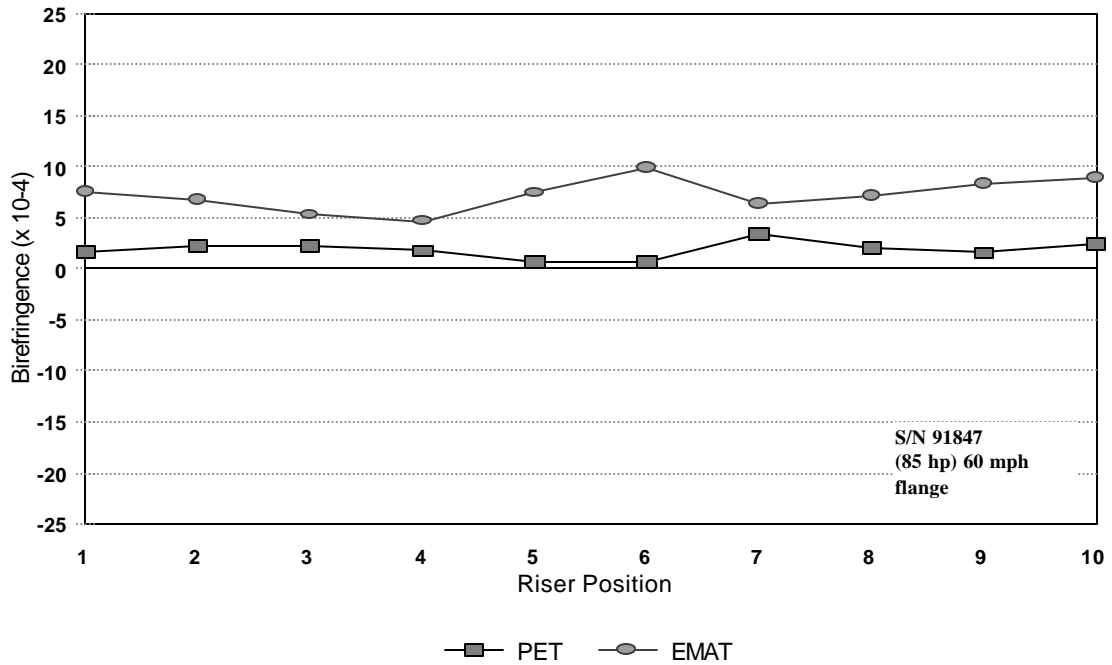


Figure 35. Residual Stress UT Birefringence Measurement Comparison Between the PET and EMAT Systems for the Railroad Wheels Drag Braked at 85 hp and 60 mph with the Brake Shoe Positioned at the Flange Corner

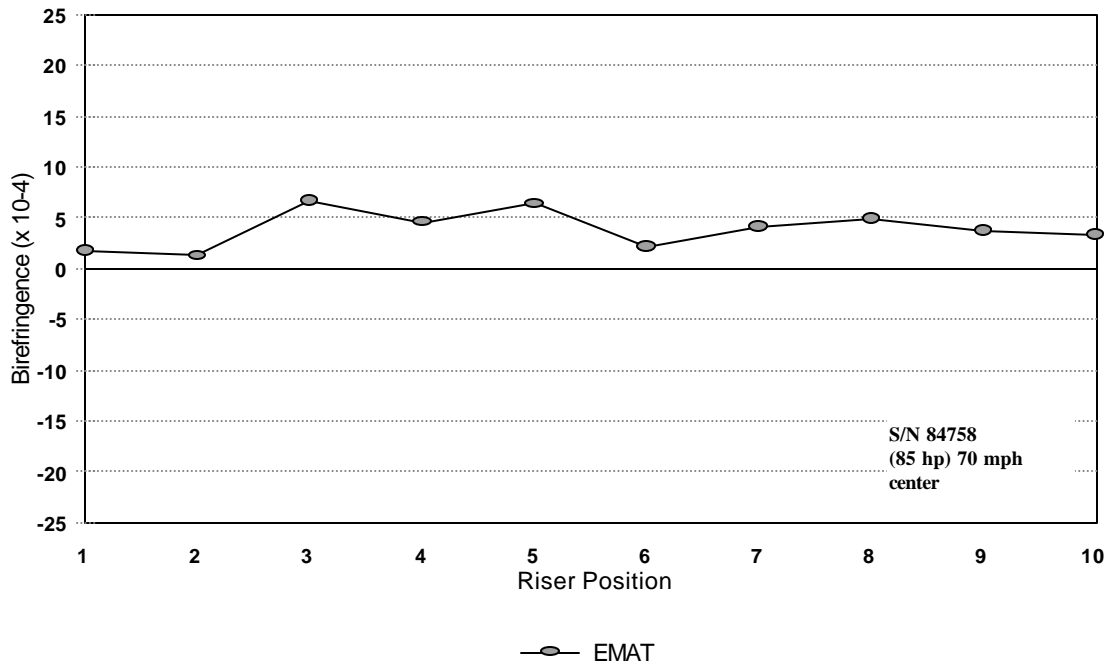
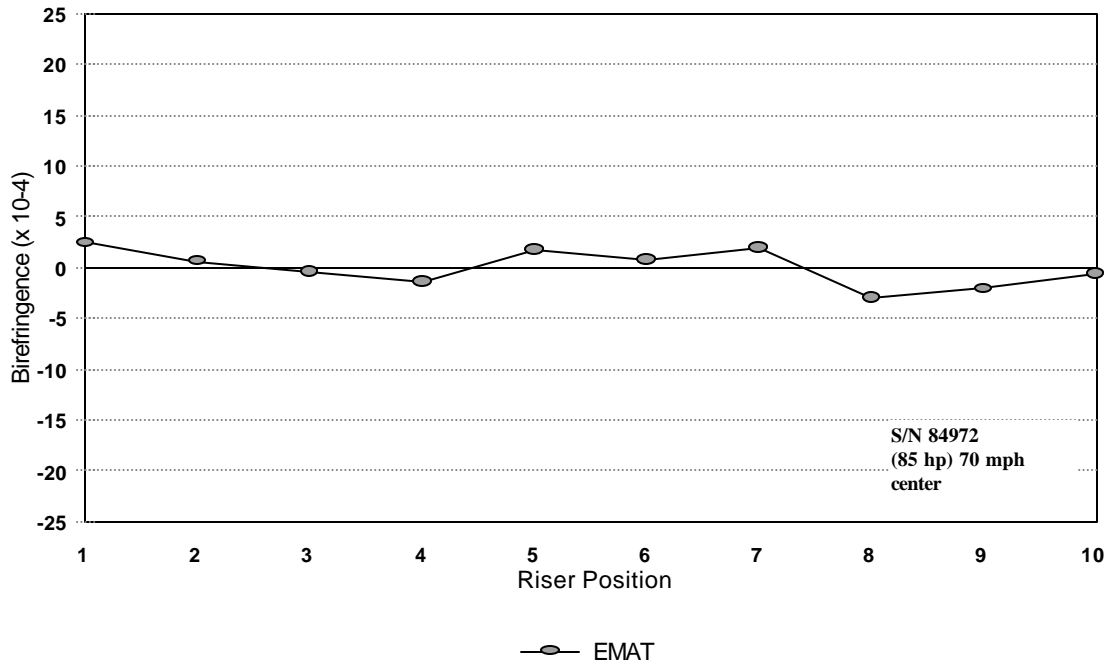


Figure 36. Residual Stress UT Birefringence Measurement from the EMAT System for the Railroad Wheels Drag Braked at 85 hp and 70 mph with the Brake Shoe Positioned at the Tread Center

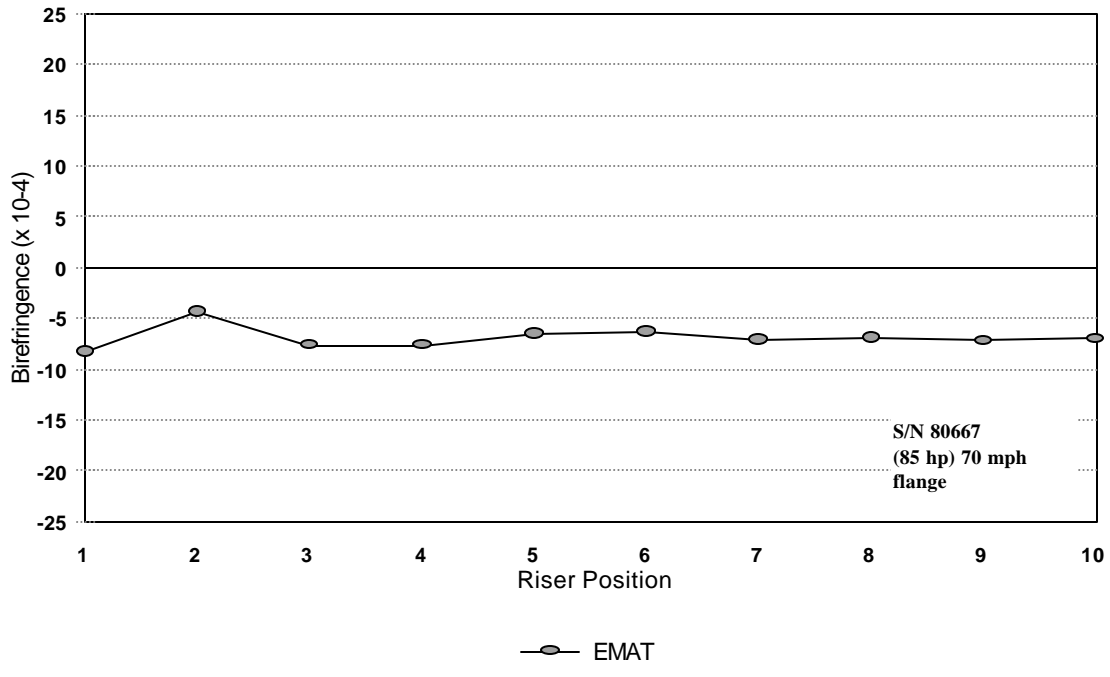
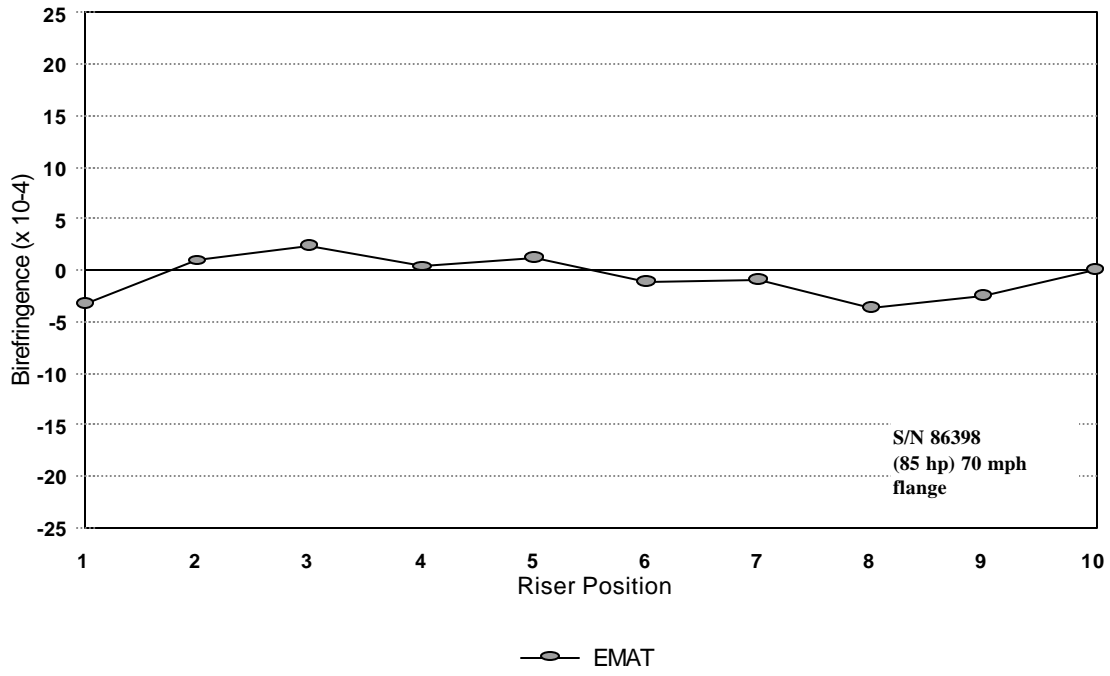


Figure 37. Residual Stress UT Birefringence Measurement from the EMAT System for the Railroad Wheels Drag Braked at 85 hp and 70 mph with the Brake Shoe Positioned at the Flange Corner

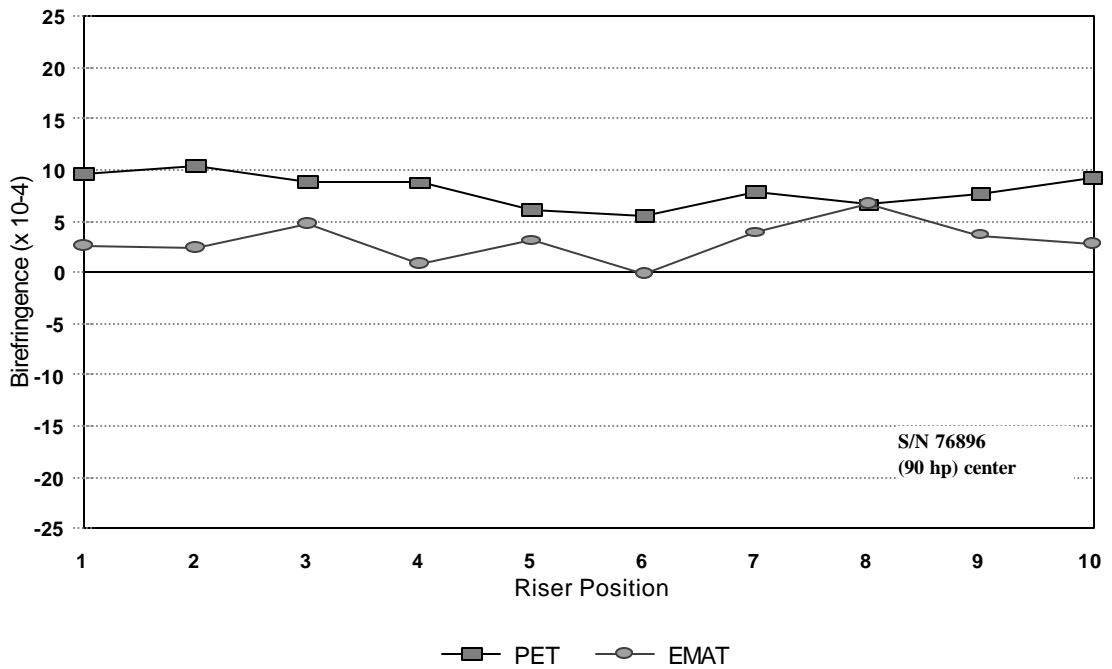
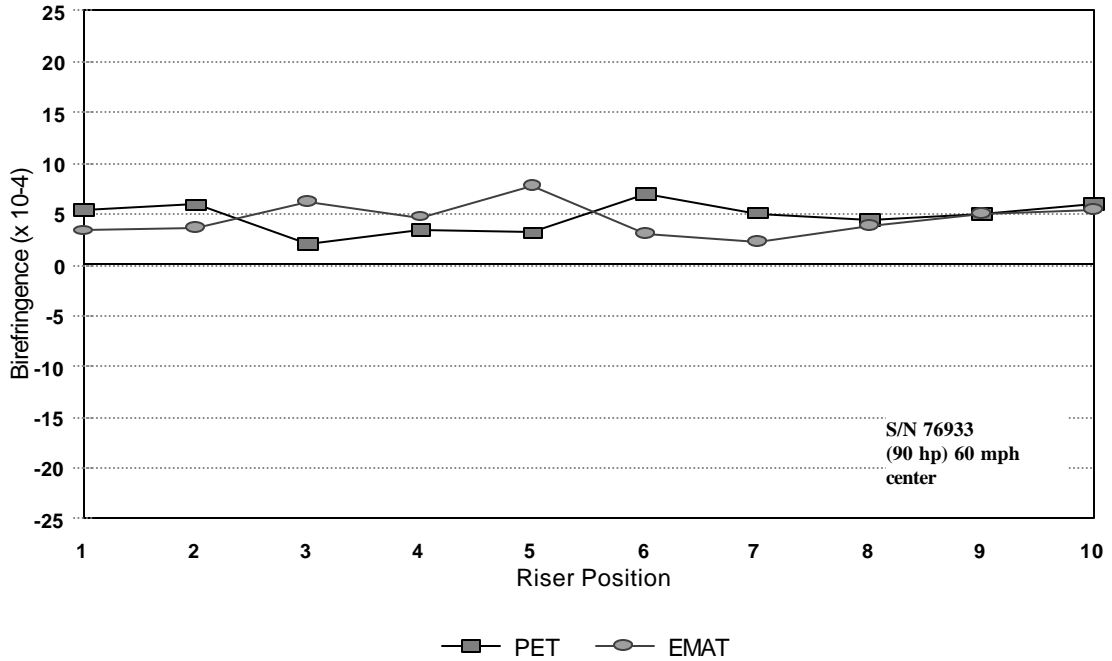


Figure 38. Residual Stress UT Birefringence Measurement Comparison Between the PET and EMAT Systems for the Railroad Wheels Drag Braked at 90 hp and the Brake Shoe Positioned at the Tread Center

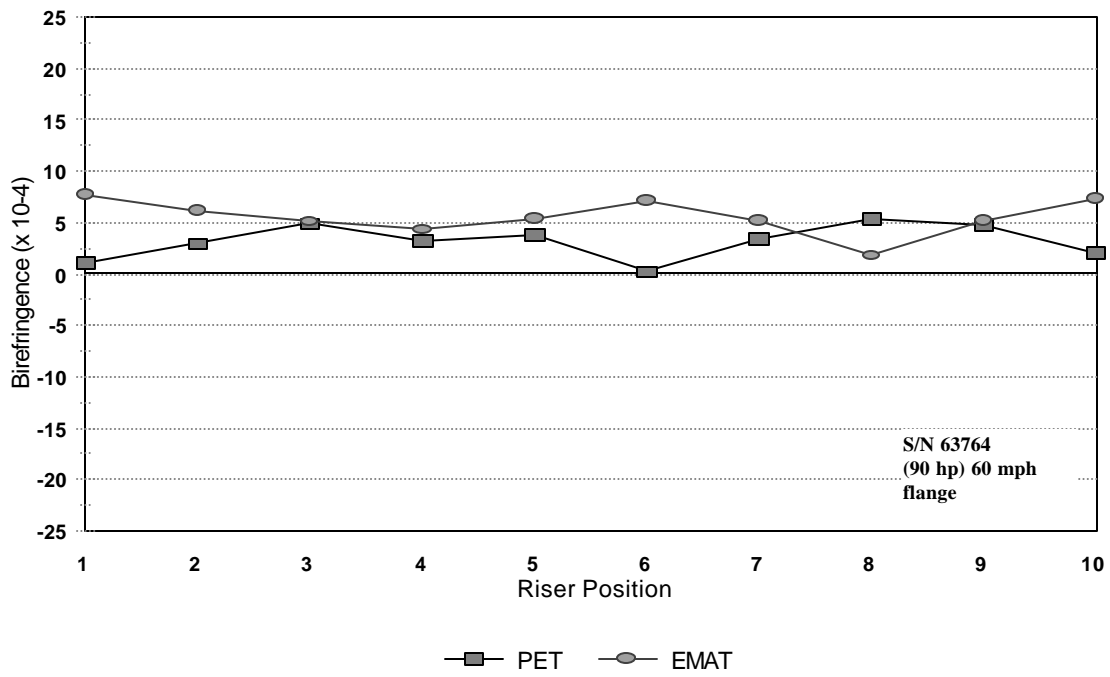
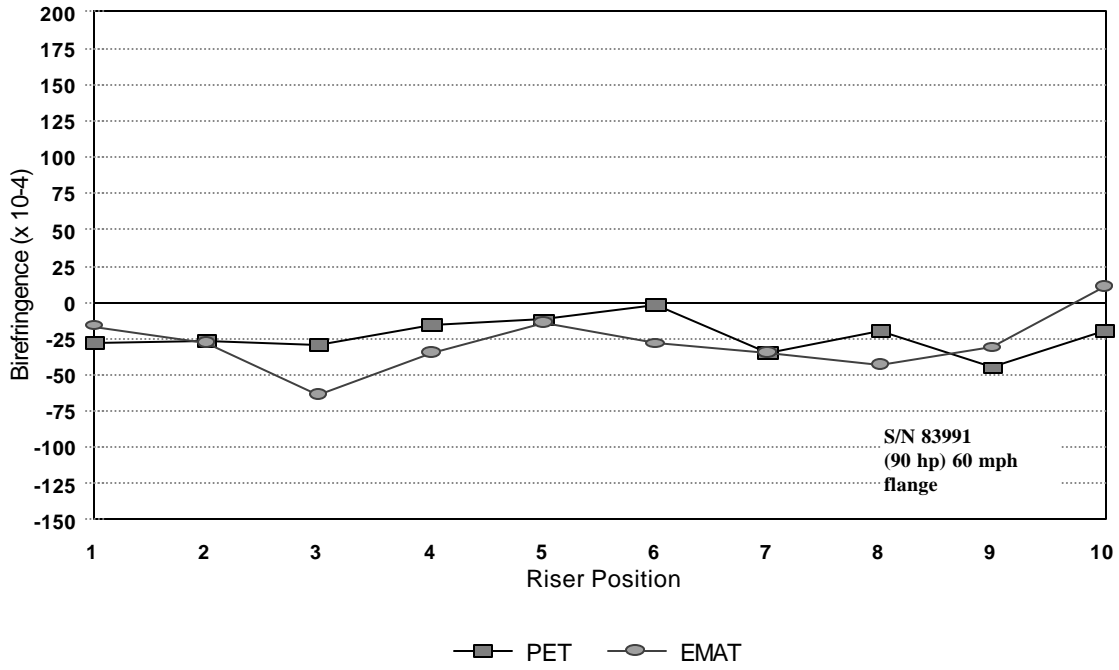


Figure 39. Residual Stress UT Birefringence Measurement Comparison Between the PET and EMAT Systems for the Railroad Wheels Drag Braked at 90 hp and the Brake Shoe Positioned at the Flange Corner

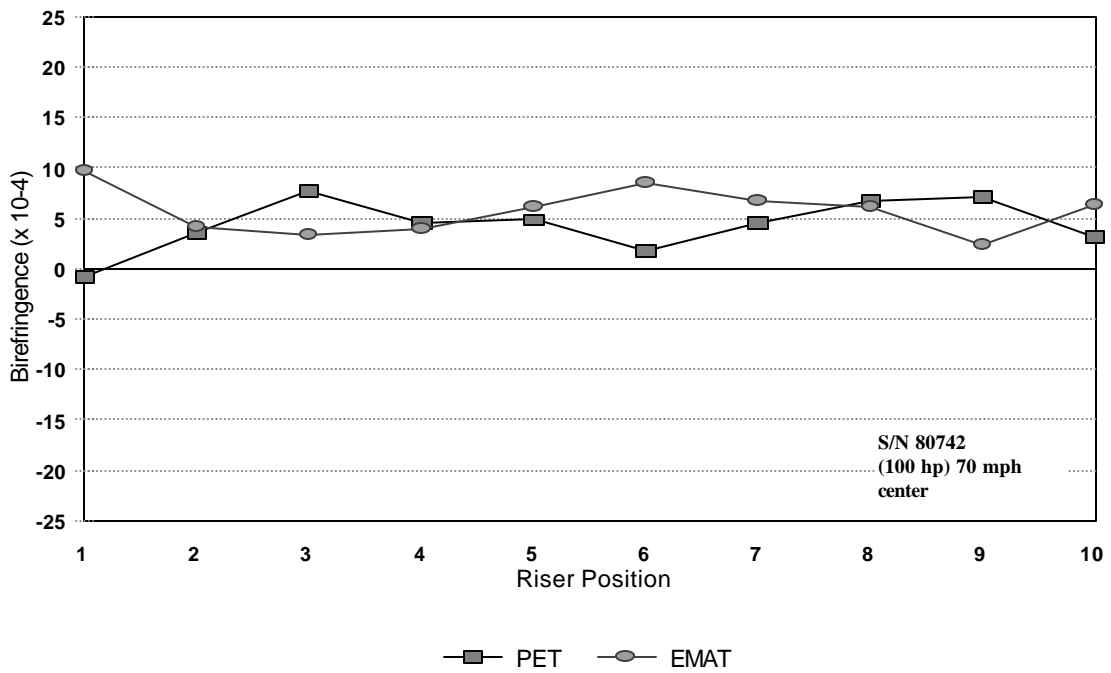
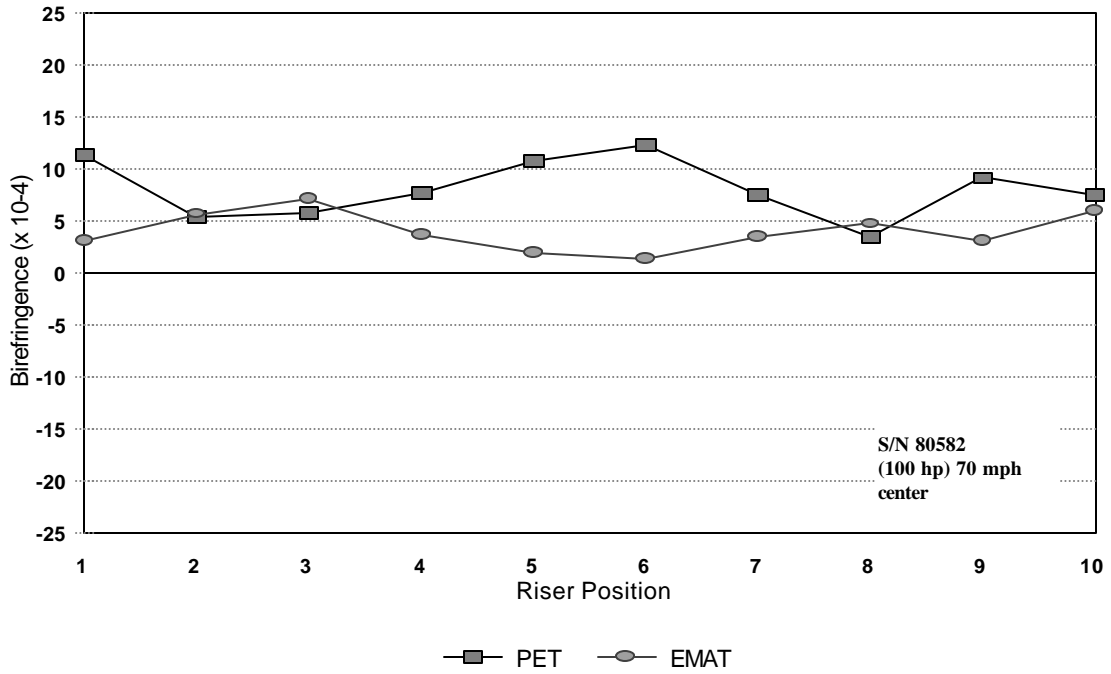


Figure 40. Residual Stress UT Birefringence Measurement Comparison Between the PET and EMAT Systems for the Railroad Wheels Drag Braked at 100 hp and 70 mph with the Brake Shoe Positioned at the Tread Center

A comparison of the PET and EMAT through thickness averaged birefringence values was obtained for each drag braked wheel. The results of those comparisons are shown in Table 6. Figure 41 gives a graphical representation of the average birefringence for each of the test wheels. The birefringence averages show the PET system consistently obtaining lower birefringence results than the EMMAP system. NIST has attributed this phenomenon to the geometric result of the beam spreads while traveling in opposite directions.¹⁴

**Table 6. PET and EMAT Ultrasonic Birefringence ($\times 10^{-4}$)
Front Rim Face Measurements**

POWER INPUT (KW (HP))	PET (MPA)	EMAT (MPA)
75 hp flange (EMAT) SN 91817	2.1	7.5
75 hp flange (EMAT) SN 91768	0	8.4
80 hp center (EMAT) SN 91807	1.9	7.6
80 hp center (EMAT) 91813	3.0	10.0
80 hp flange (EMAT) SN 91778	NA	7.8
80 hp flange (EMAT) SN 84967	NA	7.1
85 hp center (60) (EMAT) SN 91777	1.9	7.5
85 hp center (60) (EMAT) SN 91784	-6.3	9.5
85 hp flange (60) (EMAT) SN 91847	1.9	7.2
85 hp flange (60) (EMAT) SN 91843	-5.5	8.2
85 hp center (70) (EMAT) SN 84758	NA	3.9
85 hp center (70) (EMAT) SN 84972	NA	0
85 hp flange (70) (EMAT) SN 86398	NA	-0.6
85 hp flange (70) (EMAT) SN 80887	NA	-6.9
90 hp center (EMAT) SN 76933	4.8	4.5
90 hp center (EMAT) SN 76896	8.1	3.1
90 hp flange (EMAT) SN 83991	1.7	6.3
90 hp flange (EMAT) SN 63764	3.2	5.5
100 hp center (PET) SN 80582	8.0	4.0
100 hp flange (EMAT) SN 80742	4.3	5.7

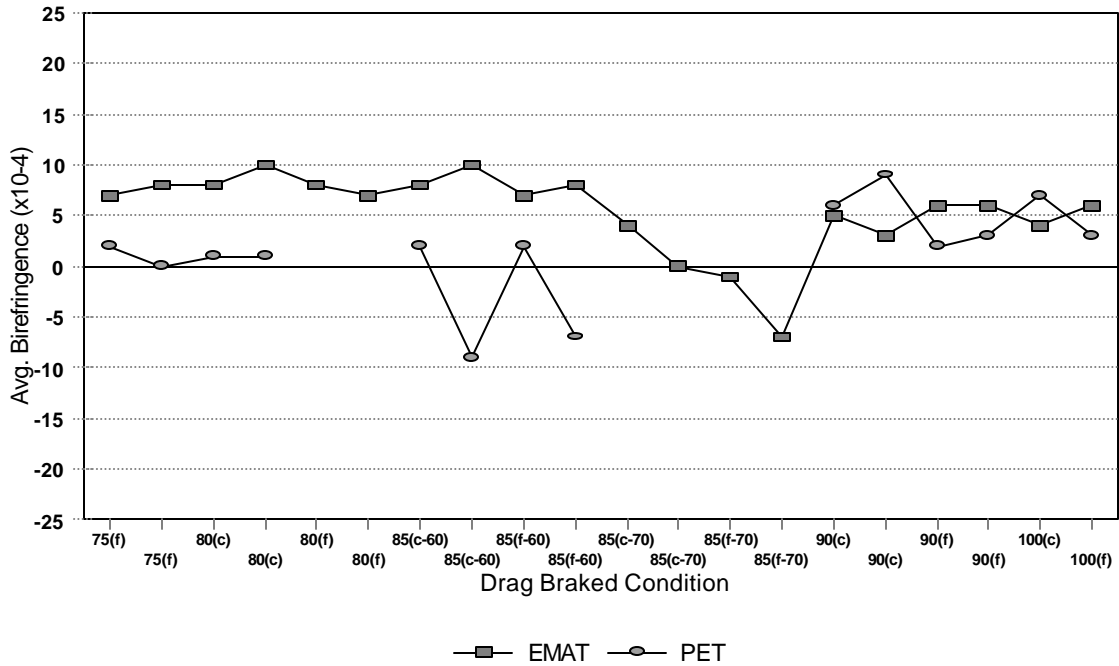


Figure 41. Average UT Birefringence Measurement Comparison Between the PET and EMAT Systems for Drag Braked Railroad Wheels

4.2 RESIDUAL STRESS MEASUREMENTS

Ultrasonic measurement comparisons between the EMAT and PET systems show that the measurements do track each other with an offset of approximately 40 MPa (6 ksi) or less, which has been identified by NIST.¹⁵ In almost all cases the PET results are higher. Variables which may contribute to this offset include:

- Initial Calibration
- Texture Effects
- Transducer Design
- Beam Spread

The primary influence will of course be determined by the areas obtained from beam spread. Beam spread affects calibration by either averaging more or less material that allows more or less influence from texture. In this evaluation, the beam spreads generated from the EMAT and PET systems were slightly different, which probably resulted in the offset between measurements.

The similarity in measurements provides confidence in the accuracy and reliability of the systems. The results also identify an offset in measurements between systems which shows a necessity for determining a proper calibration prior to testing. The ultrasonic measurements for both the EMAT and PET systems are listed in Table 7. The correlation of the two methods can be seen graphically in Figures 41 through 51.

Table 7. PET and EMAT Ultrasonic Front Rim Phase Averaged Stress Values in MPA at Each Riser Location

Wheel Description	1	2	3	4	5	6	7	8	9	10
75 hp flange (PET) SN 91817	-42	-14	-7	-3	-28	-25	-26	-21	2	-19
75 hp flange (EMAT) SN 91817	-48	-63	-50	-40	-62	-52	-35	-26	-11	45
75 hp flange (PET) SN 91768	-75	-29	-18	-46	-67	-52	-31	-41	-41	-47
75 hp flange (EMAT) SN 91768	-79	-55	-29	-76	-94	-59	-22	-52	-50	-33
80 hp center (PET) SN 91807	-31	-35	-7	-29	-7	-49	0	7	-22	-30
80 hp center (EMAT) SN 91807	-65	-47	-29	-44	-53	-73	-23	-29	-27	-63
80 hp center (PET) 91813	45	9	-16	-2	-43	-8	7	-24	2	-35
80 hp center (EMAT) 91813	-45	-54	-87	-87	-96	-77	-56	-76	-90	-88
80 hp flange (PET) SN 91778	-42	-31	-30	-35	-35	-58	-29	-21	-45	-48
80 hp flange (EMAT) SN 91778	-57	-33	-38	-43	-72	-69	-23	-35	-48	-54
80 hp flange (PET) SN 84967	-29	-40	-20	-7	23	-29	11	-48	-30	-25
80 hp flange (EMAT) SN 84967	-43	-34	-59	-46	-4	-70	-55	-59	-1	-13
85 hp center (60)(PET) SN 91777	-28	-30	5	9	-32		-57	-34	-23	-17
85 hp center (60) (EMAT) SN 91777	-42	-67	-40	2	-9	-102	-60	-62	-24	-33
85 hp center (60) (PET) SN 91784	-46	36	-59	-71	-28	-22	11	-31	-75	-74
85 hp center (60) (EMAT) SN 91784	-40	-23	-107	-87	-100	-35	-37	-75	-85	-100
85 hp flange (60) (PET) SN 91847	-24	-15	-16	-22	-37	-36	0	-18	-25	-14

Table 7. PET and EMAT Ultrasonic Front Rim Phase Averaged Stress Values in MPA at Each Riser Location (continued)

85 hp flange (60) (EMAT) SN 91847	-45	-34	-15	-7	-43	-73	-29	-40	-53	-62
85 hp flange (60) (PET) SN 91843	14	30	-45	-48	-35	-8	-20	-50	-50	-40
85 hp flange (60) (EMAT) SN 91843	-10	-26	-79	-63	-76	-30	-26	-69	-74	-67
85 hp center (70) (PET) SN 84758	NPM									
85 hp center (70) (EMAT) SN 84758	30	36	-32	-6	-29	24	0	-11	6	9
85 hp center (70) (PET) SN 84972	NPM									
85 hp center (70) (EMAT) SN 84972	21	44	58	70	31	43	27	92	79	60
85 hp flange (70) (PET) SN 86398	NPM									
85 hp flange (70) (EMAT) SN 86398	95	40	22	48	37	66	65	99	84	51
85 hp flange (70) (PET) SN 80887	NPM									
85 hp flange (70) (EMAT) SN 80887	160	109	150	150	136	134	144	140	145	142
90 hp center (PET) SN 76933	25	31	-18		-4	45	21	12	20	32
90 hp center (EMAT) SN 76933	9	6	-27	-8	-47	13	22	3	-12	-17
90 hp center (PET) SN 76896	78	88	68	67	34	27	55	40	53	73
90 hp center (EMAT) SN 76896	19	22	-8	41	13	54	3	-33	6	16
90 hp flange (PET) SN 83991	-28	-26	-29	-15	-12	-2	-35	-19	-45	-19
90 hp flange (EMAT) SN 83991	-16	-28	-63	-35	-14	-28	-35	-43	-31	11
90 hp flange (PET) SN 63764	-31	-7	18	-3	5	-42	0	25	17	-19
90 hp flange (EMAT) SN 63764	-47	-26	-13	-3	-16	-40	-14	30	-14	-41
100 hp center (PET) SN 80582	100	23	28	54	92	112	50		72	50
100 hp center (EMAT) SN 80582	14	-20	-39	6	29	36	8	-8	13	-23
100 hp flange (EMAT) SN 80742	-56	0	53	14	17	-23	14	41	47	-4
100 hp flange (EMAT) SN 80742	-72	0	10	2	-27	-56	-34	-25	23	-28

NPM-No PET measurements taken.

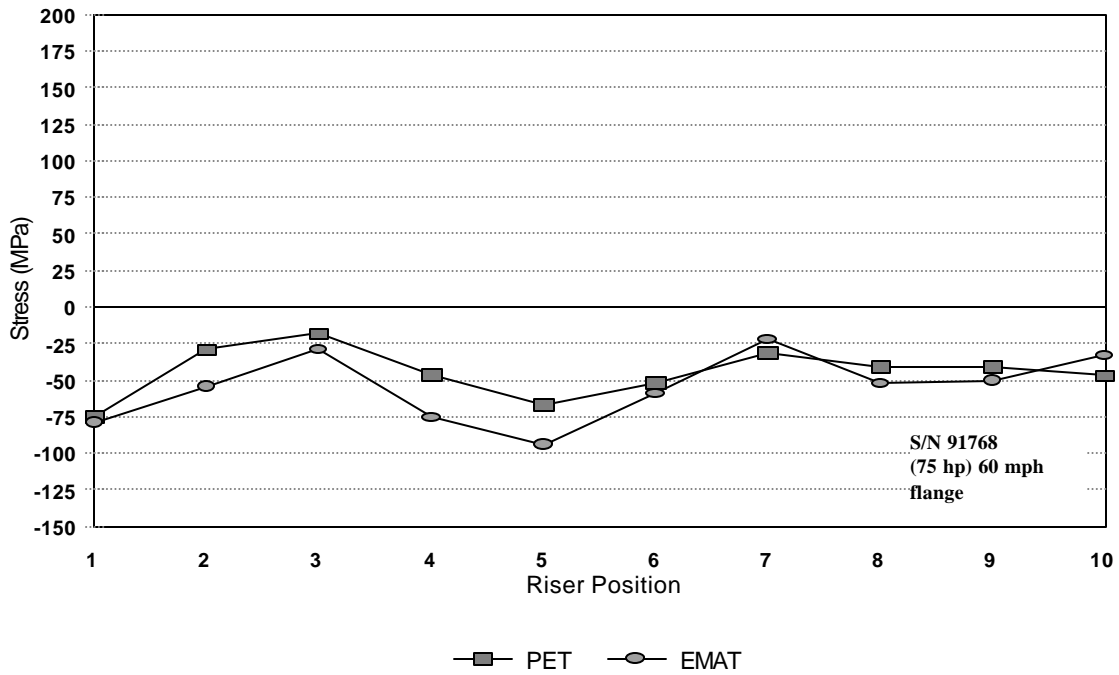
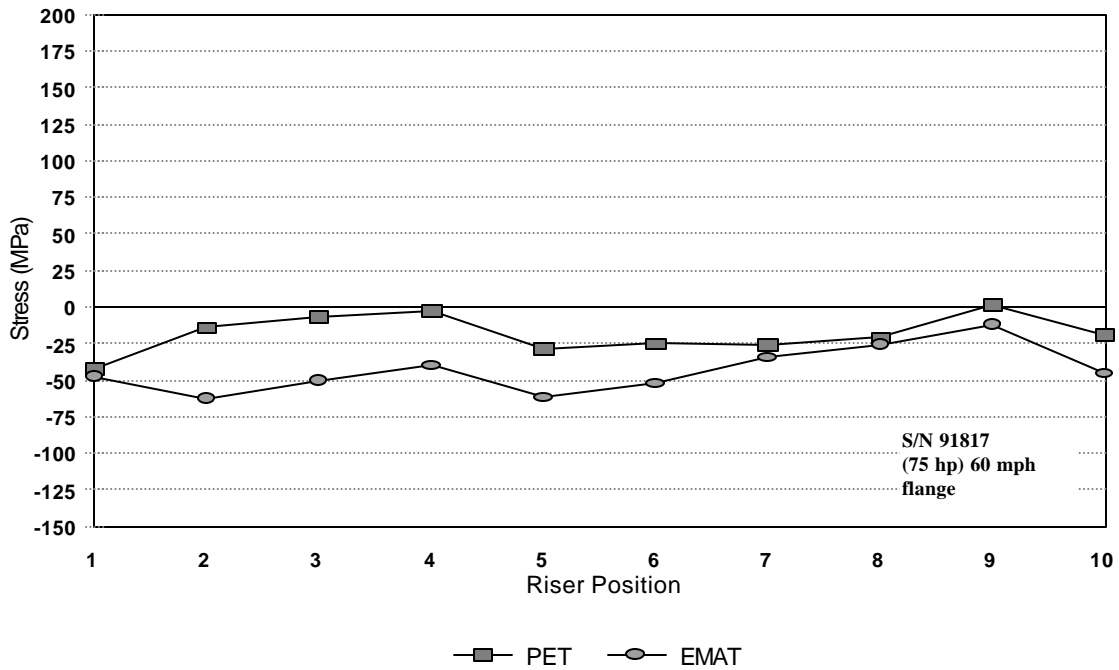


Figure 42. Residual Stress UT Measurement Comparison Between the PET and EMAT Systems for the Railroad Wheels Drag Braked at 75 hp and the Brake Shoe Positioned at the Flange Corner

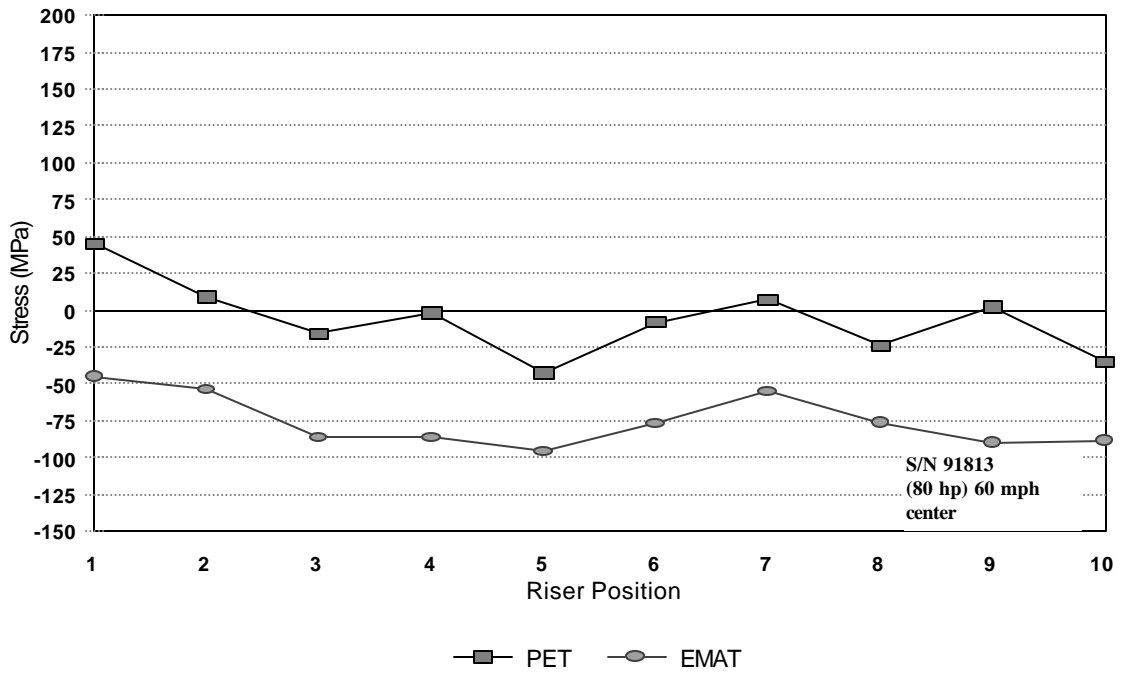
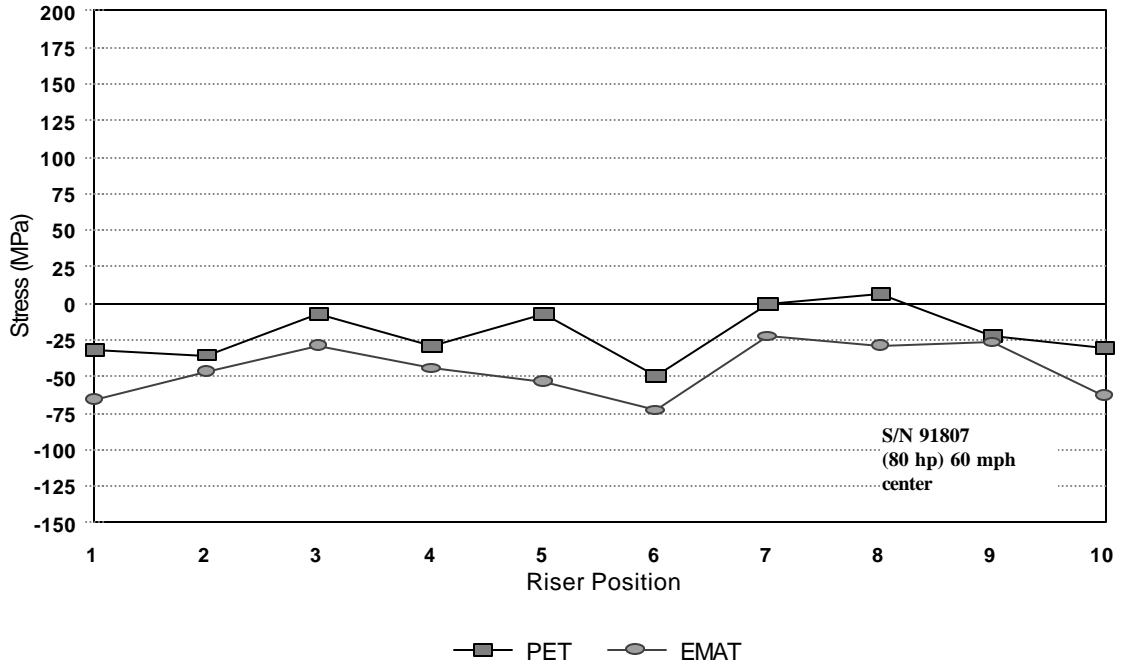


Figure 43. Residual Stress UT Measurement Comparison Between the PET and EMAT Systems for the Railroad Wheels Drag Braked at 80 hp and the Brake Shoe Positioned at Tread Center

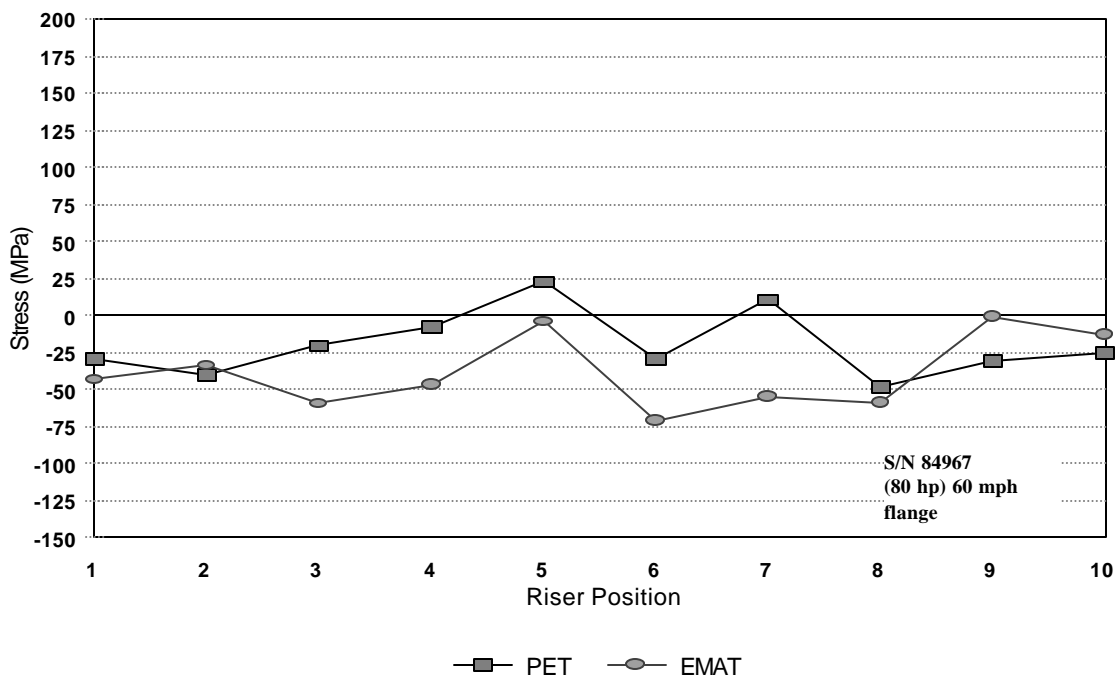
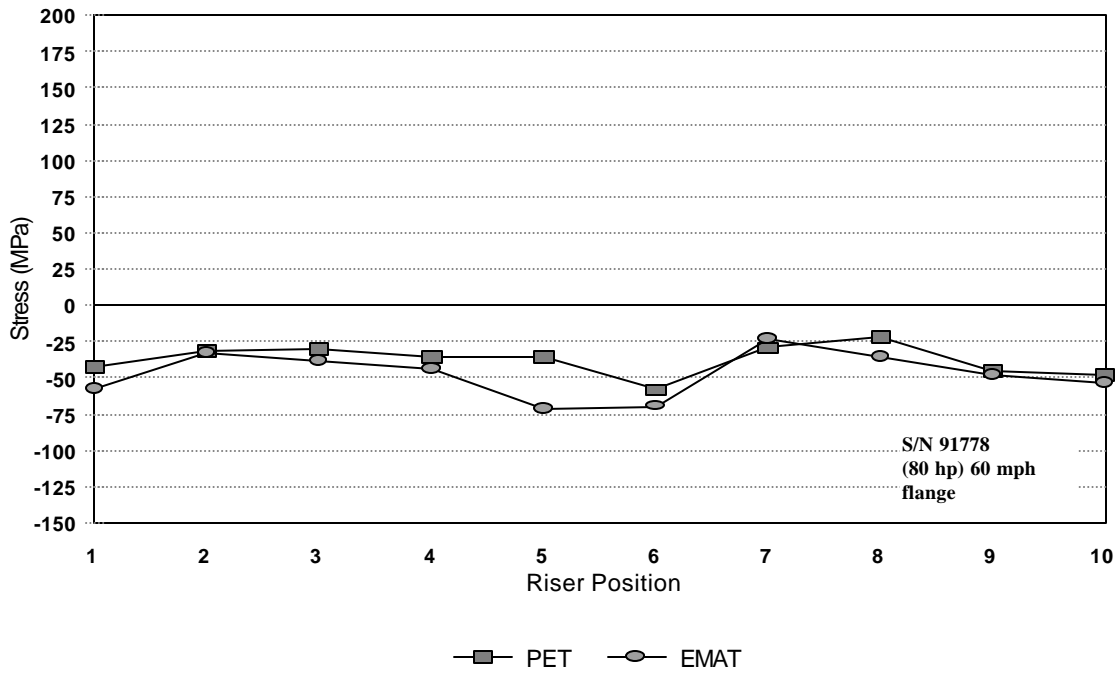


Figure 44. Residual Stress UT Measurement Comparison Between the PET and EMAT Systems for the Railroad Wheels Drag Braked at 80 hp and the Brake Shoe Positioned at the Flange Corner

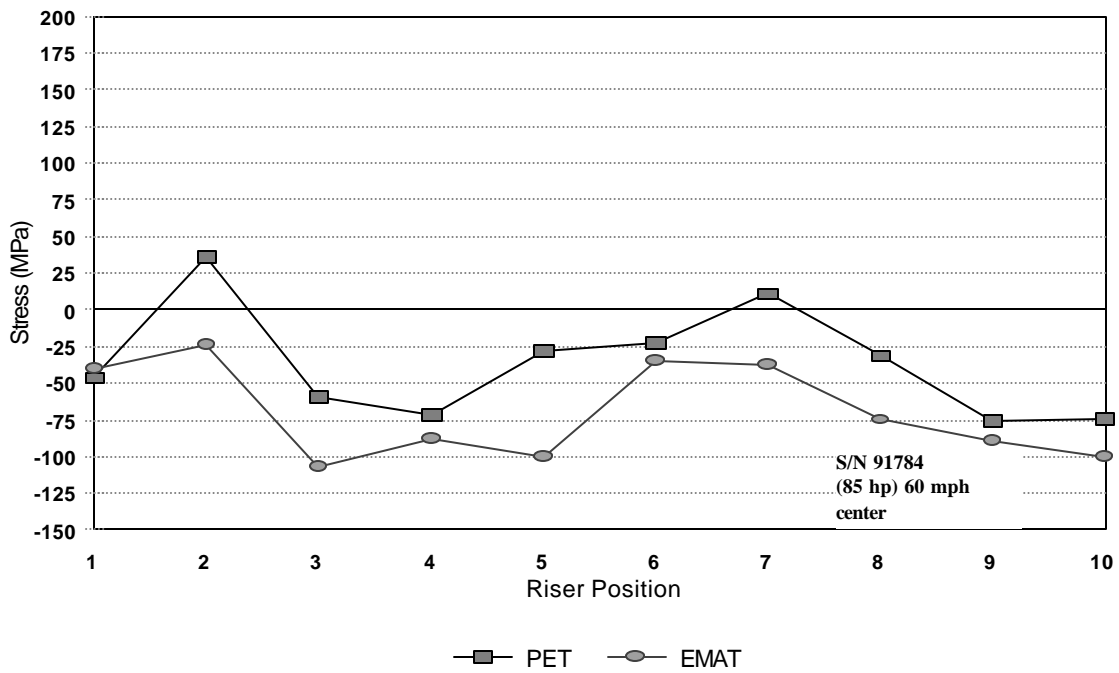
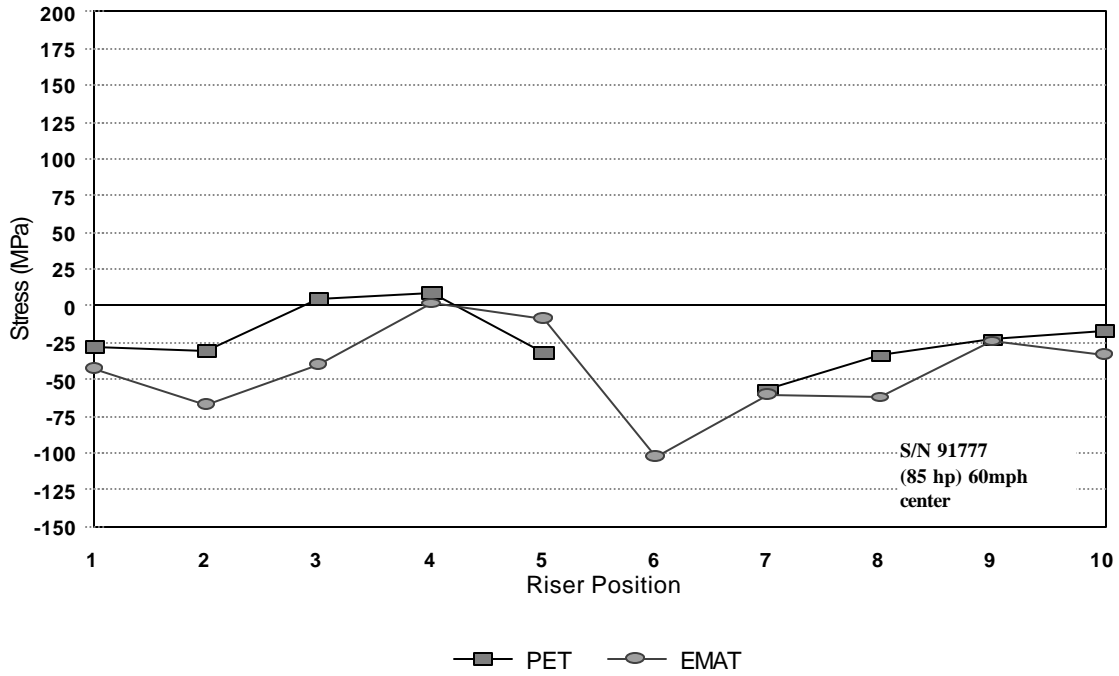


Figure 45. Residual Stress UT Measurement Comparison Between the PET and EMAT Systems for the Railroad Wheels Drag Braked at 85 hp and 60 mph with the Brake Shoe Positioned at the Tread Center

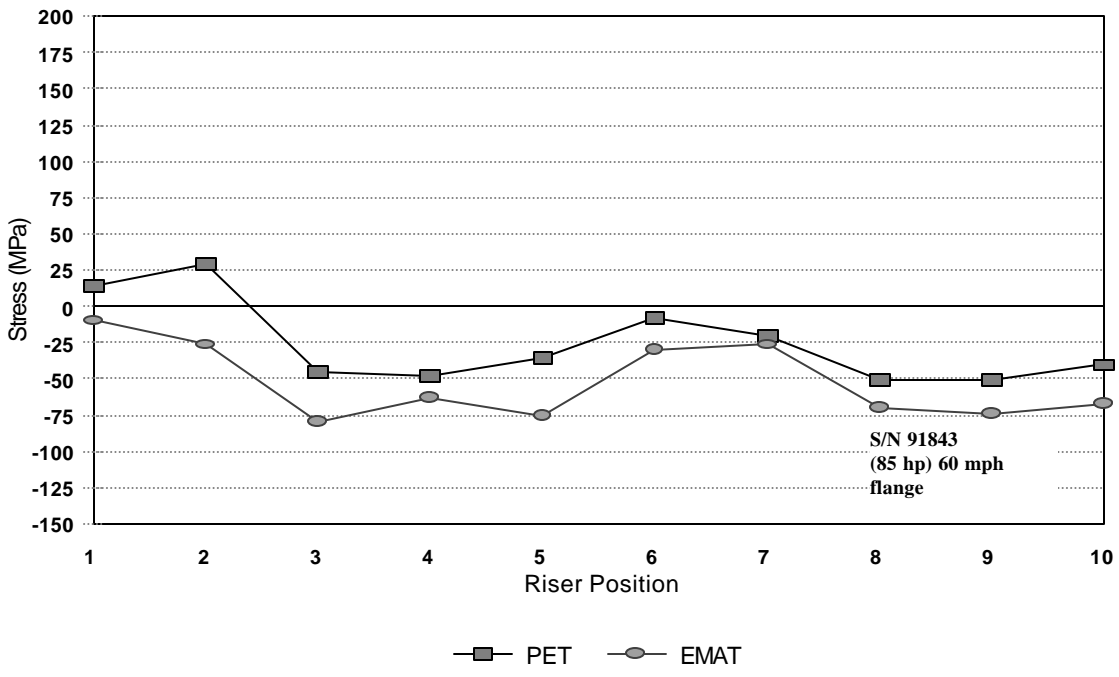
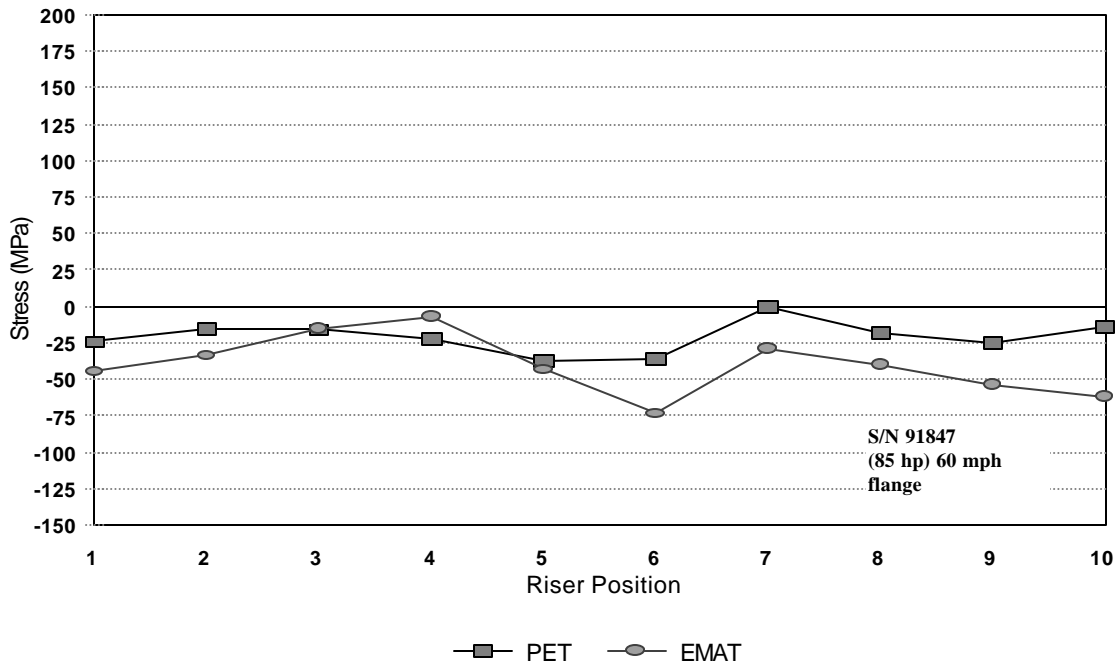


Figure 46. Residual Stress UT Measurement Comparison Between the PET and EMAT Systems for the Railroad Wheels Drag Braked at 85 hp and 60 mph with the Brake Shoe Positioned at the Flange Corner

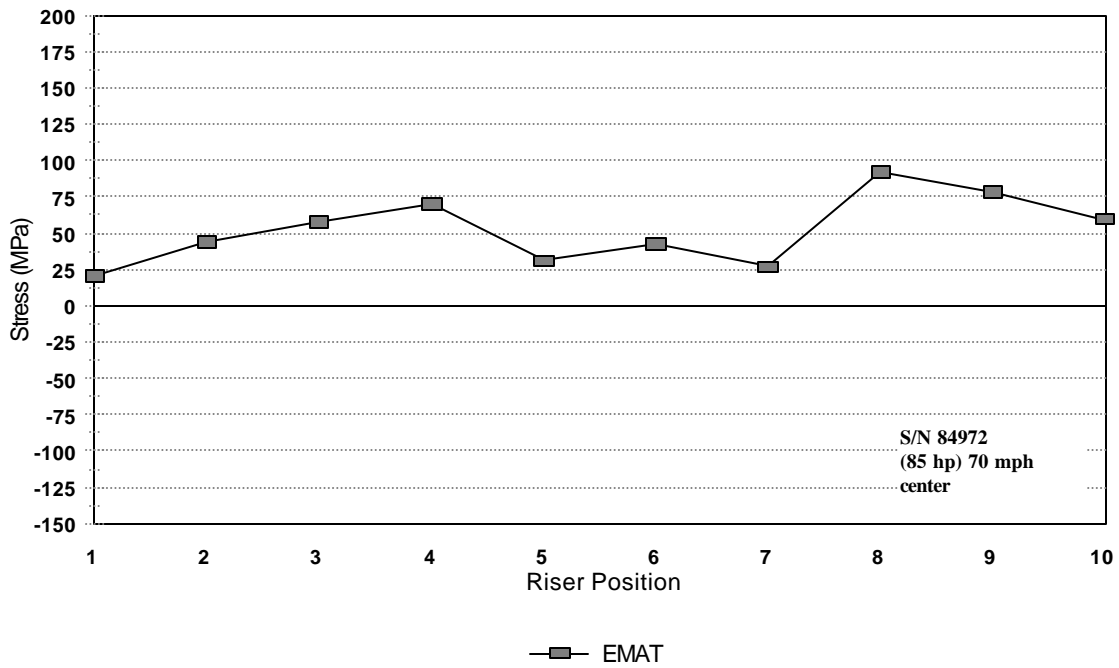
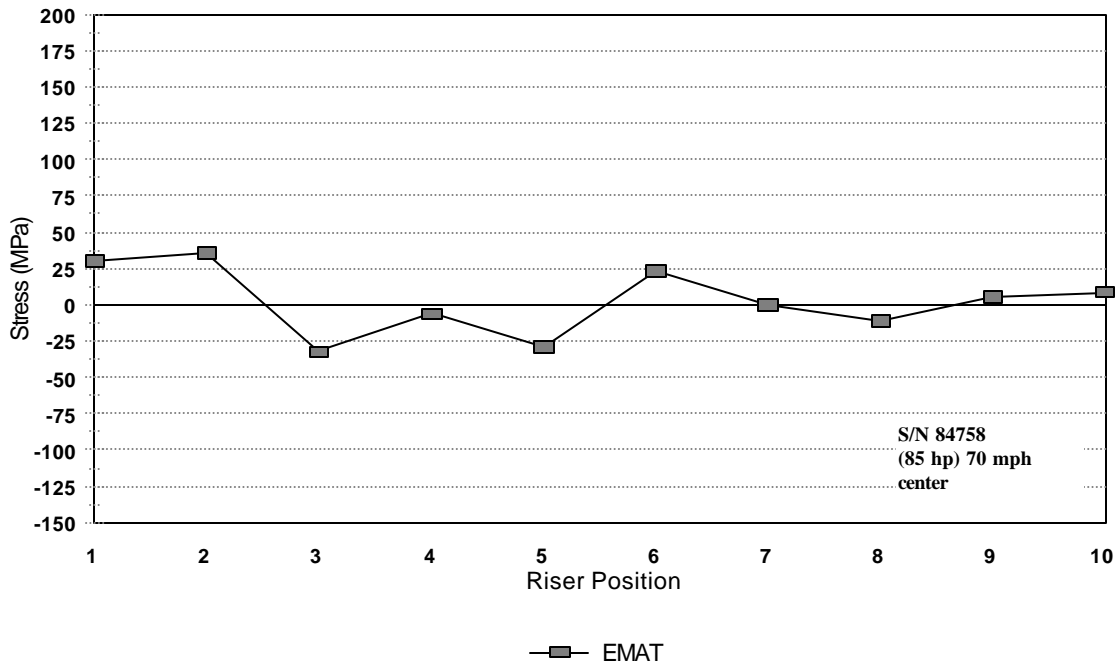


Figure 47. Residual Stress UT Measurements Using the EMAT System for Railroad Wheels Drag Braked at 85 hp and 70 mph with the Brake Shoe Positioned at the Tread Center

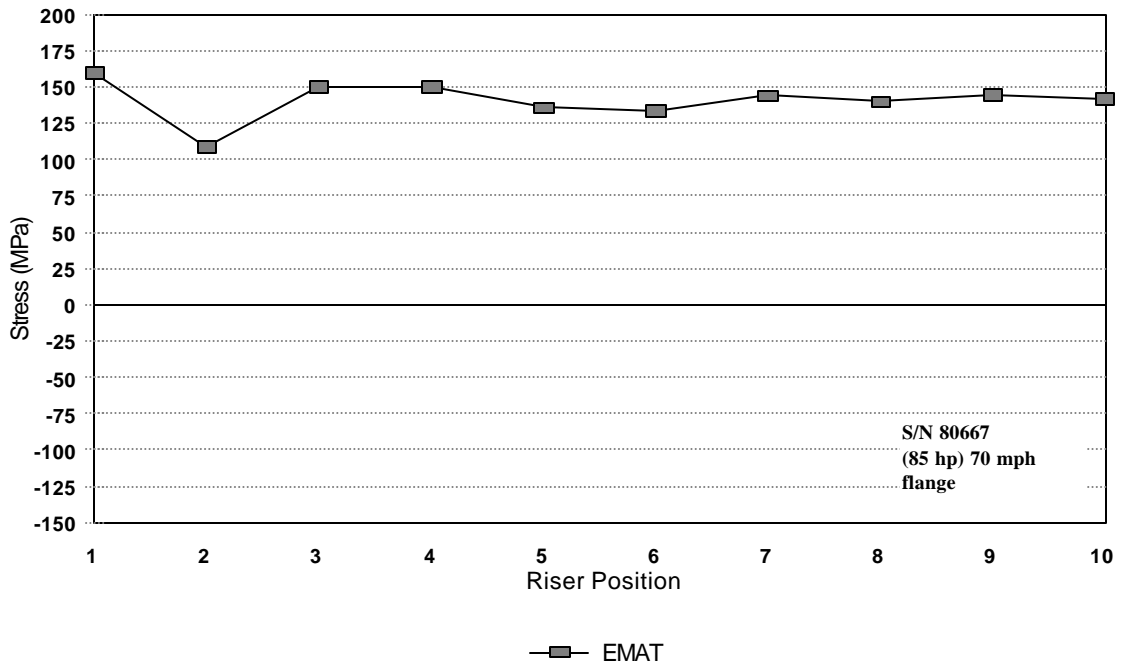
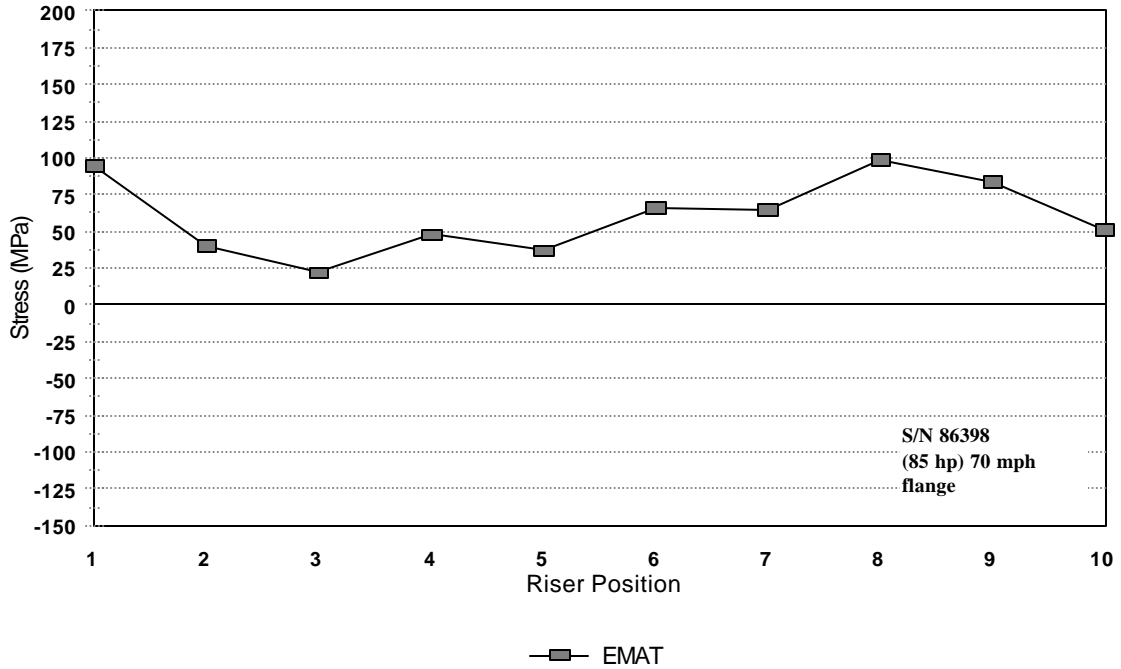


Figure 48. Residual Stress UT Measurements using the EMAT Systems for Railroad Wheels Drag Braked at 85 hp and 70 mph with the Brake Shoe Positioned at the Flange Corner

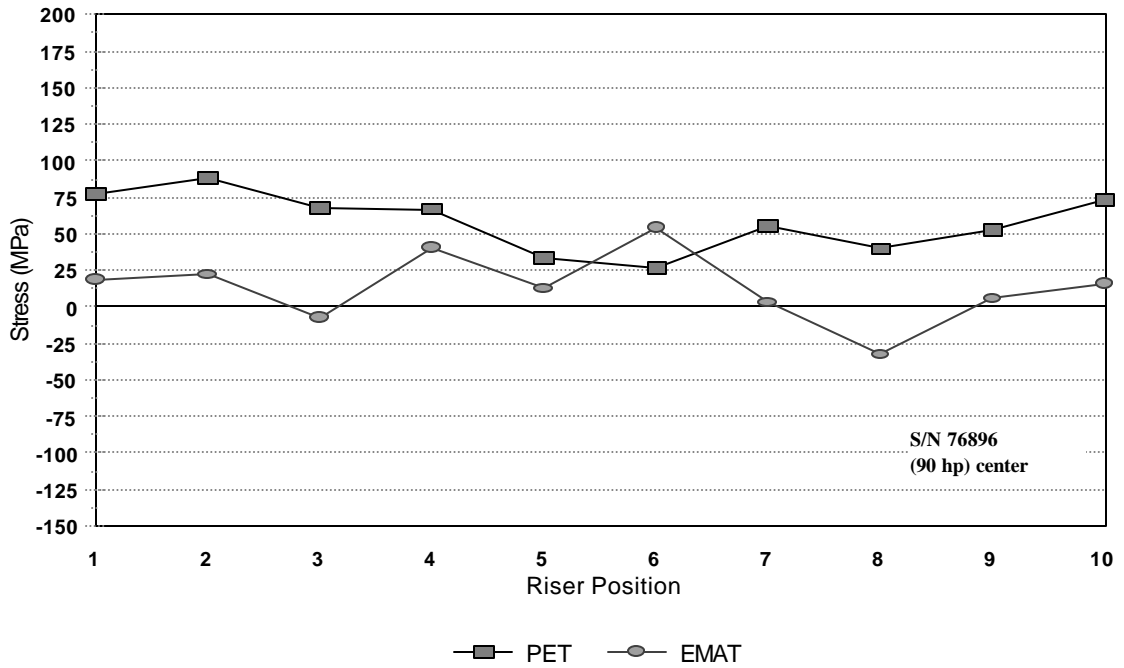
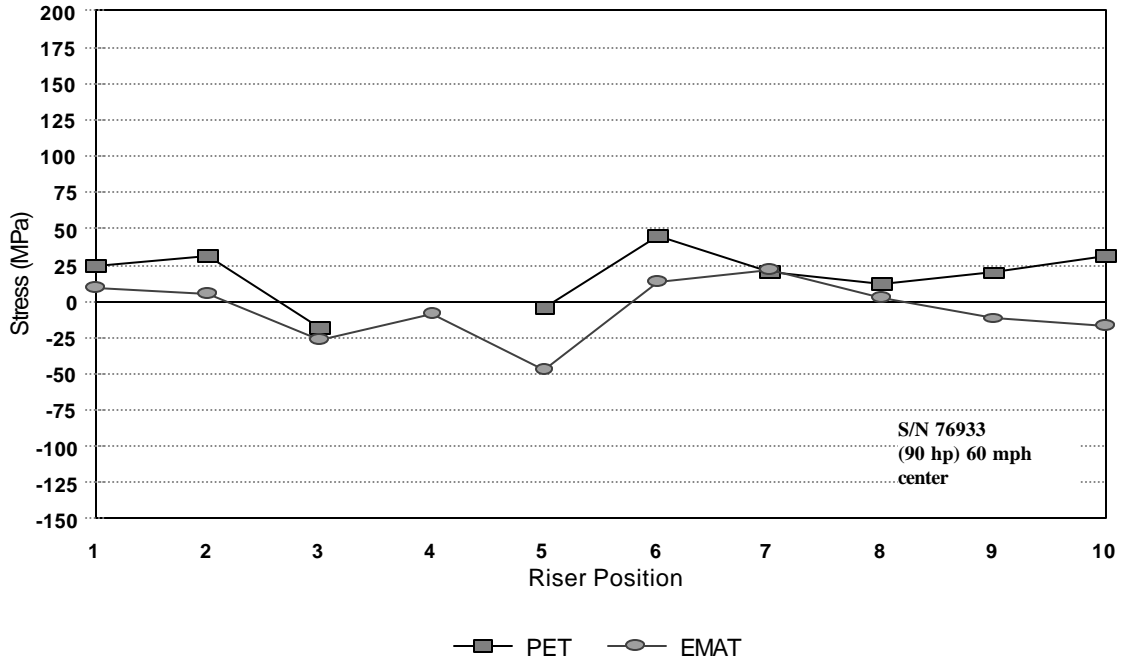


Figure 49. Residual Stress UT Measurement Comparison Between the PET and EMAT Systems for the Railroad Wheels Drag Braked at 90 hp and the Brake Shoe Positioned at the Tread Center

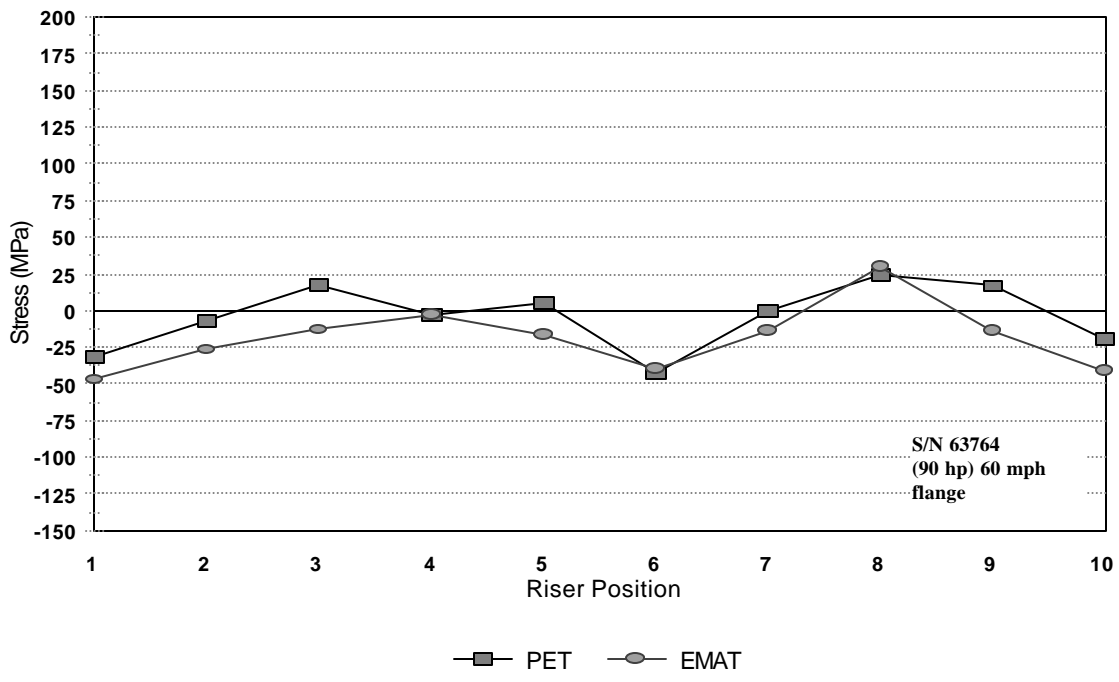
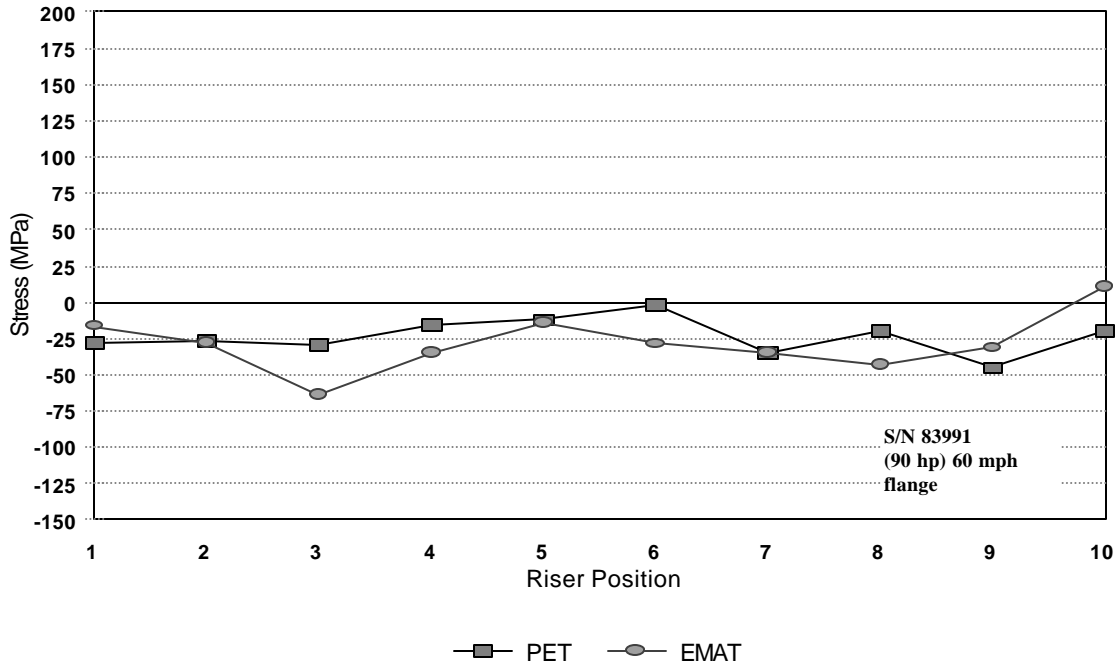


Figure 50. Residual Stress UT Measurement Comparison Between the PET and EMAT Systems for the Railroad Wheels Drag Braked at 90 hp and the Brake Shoe Positioned at the Flange Corner

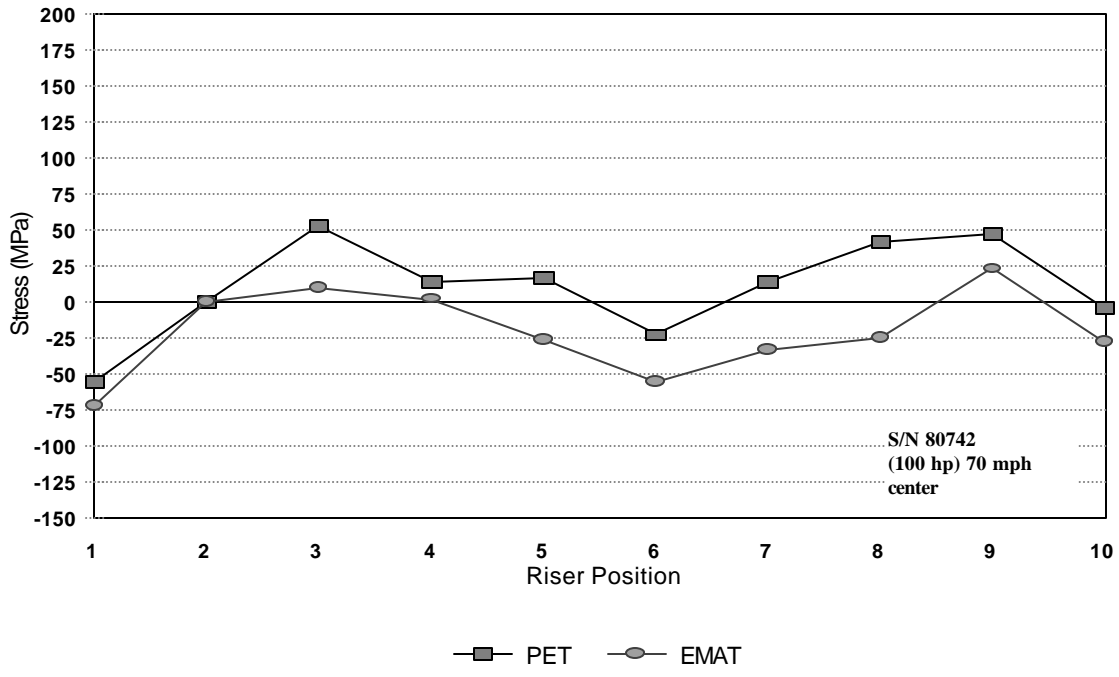
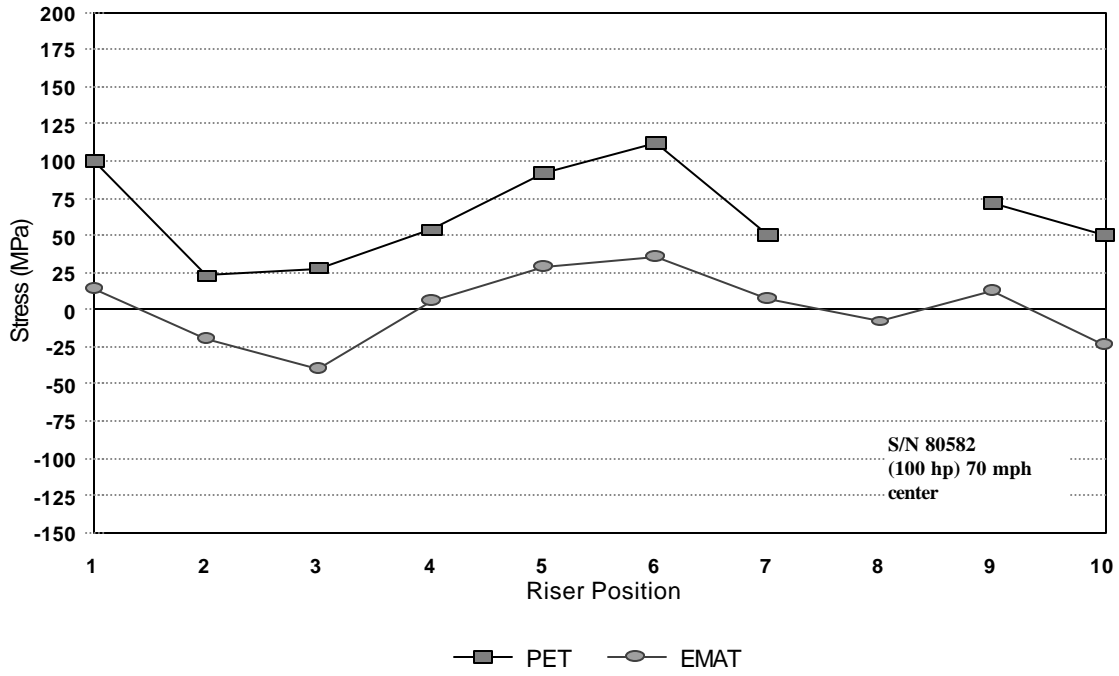


Figure 51. Residual Stress UT Measurement Comparison Between the PET and EMAT Systems for the Railroad Wheels Drag Braked at 100 hp and 70 mph with the Brake Shoe Positioned at the Tread Center

A comparison of the PET and EMAT through thickness averaged stress values was obtained for each wheel condition which includes the as-manufactured, induction heated, and drag braked conditions. As stated previously, the results show good correlation between systems with the PET readings consistently higher. The results of those comparisons are shown in Table 8. Figures 52, 53 and 54 show the average stress of the test wheels graphically. Figure 55 shows the direct comparison of the average stress measured between the EMAT and PET ultrasonic systems.

Table 8. PET and EMAT Ultrasonic Front Rim Phase Averaged Stress Values

Wheel Condition	Wheel ID No.	Power Input kW (hp)	PET MPa	EMAT MPa
As Manufactured	26508	0	-46	-82
As Manufactured	26512	0	-49	-96
Induction Heated	26515	38 (51)	-13	-65
Induction Heated	26529	38 (51)	-35	-84
Induction Heated	26506	42 (56)	2	-60
Induction Heated	26520	42 (56)	5	-59
Induction Heated	26522	42(56)	16	-57
Induction Heated	26513	45 (60)	37	-34
Induction Heated	26524	45 (60)	48	-25
Induction Heated	26526	45 (60)	34	-39
Drag Braked	91817	56 (75)	-19	-43
Drag Braked	91768	56 (75)	-47	-55
Drag Braked	91807	60 (80)	-30	-45
Drag Braked	91813	60 (80)	-35	-76
Drag Braked	91778	60 (80)	-48	-47
Drag Braked	84967	60 (80)	-25	-38
Drag Braked	91777	63 (85), 60 mph	-17	-44
Drag Braked	91784	63 (85), 60 mph	-74	-69
Drag Braked	91847	63 (85), 60 mph	-14	-40
Drag Braked	91843	63 (85), 60 mph	-40	-52
Drag Braked	84758	63 (85), 70 mph	NA	3
Drag Braked	84972	63 (85), 70 mph	NA	53
Drag Braked	86398	63 (85), 70 mph	NA	61
Drag Braked	80887	63 (85), 70 mph	NA	141
Drag Braked	76933	67 (90)	32	-6
Drag Braked	76896	67 (90)	73	13
Drag Braked	83991	67 (90)	-19	-28
Drag Braked	63764	67 (90)	-3.7	-18
Drag Braked	80582	75 (100)	50	2
Drag Braked	80742	75 (100)	-4	-21

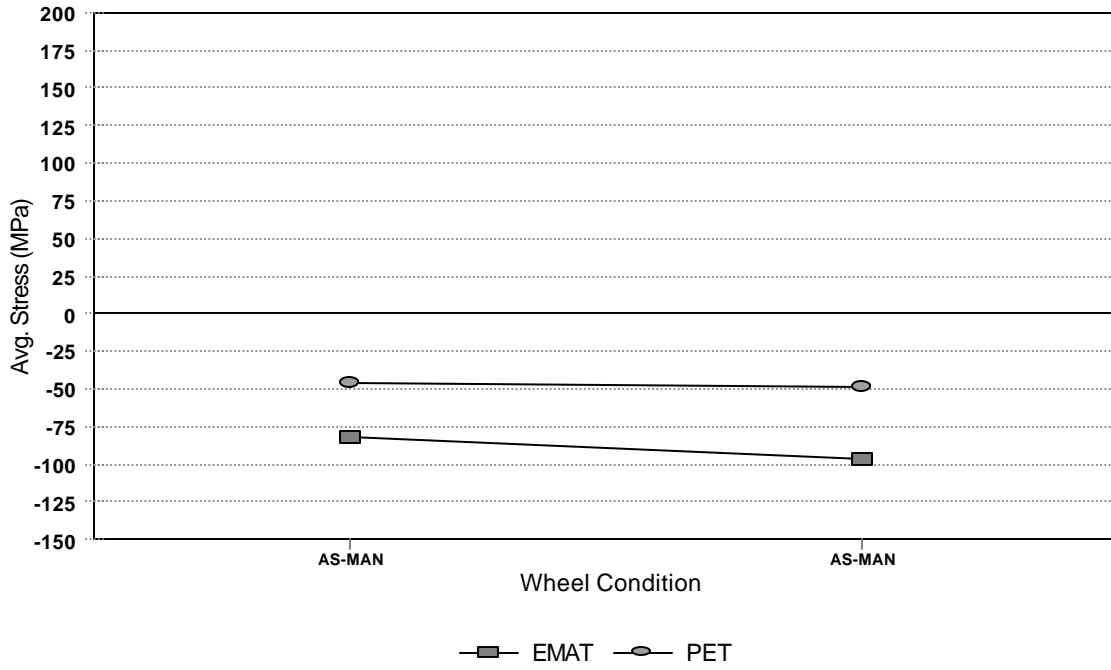


Figure 52. Average UT Residual Stress Measurement Comparison Between the PET and EMAT Systems for As-Manufactured Railroad Wheels

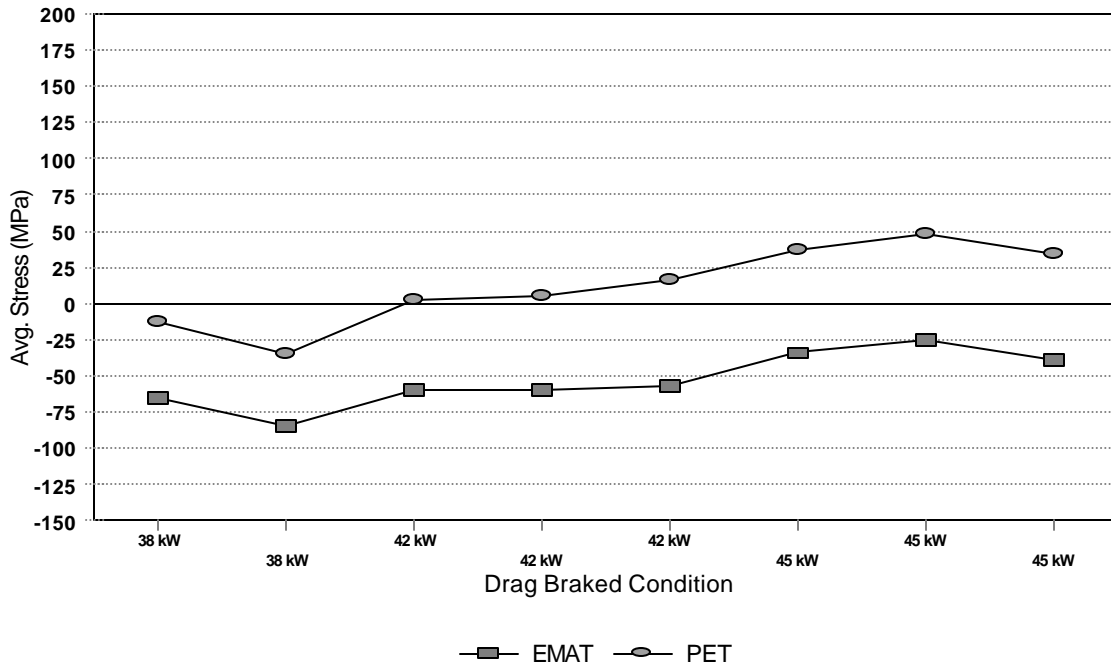


Figure 53. Average UT Residual Stress Measurement Comparison Between the PET and EMAT Systems for Induction Heated Railroad Wheels

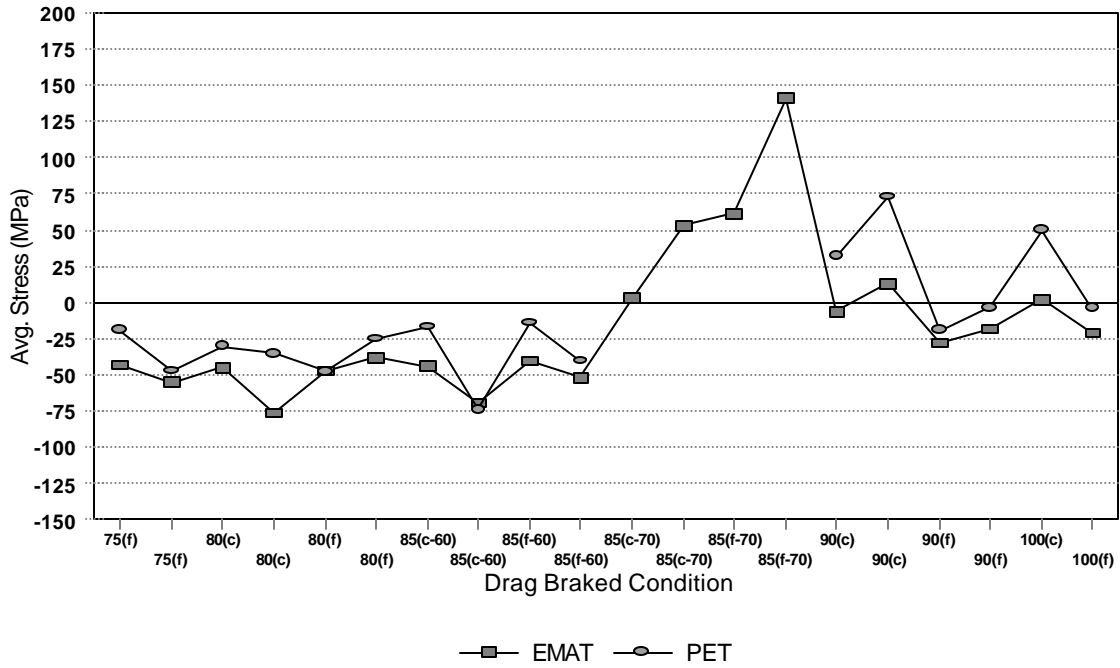


Figure 54. Average UT Residual Stress Measurements Comparison Between the PET and EMAT Systems for the Drag Braked Railroad Wheels

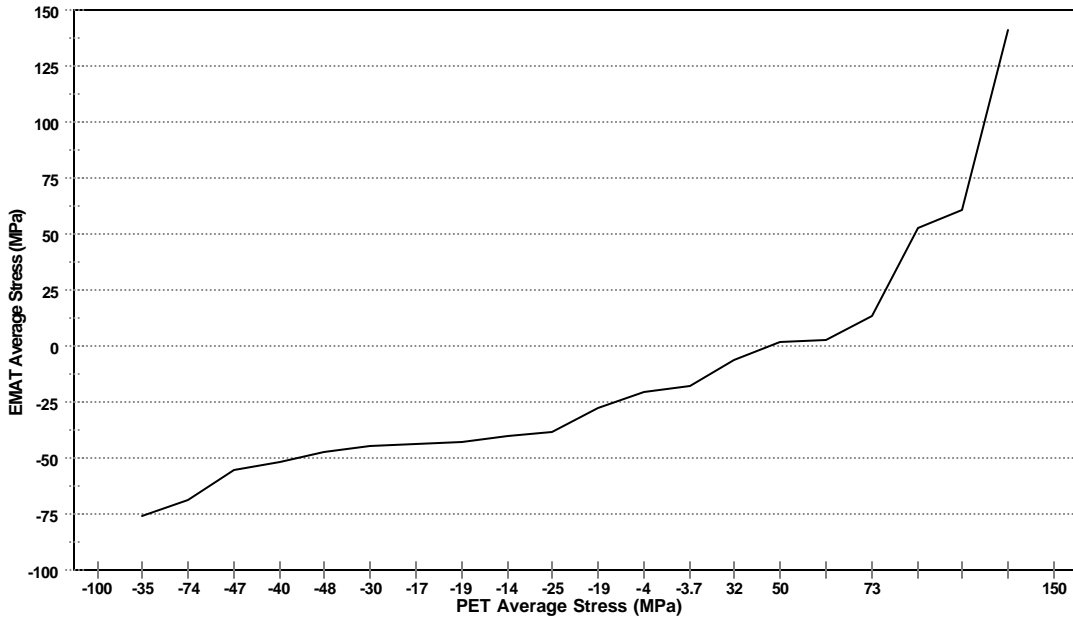


Figure 55. Direct Comparison of Average Stress Measured between EMAT and PET Ultrasonic Systems

4.3 STANDARD SAW CUT MEASUREMENTS

Tables 9 through 14 list the saw cut displacements up to a depth of 5 inches into the drag braked wheels. Figures 56 through 61 show the displacements graphically. The displacements are shown for both centered and flange crowded brake shoe positions. Table 13 and Figures 62 and 63 show displacements for the as-manufactured and induction heated wheels.

Table 9. Saw Cut Depth to Displacement Measurements for Railroad Wheels Drag Braked at 75 hp and 60 mph

Depth of Saw Cut (in.)	S/N 91817 (flange crowded) displacement (in.)	S/N 91768 (flange crowded) displacement (in.)
0.0	0.000	0.000
0.5	0.000	0.000
1.0	0.000	-0.001
1.5	-0.001	-0.002
2.0	-0.002	-0.004
2.5	-0.002	-0.006
3.0	-0.003	-0.007
3.5	-0.004	-0.009
4.0	-0.004	-0.011
4.5	-0.004	-0.012
5.0	-0.003	-0.012

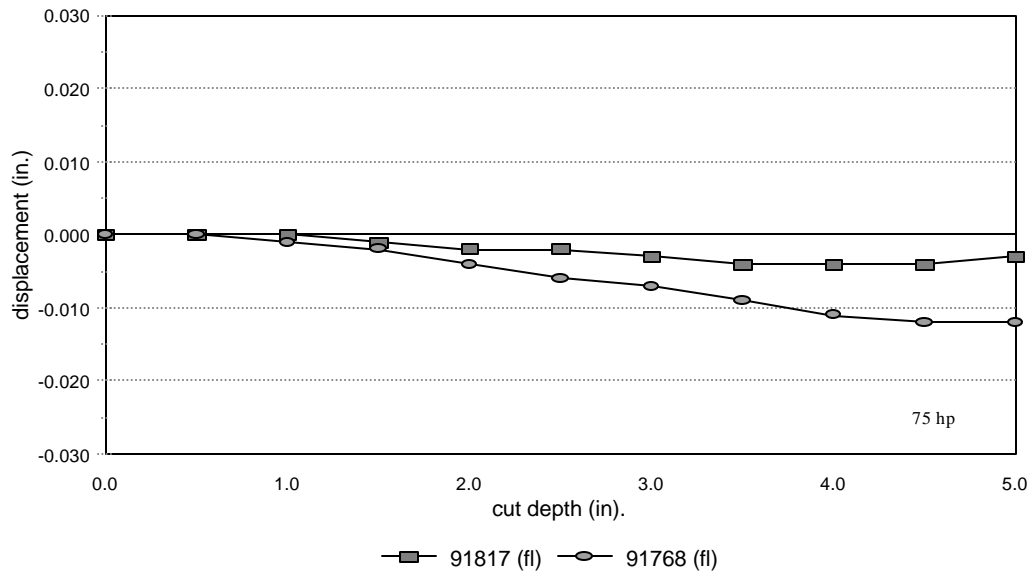


Figure 56. Radial Displacements, After Standard Saw Cutting, of the 56 kW (75 Hp) Wheels Drag Braked at 60 mph for Three 30-Minute Cycles

Table 10. Saw Cut Depth to Displacement Measurements for Railroad Wheels Drag Braked at 80 hp and 60 mph

Depth of Saw cut (in.)	S/N 91778(flange crowded) displacement (in.)	S/N 84967(flange crowded) displacement (in.)	S/N 91813(centered) displacement (in.)	S/N 91807(centered) displacement (in.)
0.0	0.000	0.000	0.000	CTC
0.5	0.000	0.000	0.000	CTC
1.0	0.000	0.000	-0.001	CTC
1.5	0.000	-0.001	-0.002	CTC
2.0	0.001	-0.001	-0.003	CTC
2.5	0.001	-0.001	-0.004	CTC
3.0	0.002	-0.001	-0.005	CTC
3.5	0.003	0.000	-0.005	CTC
4.0	0.005	0.001	-0.006	CTC
4.5	0.006	0.002	-0.006	CTC
5.0	0.007	0.003	-0.006	CTC

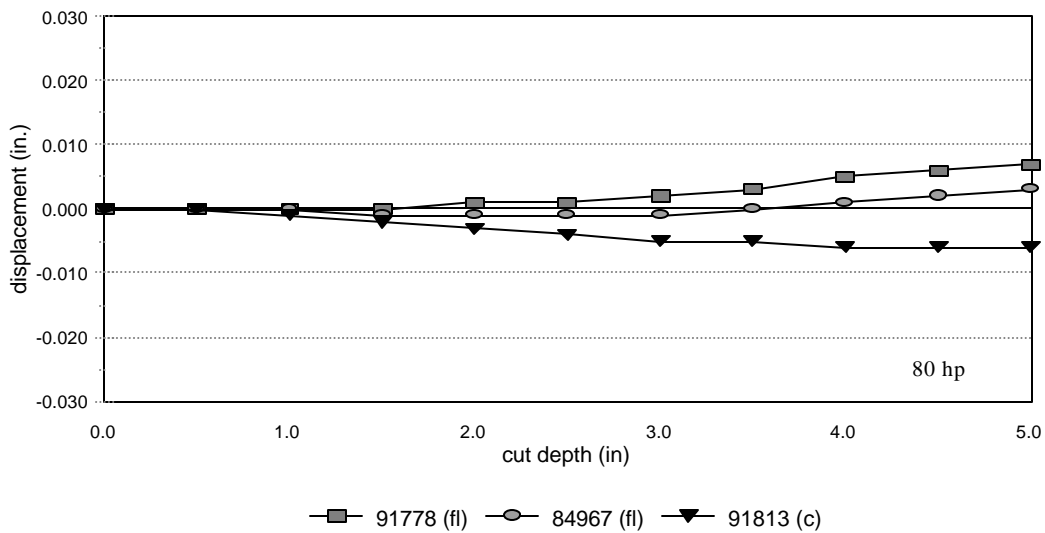


Figure 57. Radial Displacements, After Standard Saw Cutting, of the 60 kW (80 hp) Wheels Drag Braked at 60 mph for Three 30 Minute Cycles

Table 11. Saw Cut Depth to Displacement Measurements for Railroad Wheels Drag Braked at 85 hp and 60 mph

Depth of Saw Cut (in.)	S/N 91843(flange crowded) displacement (in.)	S/N 91847(flange crowded) displacement (in.)	S/N 91784 (centered) displacement (in.)	S/N 91777 (centered) displacement (in.)
0.0	0.000	0.000	0.000	0.000
0.5	0.000	0.001	0.000	0.000
1.0	0.000	0.000	-0.001	-0.001
1.5	0.000	0.000	-0.002	-0.002
2.0	0.000	0.001	-0.003	-0.003
2.5	0.001	0.001	-0.004	-0.004
3.0	0.001	0.002	-0.005	-0.004
3.5	0.002	0.003	-0.006	-0.004
4.0	0.003	0.005	-0.006	-0.004
4.5	0.004	0.006	-0.006	-0.004
5.0	0.005	0.007	-0.006	-0.004

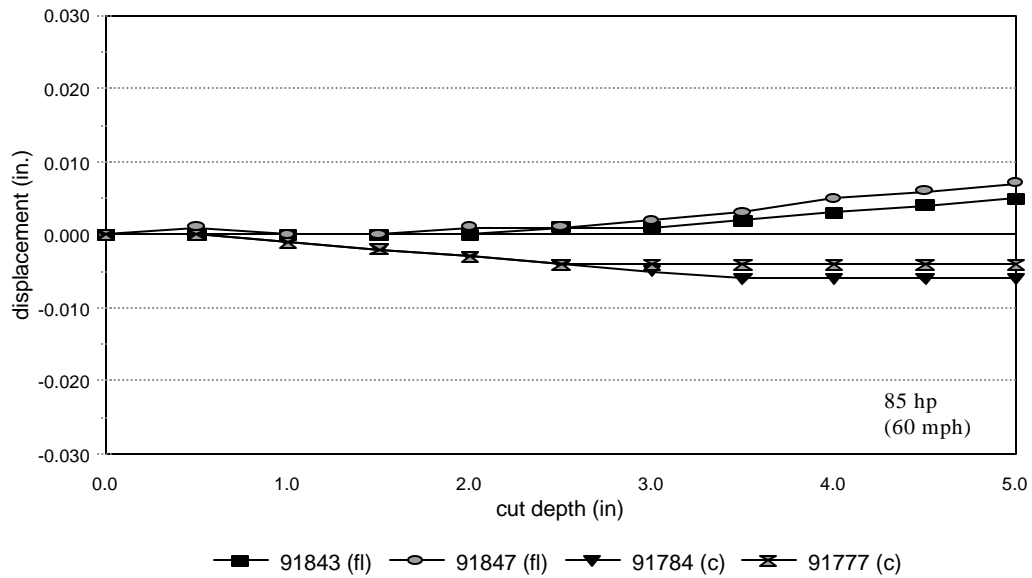


Figure 58. Radial Displacements, After Standard Saw Cutting, of the 63 kW (85 hp) Wheels Drag Braked at 60 mph for Three 30-Minute Cycles

Table 12. Saw Cut Depth to Displacement Measurements for Railroad Wheels Drag Braked at 85 hp And 70 mph.

Depth of Saw Cut (in.)	S/N 80667 (flange crowded) displacement (in.)	S/N 86398 (flange crowded) displacement (in.)	S/N 84972 (centered) displacement (in.)	S/N 84758 (centered) displacement (in.)
0.0	0.000	0.000	0.000	0.000
0.5	0.003	0.002	0.000	0.001
1.0	0.007	0.006	0.000	0.000
1.5	0.013	0.010	0.000	-0.001
2.0	0.019	0.015	0.002	0.001
2.5	see note	see note	0.004	0.001
3.0	see note	see note	0.007	0.002
3.5	see note	see note	0.012	0.004
4.0	see note	see note	0.016	0.006
4.5	see note	see note	0.019	0.008
5.0	see note	see note	0.022	0.009

Note: Wheels cracked at a cut depth of approximately 2.0 inches so no other measurements were recorded.

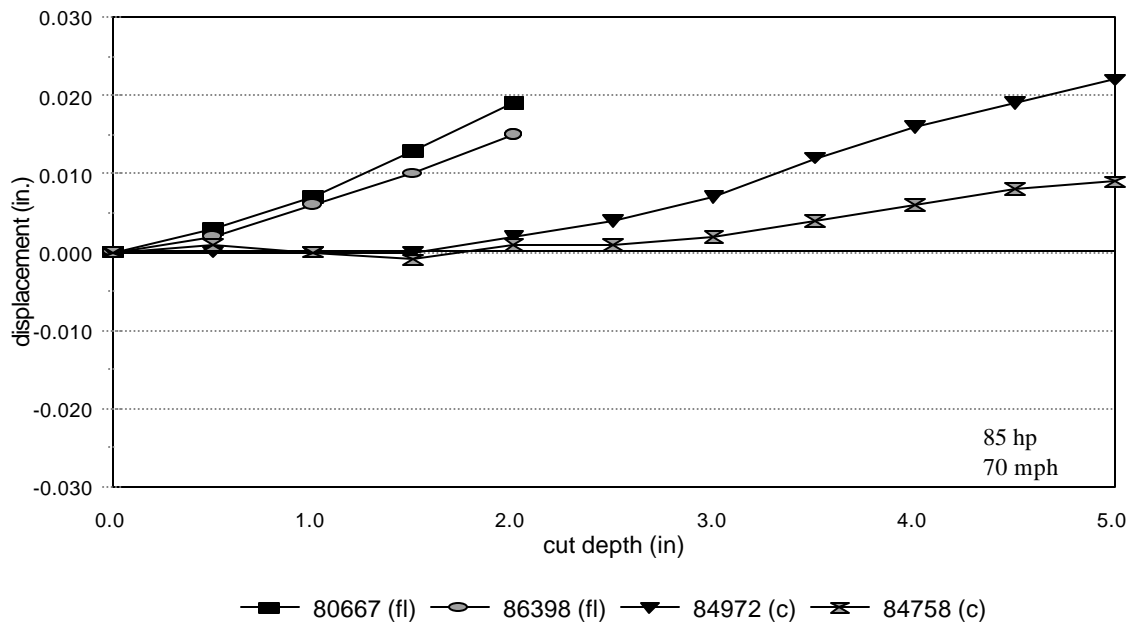


Figure 59. Radial Displacements, After Standard Saw Cutting, of the 63 kW (85 hp) Wheels Drag Braked at 70 mph for Three 30-Minute Cycles.

Table 13. Saw Cut Depth to Displacement Measurements for Railroad Wheels Drag Braked at 90 hp and 60 mph.

Depth of Saw Cut (in.)	S/N 83991 (flange crowded) displacement (in.)	S/N 63764 (flange crowded) displacement (in.)	S/N 76933 (centered) displacement (in.)	S/N 76896 (centered) displacement (in.)
0.0	0.000	0.000	0.000	0.000
0.5	0.001	0.001	0.000	0.000
1.0	0.000	0.000	0.000	-0.001
1.5	0.000	0.000	0.001	-0.001
2.0	0.001	0.001	0.003	-0.001
2.5	0.002	0.002	0.004	0.000
3.0	0.003	0.003	0.006	0.001
3.5	0.006	0.005	0.009	0.003
4.0	0.008	0.006	0.011	0.004
4.5	0.001	0.008	0.013	0.005
5.0	0.011	0.009	0.015	0.007

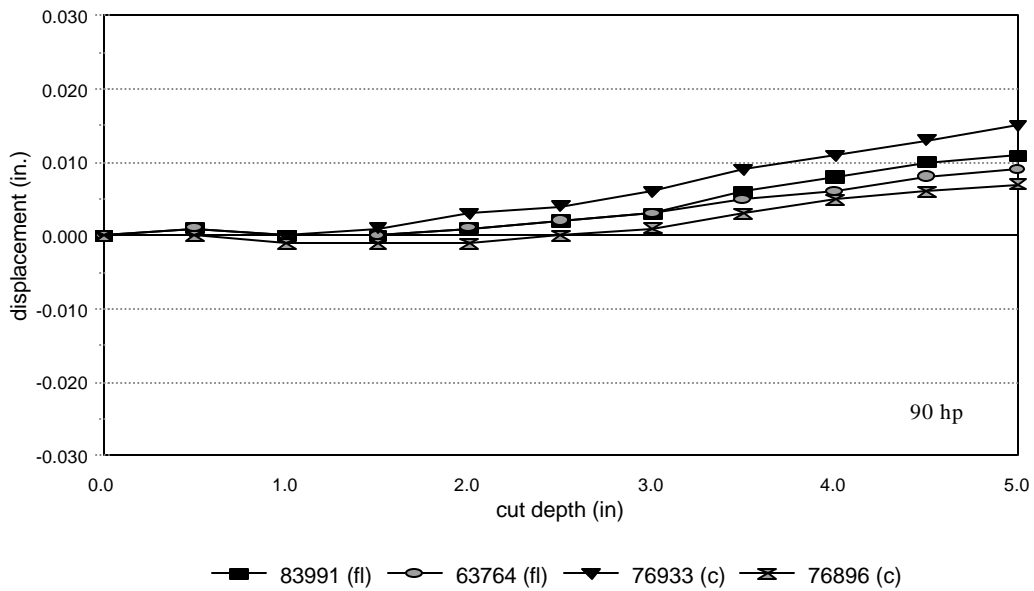


Figure 60. Radial Displacements, After Standard Saw Cutting, of the 67 kW (90 hp) Wheels Drag Braked at 60 mph for Three 30-Minute Cycles

Table 14. Saw Cut depth to displacement measurements for a railroad wheel drag braked at 100 hp and 70 mph

Depth of Saw Cut (in.)	S/N 80742 (flange crowded) displacement (in.)	S/N 80582 (flange crowded) displacement (in.)
0.0	0.000	CTC
0.5	0.000	CTC
1.0	-0.001	CTC
1.5	-0.001	CTC
2.0	-0.001	CTC
2.5	0.000	CTC
3.0	0.001	CTC
3.5	0.003	CTC
4.0	0.004	CTC
4.5	0.005	CTC
5.0	0.007	CTC

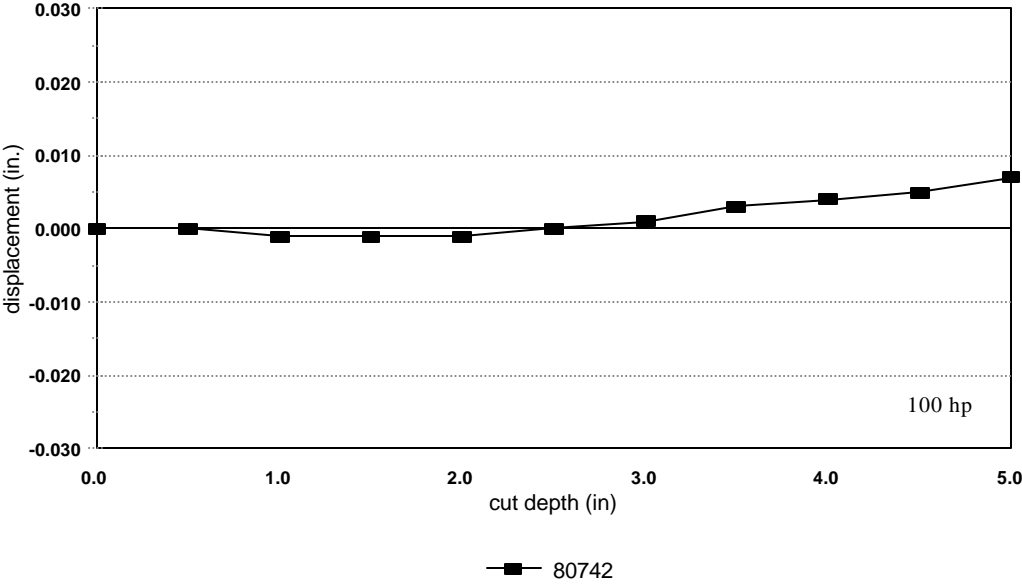


Figure 61. Radial Displacements, After Standard Saw Cutting, of the 75 kW (100 Hp) Wheel Drag Braked at 70 mph for Three 30-Minute Cycles

Table 15. Saw Cut Depth to Displacement Measurements for Railroad Wheels in the as Manufactured and Induction Heated (45 kW (60 hp)) Conditions

Depth of Saw Cut (in.)	S/N 26508 (as manufactured) displacement (in.)	S/N 26512 (as manufactured) displacement (in.)	S/N 26526 (induction heated) displacement (in.)	S/N 26524 (induction heated) displacement (in.)
0.0	-0.001	-0.005	0.058	0.082
0.5	-0.001	-0.005	0.062	0.086
1.0	-0.001	-0.001	0.062	0.086
1.5	-0.001	-0.005	0.066	0.086
2.0	-0.009	-0.017	0.066	0.062
2.5	-0.013	-0.017	0.062	0.054
3.0	0.007	-0.013	0.058	0.050
3.5	0.003	-0.005	0.054	0.050
4.0	0.003	-0.009	0.046	0.039
4.5	0.007	-0.013	0.039	0.031
5.0	0.003	-0.009	0.039	0.031

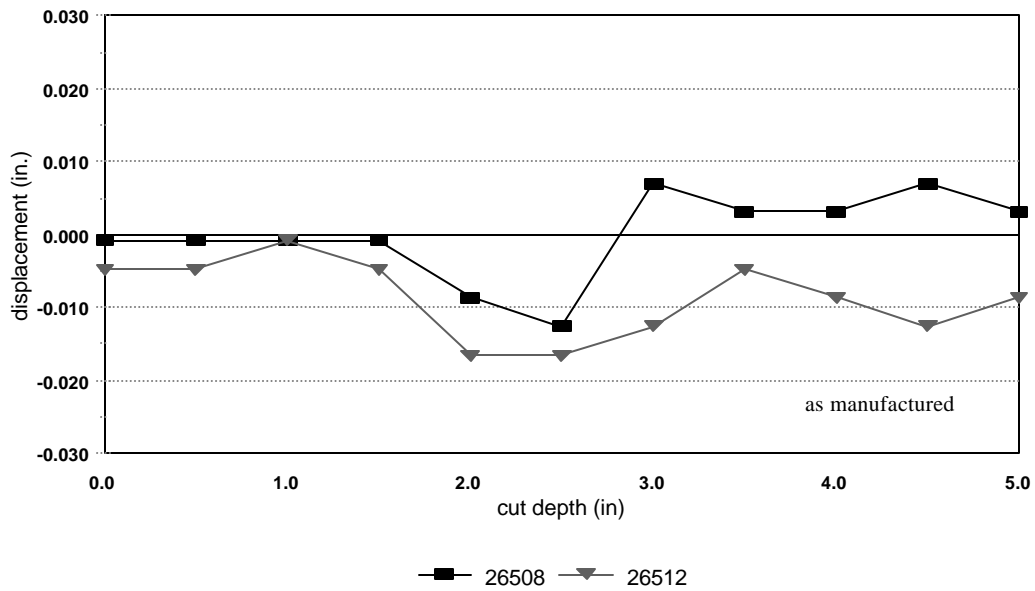


Figure 62. Radial Displacements, After Standard Saw Cutting, of Railroad Wheels in the As-Manufactured Condition

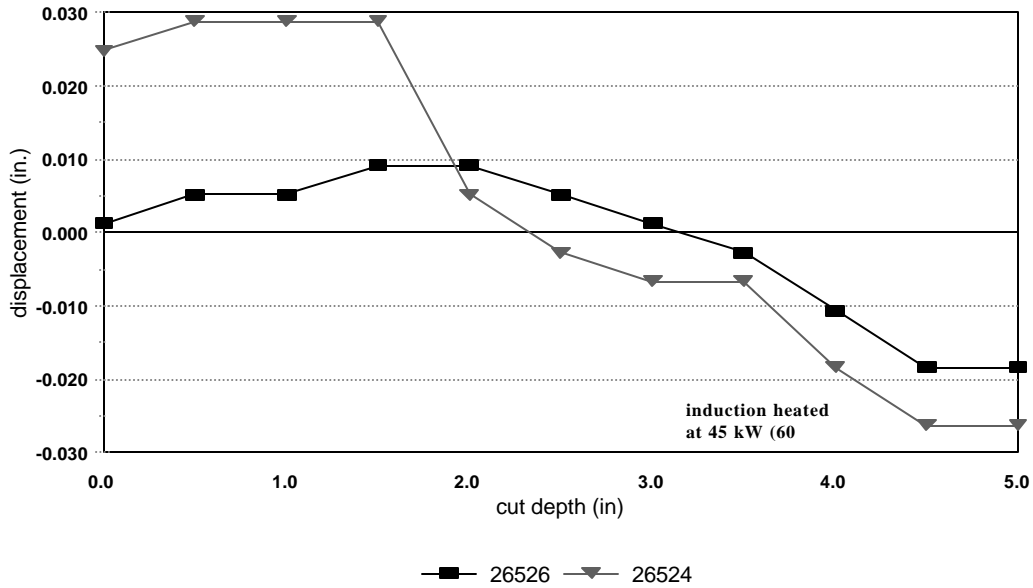


Figure 63. Radial Displacements, After Standard Saw Cutting, of Railroad Wheels Induction Heated at 45 kW (60 hp) for 30 Minutes and Air Cooled for 5 Hours

Table 16 and the graph in Figure 64 are a comparison of the displacement measurements for the test wheels. The measurement was focused at a cut depth into the wheel of 2.0 inches. This 2.0-inch cut depth was identified because this was the approximate depth at which two wheels fractured during saw cutting. The wheels that fractured (see Figures 65 and 66) had been drag braked at 70 mph for three runs of 50 minutes or longer in an 85 hp flange crowded environment.

Table 16. Saw Cut Depth To Displacement Measurements at a Cut Depth of 2 inches on as Manufactured, Induction Heated and Drag Braked Railroad Wheels

Wheel Serial Number	Wheel Condition	Wheel Displacement at 2-inch Cut Depth (in.)	Maximum Displacement (in.)
26508	as manufactured	-0.009	-0.013
26512	as manufactured	-0.017	-0.017
26526	induction heated (60 hp)	0.066	0.066
26524	induction heated (60 hp)	0.062	0.086
91817	drag braked (75 hp (fl))	-0.002	-0.003
91768	drag braked (75 hp (fl))	-0.004	-0.012
91778	drag braked (80 hp (fl))	0.001	0.007
84967	drag braked (80 hp (fl))	-0.001	0.003
91813	drag braked (80 hp (c))	-0.003	-0.006
91843	drag braked (85 hp (fl 60))	0.000	0.005
91847	drag braked (85 hp (fl 60))	0.001	0.007
91784	drag braked (85 hp (c 60))	-0.003	-0.006
91777	drag braked (85 hp (c 60))	-0.003	-0.004
80667 (*)	drag braked (85 hp (fl 70))	0.019	0.019
86398 (*)	drag braked (85 hp (fl 70))	0.015	0.015
84972	drag braked (85 hp (c 70))	0.002	0.022
84758	drag braked (85 hp (c 70))	0.001	0.009
83991	drag braked (90 hp (fl))	0.001	0.011
63764	drag braked (90 hp (fl))	0.001	0.009
76933	drag braked (90 hp (c))	0.003	0.015
76896	drag braked (90 hp (c))	-0.001	0.007
80742	drag braked (100 hp (c))	-0.001	0.007

(*)Wheels cracked at a saw cut depth of approximately 2 inches.

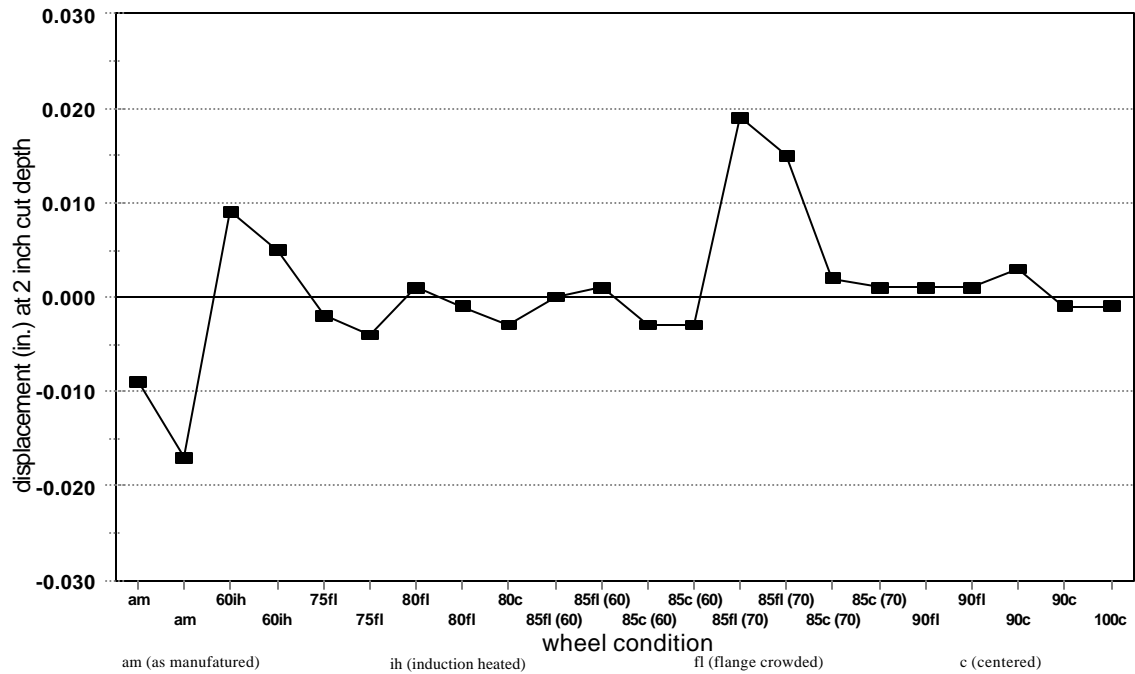


Figure 64. Radial Displacement Comparison at a Cut Depth of 2 Inches for As-Manufactured, Induction Heated and Drag Braked Railroad Wheels

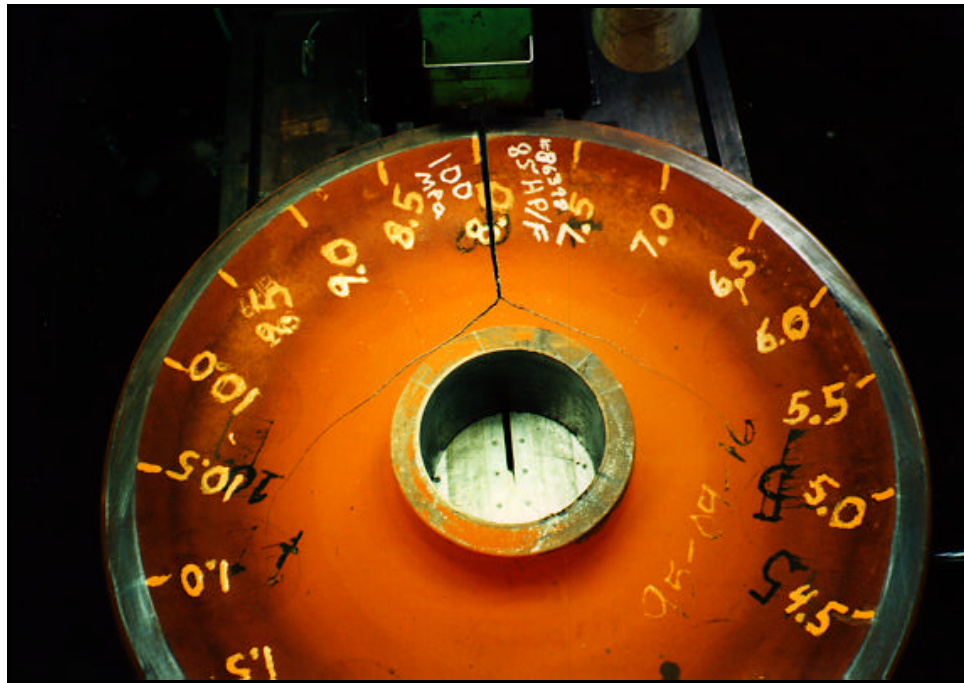


Figure 65. Fractured Railroad Wheel C Drag Braked at 70 mph, 3 Runs at a Minimum of 50 Minutes Each Run



Figure 66. Fractured Railroad Wheel C Drag Braked at 70 mph,
3 Runs at a Minimum of 50 Minutes Each Run

4.4 FINITE ELEMENT ANALYSIS (FEA)

4.4.1 Induction Heat FEA

The finite element analysis conducted for 51, 56, and 60 hp heat inputs and the average element hoop stress in the NDT zone at the end of each analysis has been calculated. Each analysis was conducted in two steps. The first step solves for the temperature distribution in the wheel at discrete time steps. The second solves for the resulting temperature induced wheel stresses at those time steps. The results from the analysis are shown in Table 17.

Table 17. Average Hoop Stress as Generated by the FEA Heat Model

Heat Input kW (Hp)	NDT zone average hoop stress MPa (ksi)
38, (51)	34 (5)
42, (56)	55 (8)
45, (60)	82 (12)

Comparing the FEA results with the actual ultrasonic measurements show a similar trend in hoop stress identification. As mentioned previously, an offset between the FEA results and the ultrasonic measurements is expected. The offset is due to the FEA being evaluated from a point of zero stress and ultrasonic measurements taken on actual wheels which have compressive stresses generated into the wheels during the manufacturing process. Figure 67 shows the comparison between the FEA results and the ultrasonic measurements. Figure 68 shows the same comparison as before but with a -80 MPa offset. The offset has been added to simulate the railroad wheel state after manufacturing.

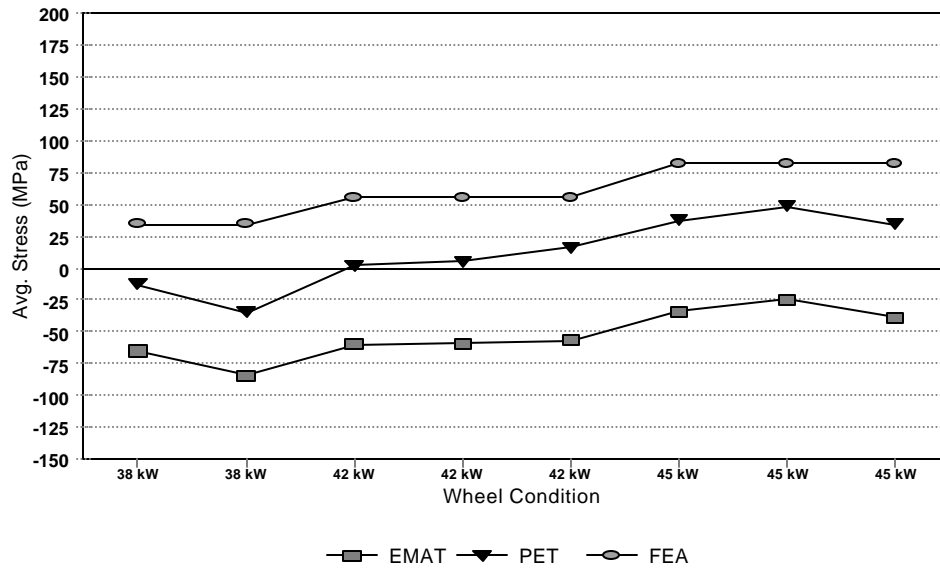


Figure 67. Residual Stress Comparison Between Finite Element Analysis and Ultrasonic Measurements Using PET and EMATs for Evaluating Induction Heated Railroad Wheels

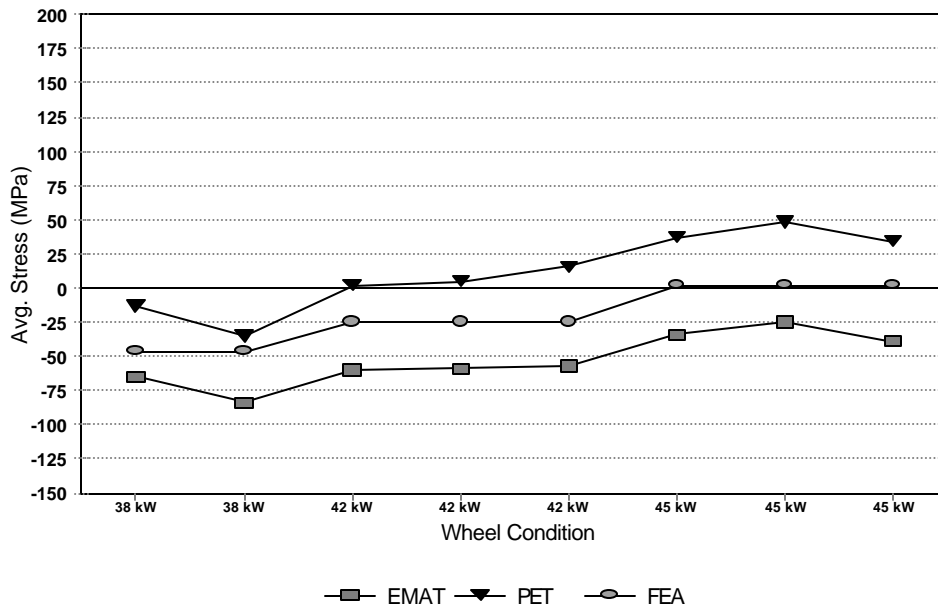


Figure 68. Residual Stress Comparison Between the Finite Element Analysis Heat Model and Ultrasonic Measurements Using PET and EMATs with a -80 MPa Offset to Compensate for Stresses Generated During Manufacturing

4.4.2 Saw Cut FEA

The saw cut FEA model was derived by allowing it to reach equilibrium with the specified hoop displacement data. This amounts to “unsawcutting” the wheel. The average element hoop stress for the NDT zone was then calculated. The average hoop stress at the NDT zone for the four wheels that saw cut opening measurements were made are given in Table 18. Figure 69 shows the trend comparison between FEA from the unsawcutting process and ultrasonic measurements.

Table 18. Average Hoop Stress as Generated by the Saw Cut Displacement Model

Wheel No.	NDT Zone Average Hoop Stress MPa (ksi)
5 (45 kW (60 hp))	35, (5)
6 (as manufactured)	-28, (-4)
7(45 kW (60 hp))	-55, (-8)
8 (as manufactured)	-41, (-6)

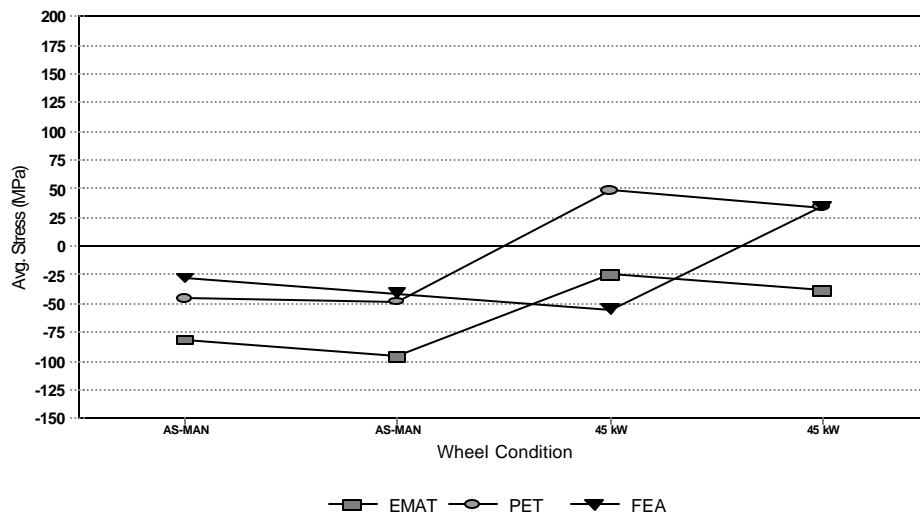


Figure 69. Residual Stress Comparison Between the Finite Element Analysis Saw Cut Displacement Model and Ultrasonic Measurements Using PET and EMATs

The result from wheel 7 was not expected since wheel 5 and 7 were showing the saw cut to be opening. Because of this both should be in tension, but wheel 7 is indicating compression in the NDT zone. This is even more surprising since wheel 7 has much larger opening displacements on the tread surface than wheel 5.

The explanation is that wheel 5 and 7 have a neutral axis that cuts through the NDT zone (leaving the gage and field face elements in compression and the rest in tension). Since wheel 7 had much larger displacements on the tread the compressive stress on the gage and field face elements intensified and caused the average NDT zone hoop stress to be in “compression” even though all the other elements in the NDT zone were in tension.

4.4.3 Saw Cut FEA Relevant Error Sources

There are three relevant error sources for the saw cut FEA. They are:

- (1) Assumption of homogeneous material properties may be in error.
- (2) Inaccurate boundary conditions may have been caused by test measurement errors, when recording saw cut displacements both electronically and manually.
- (3) Hoop stress may vary around the wheel (demonstrated by NDT measurements at different positions on the wheels).

5.0 CONCLUSIONS

The nondestructive testing system developed by NIST has demonstrated both accuracy and reliability in determining the residual “hoop” stress in as-manufactured, induction heated and drag braked cast railroad wheels. Comparison with the DEBRO-30 ultrasonic system, available commercially in Europe, showed excellent correlation in measurement trends with a maximum offset of approximately 40 MPa (6 ksi).¹⁷ Both ultrasonic systems correlate with induction heated finite element analysis trends as shown in Figure 70. The graph in Figure 70 contains an -80 MPa offset to compensate for the compressive stressed wheel condition produced as part of the manufacturing

design process. A correlation also exists between ultrasonic and saw cutting data as shown in Figure 71. Nondestructive and destructive data trends show a correlation in identifying the residual stress states of railroad wheels to be either compressive or tensile.

As mentioned previously in order for thermal failure to occur in a railroad wheel, three conditions must be present. First a thermal crack must be present on the rim of the wheel; this condition can usually be determined with visual inspection. Second, a residual tensile stress must be present to permit crack opening; this condition could be addressed by using the EMAT system to identify wheel residual “hoop” stresses in the rim. And third, the wheel must be subjected to a set of alternating loads to advance the thermal crack until it reaches a critical size and fracture occurs. If any of the preceding three conditions are missing, failure will not occur.

By implementing the EMAT system to determine wheel residual stress states during both wheel manufacturing, as a quality control tool, and wheel-shop inspection, as a safety inspection tool, two of the three conditions for thermal failure in a railroad wheel would be addressed. Combining visual inspection with residual stress monitoring would help to assure that wheels containing both thermal cracks and a residual tensile stress are identified and removed from service. The EMAT also serves as a tool in identifying wheels which may contain thermal cracks on the rim, but the stress state of the wheel is compressive allowing the wheel to remain in service, thus reducing wheel replacement costs.

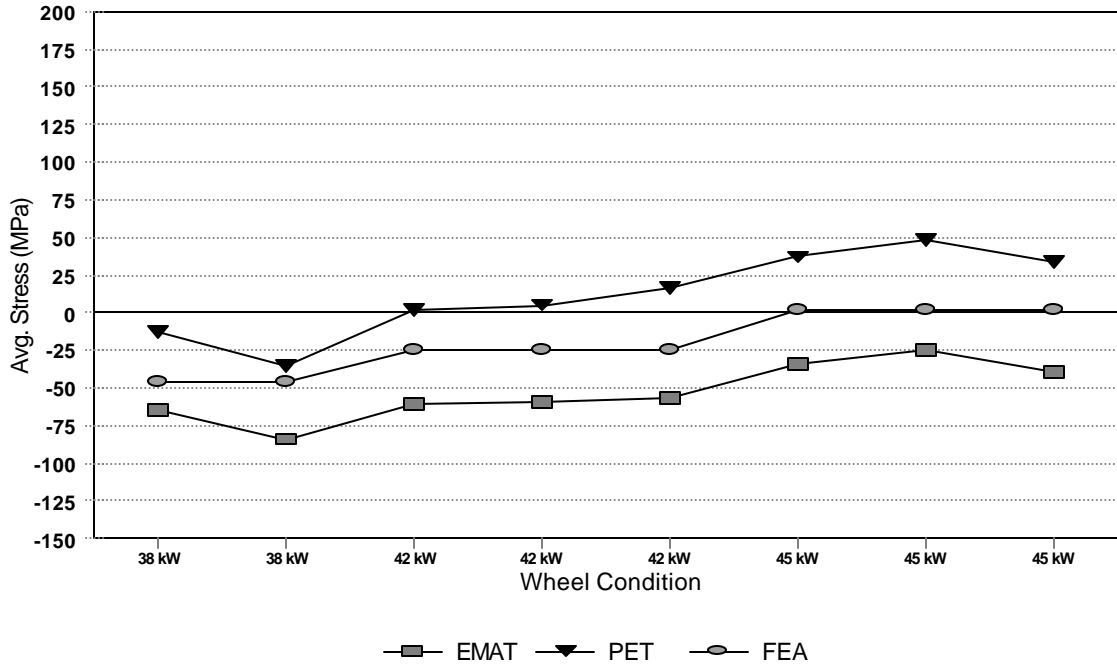


Figure 70. Ultrasonic Measurement to Finite Element Analysis Comparison of Induction Heated Railroad Wheels (The FEA Represents an Offset Included For Manufacturing)

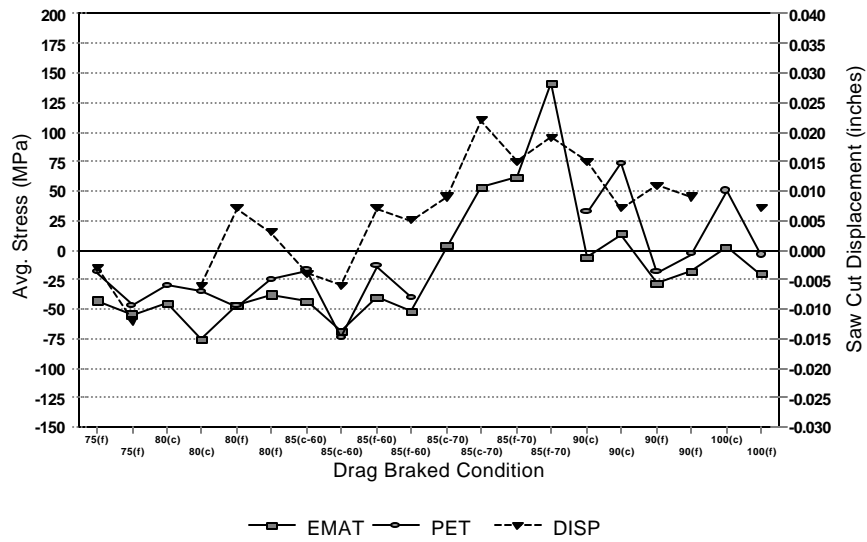


Figure 71. Comparison of Test Results obtained from Destructive and Non-destructive Evaluation of Drag Braked Railroad Wheels

6.0 RECOMMENDATIONS

The NIST ultrasonic EMAT system has demonstrated the accuracy and reliability for determining the residual “hoop” stress state of as-manufactured, induction heated and drag braked CH-36 railroad wheels. AAR recommends that the system be further evaluated by measuring residual stresses of in-service railroad wheels. An EMAT system should be setup in a wheel inspection shop and used to measure stress states on a minimum of 100 wheels. The wheels would be identified as containing either compressive or tensile “hoop” stress as measured by the EMAT system. From the wheels sampled a minimum of 50 of these wheels should be saw cut to verify any correlation with the ultrasonic data. It is suggested that the wheels identified for saw cutting be equally selected with 25 of the wheels suspected of containing a compressive residual stress and the other 25 a tensile residual stress. If the evaluation provides sufficient correlation between nondestructive (EMAT) and destructive (sawcutting) results then the EMAT system should be considered for commercial application.

The primary areas to benefit from the EMAT technology would be wheel manufacturers and wheel inspection shops. The use of the EMAT as a quality control tool should allow the wheel manufacture to re-evaluate destructive inspection requirements thus allowing more product available for sale to customers. Wheel shops could use the EMAT system to assess the safety of wheels entering and leaving their shops. By identifying the residual stress state of the wheel, a greater level of confidence in decisions to return or remove wheels from service would be provided.

REFERENCES

1. R. L. Kenyon and Harry Tobin, "Stresses in Car Wheels," *Railway Mechanical Engineer*, December, 1941.
2. H. R. Wetenkanp, O. M. Sidebottom, and H. J. Schrader, "The Effect of Brake Shoe Action on Thermal Cracking and on Failure of Wrought Steel Railway Car Wheels," *Univ. of Illinois Bulletin*, Vol. 47, No. 77, June, 1950.
3. H. N. Jones III, "The Characterization of the Residual Stress State of Railroad Wheels," *ASME Rail Transportation Spring Conference Proceedings-1985*, ASME (New York, 1995)
4. B. R. Rajkumar and D. H. Stone, "Wheel Thermal Failure Mechanisms of Railroad Cars, Volume 1 - Final Summary Report," AAR Report R-679, November, 1987.
5. M. R. Johnson, R. R. Robinson, A. J. Opinsky, M. W. Joerms , and D. H. Stone, "Calculation of Residual Stresses in Wheels from Saw Cut Displacement Data," ASME Paper 85-WA/RT-17, November, 1985.
6. D. M. Engle and D. E. Bray, "Nondestructive Measurement of longitudinal Stress in Rail," FRA Report FRA/ORD 77/34.I, January, 1978.
7. G. L. Burkhart, W. D. Perry, P. J. Pantermuehl, M. Smith, and J. R. Barton, "Determination of Thermal Damage in Freight Car Wheels by Barkhausen Noise Analysis," *Proceedings of the Ninth International Wheelset Congress*, Montreal, September, 1988, Paper 3-5..
8. P. J. Mutton, M. D. O'Rourke, and R. A. Langman, "Non-destructive Measurement of Residual Stresses in Railway Wheels, Based on the Magnetomechanical Effect," *Proceedings of the Tenth International Wheelset Congress*, Sydney, September, 1992, p.135.
9. C. W. Simmons, P. A. Robinson, and G. S. Neal, "Operational Experience in the Use of a Wheel Stress Measurement Device," *Proceedings of the Tenth International Wheelset Congress*, Sydney, September, 1992, p. 145.
10. H. Fukuoka, H. Toda, K. Hirakawa, H. Sakamoto, and Y. Toya, "Nondestructive Assessments of Residual Stresses in the Rim by Acoustoelasticity," *Journal of Engineering for Industry*, Volume 107, August, 1985, pp. 281-287.

11. E. Schneider, H. Hintze, M. Dalichow, "Ultrasonic Techniques for the Evaluation of Stress States in Railroad Wheels and Rails," ***Proceedings of the World Congress of Railway Research 1996***, Colorado Springs, 1996, pp. 425-430.
12. V. Del Fabbro and B. Catot, "Ultrasonic Measurement of Stresses in New Wheels," ***Proceedings of the Eleventh International Wheelset Congress***, Volume 1, Paris, 1995, pp. 251-259.
13. Deputat, A. Kwaszczynska-Klimek, and J. Selazek, "Monitoring Residual Stresses in Railroad Wheels with Ultrasound," ***Proceedings of the Twelfth World Conference on Nondestructive Testing***, (Amsterdam, 1989), Paper 181.
14. R. E. Schramm, J. Szelazek and A. V. Clark, Jr., NIST Report No. 30 Dynamometer-Induced Residual Stress in Railroad Wheels: Ultrasonic and Saw Cut Measurements, March 1995, NISTIR 5043.
15. R. E. Schramm, J. Szelazek and A. V. Clark, Jr., NIST Report No. 28 Residual Stress in Induction-Heated Railroad Wheels: Ultrasonic and Saw Cut Measurements, May 1995, NISTIR 5038.
16. R. Czarnek, Ph.D. and S. y. Lin, Ph.D., Concurrent Technologies Corporation, Final Report Contract No. DTRF-53-93-C-00001: Experimental Determination of Release Fields in Cut Freight Railroad Car Wheels, 28 March 1996.
17. DEBRO Ultrasonic Stress Meter, Institute of Fundamental Technological Research, Polish Academy of Sciences, Warsaw, Poland, 1990.